MitoRibo-Tag mice –

a novel tool to study the composition of the mitochondrial ribosome *in vivo*

Inauguraldissertation

zur

Erlangung des Doktorgrades

der Mathematisch-Naturwissenschaftlichen Fakultät

der Universität zu Köln

vorgelegt von

Jakob D. Busch

aus Köln, Deutschland

Köln, 2019

Berichterstatter:

Prof. Dr. Nils-Göran Larsson (1. Gutachter)

Prof. Dr. Elena Rugarli (2. Gutachter)

Prof. Dr. Jan Riemer (Vorsitzender)

Tag der mündlichen Prüfung: **26. März 2019**

“Satisfaction of one's curiosity is one of the greatest sources of happiness in life.”

“I believe all complicated phenomena can be explained by simpler scientific principles.”

Linus Pauling

Table of contents

Summary

Mitochondria, semi-autonomous organelles of eukaryotic cells derived from an α-proteobacterium, are essential for synthesis of iron-sulfur clusters, amino acids, lipids and for maintaining the cellular ATP levels by the oxidative phosphorylation (OXPHOS). During evolution, mitochondria retained a compact double stranded circular mitochondrial DNA (mtDNA) genome, which harbors organelle-specific rRNA, tRNA and mRNA genes. The mitochondrial mRNAs encode highly hydrophobic protein constituents of the OXPHOS system and are translated by mitochondrial ribosomes (mitoribosomes). The coordinated synthesis of mtDNA- and nuclear- encoded OXPHOS proteins is required for mitochondrial integrity and cell survival. Mitoribosomes are structurally and functionally adapted as they have acquired 36 specific proteins, different from bacterial ribosomal proteins, and putatively interact with inner mitochondrial membrane. The regulation of translation and mitoribosome assembly in mitochondria is well studied in *Saccharomyces cerevisiae* but remains largely unexplored in mammals due to the limited number of available animal models. To obtain new insights into regulatory mechanisms underlying the process of mitochondrial translation, we generated a knock-in mouse model, denoted MitoRibo-Tag mice, expressing a FLAG-tagged mitoribosome protein. We used MitoRibo-Tag mice to determine the mitoribosome interactome across various mouse tissues by proteomics. This mitoribosome protein catalog unravels several novel mitoribosome-interacting proteins (MIPs) and demonstrates intriguing tissue-specific compositional differences. Moreover, the proteomic definition of a biogenesis intermediate, formed in the absence of the mitoribosome assembly factor MTERF4, unveils PUSL1 as a novel MIP. We find that PUSL1 is peripherally associated with the mitochondrial inner membrane from the matrix side and part of a yet unknown mitoribosome biogenesis intermediate. Additionally, depletion of PUSL1 reveals that the protein is required for efficient *de novo* synthesis of mtDNA-encoded proteins. In summary, this PhD thesis establishes MitoRibo-Tag mice as a novel tool to study mitoribosomes *in vivo*, enabling future studies on translation and dynamics during different physiological states, including ageing, exercise and fasting or disease.

Zusammenfassung

Mitochondrien sind semiautonome Organellen eukaryotischer Zellen α-proteobakteriellen Ursprungs, welche essentielle Eisen-Schwefel-Kofaktoren, Aminosäuren und Lipide synthetisieren. Ferner regulieren Mitochondrien das zelluläre Verhältnis von ATP zu ADP und Phosphat durch die oxidative Phosphorylierung (OXPHOS). Trotz der evolutionären Entwicklung haben Mitochondrien ein kompaktes zirkuläres doppelsträngiges Genom, die mitochondriale DNA (mtDNA), behalten, welches organellenspezifische rRNA, tRNA und mRNAs kodiert. Mitochondriale mRNAs chiffrieren hydrophobe Kernproteine der OXPHOS, welche von mitochondrienspezifischen Ribosomen (Mitoribosomen) translatiert werden. Die koordinierte Synthese von mtDNA- und zellkernkodierten OXPHOS-Proteinen ist essentiell für die mitochondriale Integrität und das Überleben der Zelle. Mitoribosomen sind strukturell und funktionell angepasst, weil sie im Vergleich zu bakteriellen Ribosomen 36 zusätzliche Proteine erworben haben und mit der inneren mitochondrialen Membran interagieren. Die Biogenese von Mitoribosomen ist überwiegend in der Bäckerhefe *Saccharomyces cerevisiae* untersucht, jedoch in Säugetieren größtenteils unbekannt. Um neue Erkenntnisse über die regulatorischen Mechanismen der mitochondrialen Proteinbiosynthese zu gewinnen, haben wir gentechnisch veränderte Knock-in Mäuse generiert, genannt MitoRibo-Tag Mäuse, welche ein mitoribosomales FLAG-tag-Fusionsprotein exprimieren. Mittels Massenspektrometrie haben wir das Mitoribosomeninteraktom in verschiedenen Geweben von MitoRibo-Tag Mäusen bestimmt. Der erstellte Proteinkatalog enthüllt bisher unbekannte Mitoribosomen-interagierende Proteine (MIPs) und gewebespezifische Proteinzusammensetzungen. Des Weiteren haben wir mittels Massenspektrometrie die Zusammensetzung eines Biogeneseintermediates von Mitoribosomen analysiert, welches in der Abwesenheit des Assemblierungsfaktors MTERF4 in Herzzellen von Mäusen akkumuliert. Die Untersuchung führte zur Identifikation des noch unerforschten Proteins PUSL1 als ein neues MIP. Die biochemische Lokalisierung von PUSL1 zeigt, dass PUSL1 ein mitochondriales Matrixprotein ist und mit der inneren Membran, sowie einem Biogeneseintermediat von Mitoribosomen, assoziiert. Ferner führt die RNA-Interfenz von PUSL1 zu einer

spezifischen Reduktion der mitochondrialen *de novo*-Proteinbiosynthese. Zusammengefasst etabliert die vorliegende Dissertation MitoRibo-Tag Mäuse als ein neues Tool, um Mitoribosomen *in vivo* zu studieren, und ermöglicht zukünftige experimentelle Studien der mitochondrialen Translation unter verschiedenen physiologischen Bedingungen wie dem Altern, Diäten oder Krankheiten.

List of abbreviations

Abbreviation	Full name
°C	Celsius
µCi	Micro Curie
µg	Microgram
12S mt-rRNA	12S mitochondrial ribosomal RNA
16S mt-rRNA	16S mitochondrial ribosomal RNA
28S	28S small subunit
39S	39S large subunit
55S	55S (mitoribosome) monosome
A	Adenine
AAA	ATPase associated with diverse cellular activities
ADP	Adenosine diphosphate
A-site	Aminoacyl site
Asn	Asparagine
ATP	Adenosine triphosphate
bp	Base pair
BSA	Bovine serum albumin
bxx	Ribosomal protein conserved from bacteria
C	Cytosine in sequences or carboxyl terminus of peptides or proteins
CAA	2-Chloracetamid
CCA	Cytosine-cytosine-adenine-linker
Ckmm	Muscle creatinine kinase promoter
cm	Centimeter
CMIB	Cell mitochondrial isolation buffer
CO_2	Carbon dioxide
Complex I,	NADH:ubiquinone oxidoreductase
Complex II, SDH	Succinate dehydrogenase
Complex III	Coenzyme Q-cytochrome *c* reductase
Complex IV, COX	Cytochrome *c* oxidase
Complex V	ATP synthase
CoRR	Colocation (of gene and gene product) for redox regulation of gene expression
CP	Central protuberance
Cre	Cre recombinase
CRISPR	Clustered regularly interspaced short palindromic repeats
CRISPR/Cas9	Gene editing technique based on the prokaryotic CRISPR/Cas9 system
Cryo-EM	Cryo-electron microscopy
CxORFx	Chromosome x open reading frame x
DMEM	Dulbecco's Modified Eagle Medium
DMSO	Dimethyl sulfoxide
DNA	Deoxyribonucleic acid
E	Eluate

e.g.	*Exempli gratia*
EDTA	Ethylenediaminetetraacetic acid
EF-x_{mt}	Translation elongation factor, mitochondrial
ERAL1	Era-like 12S mitochondrial rRNA chaperone 1
FA	Formic acid
FASTKD	FAST kinase domain-containing protein
FBS	Fetal bovine serum
FL	Full-length
FLAG-tag	DYKDDDDK-Tag (FLAG© Sigma-Aldrich)
FLP	*FLP* recombination site
FT	Flow-through
g	Gravitational force
G	Guanine
GDP	Guanosine diphosphate
GLN, Q	Glutamine
GLU, E	Glutamate
GOI	Gene-of-interest
GTP	Guanosine triphosphate
GTPBP	GTP-binding protein
GuCl	Guanidinium chloride
h	Hours
H^+	Proton
H_2O	Water
HA-tag	Hemagglutinin-tag
HCl	Hydrochloric acid
HEK293T	Flp-In TREx HEK293 cells
HEPES	4-(2-Hydroxyethyl)piperazine-1-ethanesulfonic acid
HRP	Horseradish peroxidase
HSP	Heavy strand promoter
HSP60	Mitochondrial heat shock protein 60
i.e.	*Id est*
IFx_{mt}	Translation initiation factor, mitochondrial
IN	Input
KCl	Potassium chloride
KGD4	α-Ketoglutarate dehydrogenase
L	LoxP
L0R8F8, MIEF1	Smith-Magenis syndrome chromosomal region candidate gene 7 protein-like
LC-MS/MS	Liquid-chromatography mass spectrometry
Leu	Leucine
LFQ	Label-free quantification
LFQ-MS/MS	Label-free quantitative mass spectrometry experiments or proteomics
LRPPRC	Leucine-rich PPR motif-containing protein
LSP	Light strand promoter
m/z	Mass/charge ratio of peptides
mA	Milliampere
m-AAA	Mitochondrial AAA protease

MALSU1	Mitochondrial assembly of ribosomal large subunit 1
Mam33	Mitochondrial acidic matrix protein 33
Mba1	Membrane-associated mitoribosome receptor 1, yeast
MDa	Megadalton
mg	Milligram
$MgCl_2$	Magnesium di-chloride
MIB	Mitochondrial isolation buffer
mio	Million
MIP	Mitoribosome-interacting protein
Mitoribosome(s)	Mitochondrial ribosome(s)
MITRACx	Mitochondrial translation regulation assembly intermediate of cytochrome *c* oxidase
ml	Milliliter
mL62, ICT1	Mitoribosome-specific large subunit protein 62, Immature colon transcript 1
mLx	Mitochondrial-specific 39S protein
mM	Millimolar
MR	MitoRibo-Tag
MRM	Mitochondrial RNA methyltransferase
MS	Mass spectrometry
ms	Milliseconds
mS39 or PTCD3	Pentatricopeptide repeat-containing protein 1, mitochondrial
MSH	Mannitol-sucrose-HEPES buffer
Mss51	Mitochondrial splicing suppressor 51
mSx	Mitochondrial-specific 28S protein
mt	mitochondrial
mt-ACP	Mitochondrial acyl carrier protein
mt-CytB	Cytochrome *b*, mitochondrial
mtDNA	Mitochondrial DNA
MTERFx	Mitochondrial transcription termination factor x
MTFMT	Mitochondrial methionyl-tRNA formyltransferase
mt-mRNA	Mitochondrial messenger RNA
mtPAP	Mitochondrial polyadenine polymerase
mt-rRNA	Mitochondrial ribosomal RNA
mt-tRNA	Mitochondrial transfer RNA
$m^x{}_2A^x$	Adenine dimethylation
m^xC^x	Cytosine methylation
N	Amino terminus of peptides or proteins
Na_2CO_3	Disodium carbonate
NaCl	Sodium chloride
NaCl	Sodium chloride
NaOH	Sodium hydroxide
NC	Negative control
NCR / D-loop	Non-coding regulatory control region, displacement loop
nDNA	Nuclear DNA
ng	Nanogram

NGRN	Neugrin
nm	Nanometer
NOA1, MTG3	Nitric oxide-associated protein 1
NSUN4	Mitochondrial NOP2/Sun-RNA methyltransferase family member 4
O_H	Origin of replication of the heavy strand
O_L	Origin of replication of the light strand
OXA1L	Oxidase (cytochrome *c*) assembly 1-like
OXPHOS	Oxidative phosphorylation
P	Phosphate
PAGE	Polyacrylamide gel electrophoresis
PARE	Parallel analysis of RNA ends sequencing
PBS	Phosphate-buffered saline
PCMV	Cytomegalovirus promotor
PCR	Polymerase chain reaction
Pet309	PETite colonies 309
Phe	Phenylalanine
PIC	Complete EDTA-free protease inhibitor cocktail
PMSF	Phenylmethylsulfonyl fluoride
POLRMT	Mitochondrial RNA polymerase
Poly(A)	Polyadenine
PPR	Pentatricopeptide Repeat
PPTC7	PTC7 protein phosphatase homolog
PTC	Peptidyl transfer center
PTCD1	Pentatricopeptide repeat-containing protein 1, mitochondrial
PuroR	Puromycin resistance selection marker
PUS	Pseudouridine synthase
Q	Coenzyme Q
qRT-PCR	Quantitative real-time PCR
RBFA	Ribosome-binding factor A, mitochondrial
Redox	Reduction-oxidation reaction
RNA	Ribonucleic acid
RNAi	RNA interference
RNase P / MRPP	Mitochondrial RNase P subunit
RNAse Z / ELAC2	ElaC ribonuclease Z 2
RNMTL1 or MRM3	RNA methyltransferase-like 1
rpm	Rounds per minute
RPUSD4	RNA pseudouridylate synthase domain-containing protein 4
$RRF1_{mt}$	Mitochondrial ribosome recycling factor
RT	Room temperature
S	Svedberg sedimentation unit
SDS	Sodium dodecylsulfate
sec	Seconds
Ser	Serine
SILAC	Stable isotope labeling with amino acids in cell culture
siRNA	Silencing RNA

SLIRP	SRA stem-loop-interacting RNA-binding protein
T	Thymine in sequences or transgenic for genetically modified animals
TACO1	Translation activator of COX1
TBS	Tris buffer saline
TCA	Trichloroacetic acid
TCEP	Tris(2-carboxyethyl)phosphine
TE	polypeptide tunnel exit
TEFM	mitochondrial transcription elongation factor
Tet	Tetracycline
TetR	Tetracycline repressor
TFAM	Mitochondrial transcription factor A
TFB1M	Mitochondrial transcription factor B1
TFB2M	Mitochondrial transcription factor B2
TIM	Translocase of inner mitochondrial membrane
Tk	Thymidine kinase
TOM	Translocase of inner mitochondrial membrane
Tris	Tris(hydroxymethyl)aminomethane
TRNT1	CCA-adding tRNA-nucleotidyltransferase
Trp	Tryptophan
U	Uracil
UTR	Untranslated region
uxx	Universal conserved ribosomal protein
V	Voltage
Val	Valine
VDAC	Voltage-dependent anion channel
vs.	*Versus*
w	Weeks
WT	Wild type
Y	Pyrimidine
βCre	Beta-actin Cre recombinase
ψ	Pseudouridine

1. Introduction

1.1. Origin of mitochondria

The endosymbiotic theory postulates that modern mitochondria descend from free-living molecular hydrogen-producing α-proteobacteria (Sagan, 1967). Approximately 2 billion years ago, the α-proteobacteria were engulfed by a anaerobic hydrogen-dependent archaeal host cell by a still enigmatic process called phagocytosis (Martin et al., 2017; Martin & Müller, 1998; Sagan, 1967). These evolutionary events are inferred from large-scale comparative (meta-)genomic studies of present day cell and organellar genomes (Gray, 2017; Martin et al., 2017).

During evolution of the symbiotic relationship, some of the ancient α-proteobacterial genes were copied into to the developing nucleus of the host cell while other genes were lost or functionally replaced by other genes (Gray, 2017; Martin et al., 2017). These events reduced the proteobacterial DNA coding capacity from ~5000 genes to an extremely compact circular genome called mitochondrial DNA (mtDNA) harboring only 37 genes and a non-coding regulatory control region (NCR or displacement loop, D-loop) in contemporary mammalian mitochondria (Allen, 2015; Anderson et al., 1981; Bibb et al., 1981). It is still not exactly clear why a mitochondrial genome remained, especially as the length and organization of the mitochondrial genome can greatly vary between different eukaryotic lineages with some completely lacking mtDNA (Allen, 2015; Allen & Martin, 2016; Gray et al., 2008).

There are several different hypotheses explaining the retention of mtDNA in eukaryotes. The hydrophobicity theory suggests that the hydrophobic nature of mtDNA-encoded proteins prevents import to mitochondria (Allen, 2015). The second theory postulates that mtDNAs remained due to the different codon usage in mitochondria and nucleus, which would not allow proper translation of mtDNA-encoded proteins (Allen, 2015; Suzuki et al., 2011). Furthermore, it may be that remaining mtDNA genes are slowly copied and remnant intermediates towards a complete transfer to the nucleus with proceeding evolution. Lastly, a widely accepted is the “colocation (of gene and gene product) for redox regulation of gene expression” (CoRR) theory, which proposes that localization

mtDNA close to the respiratory chain or oxidative phosphorylation system (OXPHOS) allows to precisely control the stoichiometric expression of mtDNA-encoded and nuclear encoded proteins by a redox reaction-based feedback mechanism (Allen, 2015; Allen & Martin, 2016). Moreover, it is important to point out that in eukaryotes the presence of mtDNA and a mitochondrial respiratory chain always correlate (Allen, 2015; Allen & Martin, 2016).

1.2. Structure and functions of mitochondria

Mitochondria are cellular organelles surrounded by two phospholipid bilayers forming at least four mitochondrial subcompartments, the outer mitochondrial membrane, the inter-membrane space, the inner mitochondrial membrane and the matrix harboring mtDNA molecules (Westermann, 2010). The inner membrane further invaginates into tear-like structures called cristae. In yeast and cultured mammalian cells mitochondria form a dynamic network undergoing constant fusion and fission events, which seems to be linked to the bioenergetic status as dysfunction can cause complete fragmentation (figure 1.1; Rugarli & Langer, 2012; Westermann, 2010).

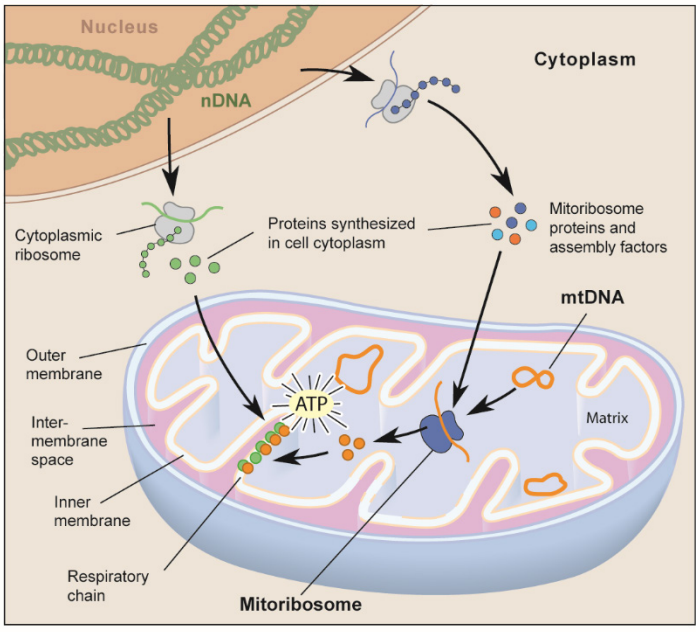

Larsson - Annu. Rev. Biochem. 2010. 79:683–706, 2010, Copyright © Annual Reviews.

Figure 1.1 – Overview of mitochondrial ultrastructure and protein biogenesis. Approximately 99 % of genes encoding mitochondrial proteins are located in the nuclear DNA (nDNA). These proteins are synthesized in the cytosol and post-translationally imported into one of the mitochondrial compartments, the outer membrane, the inter membrane space, the inner membrane and the matrix. Many of the imported proteins promote expression of mtDNA-encoded genes and form mitochondrial-specific mitoribosomes, which synthesize mtDNA-encoded proteins to build the oxidative phosphorylation (OXPHOS) system. Adapted from Larsson - Annu. Rev. Biochem. 2010.

Mitochondria are crucial regulators of cellular metabolism, encompassing enzymatic machineries to synthesize essential iron-sulfur clusters, amino acids, lipids and the OXPHOS system in the inner membrane to maintain the cellular ATP to ADP and phosphate ratio (figure 1.1; Lill & Mühlenhoff, 2008; Mitchell, 1961; Spinelli & Haigis, 2018). The most essential function of mitochondria is iron-sulfur cluster synthesis (Braymer & Lill, 2017). This assumption is supported by the fact that mitochondrial lineages, including mitosomes and hydrogenosomes, mostly retained machineries to synthesize iron-sulfur clusters (Allen, 2015; Braymer & Lill, 2017).

Due to their nuclear encoding, ~99 % of mitochondrial proteins are synthesized in the cytosol and imported into their corresponding submitochondrial compartment (figure 1.1; Wiedemann & Pfanner, 2017). Mitochondrial protein precursors harbor specific targeting signals, *e.g.* N-, C-terminal or internal signals, that direct them to mitochondrial import machineries that are distributing them to the respective mitochondrial compartments (Rugarli & Langer, 2012; Wiedemann & Pfanner, 2017).

The expression of mtDNA-encoded proteins is essential to establish the chemiosmotic proton gradient across the inner membrane by the respiratory chain in many eukaryotic species (Larsson, 2010; Mitchell, 1961; Neupert, 2016). The respiratory chain consists of four complexes NADH:ubiquinone oxidoreductase (complex I), succinate dehydrogenase (complex II), coenzyme Q-cytochrome *c* reductase (complex III), cytochrome *c* oxidase (complex IV) and two electron shuttles coenzyme Q and cytochrome *c* (figure 1.2; Larsson, 2010).

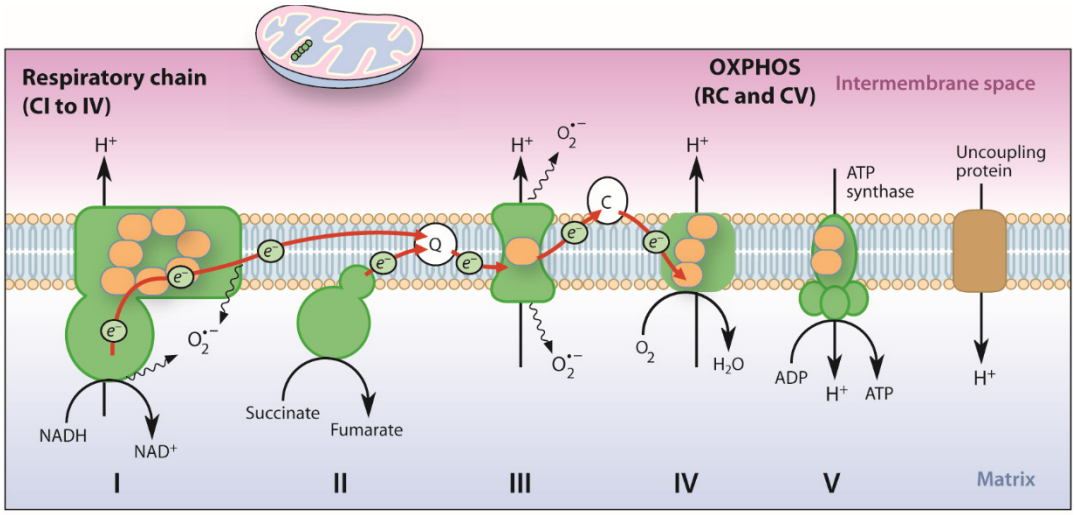

Larsson - Annu. Rev. Biochem. 2010. 79:683–706, 2010, Copyright © Annual Reviews.

Figure 1.2 – The respiratory chain and oxidative phosphorylation system in the inner mitochondrial membrane. The OXPHOS can be functionally divided into two functional entities, the respiratory chain (complex I to IV), which pumps protons (H^+) from the matrix into the inter-membrane space, transferring electrons (e^-) to coenzyme Q (Q) and cytochrome *c* (C), and the OXPHOS system including the ATP synthase (complex V) using the chemiosmotic gradient to synthesize ATP from ADP and phosphate. Nuclear-encoded subunits (green), mtDNA-encoded proteins (orange) and the uncoupling protein (brown) are indicated. Adapted from Larsson - Annu. Rev. Biochem. 2010. 79:683–706, 2010, Copyright © Annual Reviews, Copyright clearance license ID: 4507750910457.

All OXPHOS complexes catalyze series of redox reactions ultimately reducing molecular oxygen to water at complex IV (figure 1.2; Larsson, 2010). The redox reactions and the electron transfer enable the translocation of protons and thereby generate a chemiosmotic gradient between the matrix and the inter membrane space (figure 1.2; Larsson, 2010; Mitchell, 1961). The ATP synthase (complex V) uses the proton gradient to produce ATP from ADP and phosphate (Mitchell, 1961).

Interestingly, three of the four respiratory complexes (complex I, III and IV) and complex V are of dual genetic origin, with majority of components being nuclear encoded, whereas some essential hydrophobic core subunits are encoded by mtDNA (Larsson, 2010; Wiedemann & Pfanner, 2017). Hence, synthesis and assembly of mtDNA-encoded and nuclear-encoded subunits has to occur in a coordinated manner, a phenomenon that is still poorly understood (Couvillion et al., 2016; Signes & Fernandez-Vizarra, 2018).

1.2.1. The mammalian mitochondrial genome

mtDNA is a double stranded circular ~16.6 kb molecule (Anderson et al., 1981; Bibb et al., 1981; Nass & Nass, 1963). In addition to the 13 proteins, which are encoded by 11 messenger RNAs (mt-mRNAs), mtDNA encodes for two mitochondrial ribosomal RNAs (mt-rRNAs) and 22 mitochondrial tRNAs (mt-tRNAs; figure 1.3; Anderson et al., 1981; Bibb et al., 1981; Gustafsson et al., 2016).

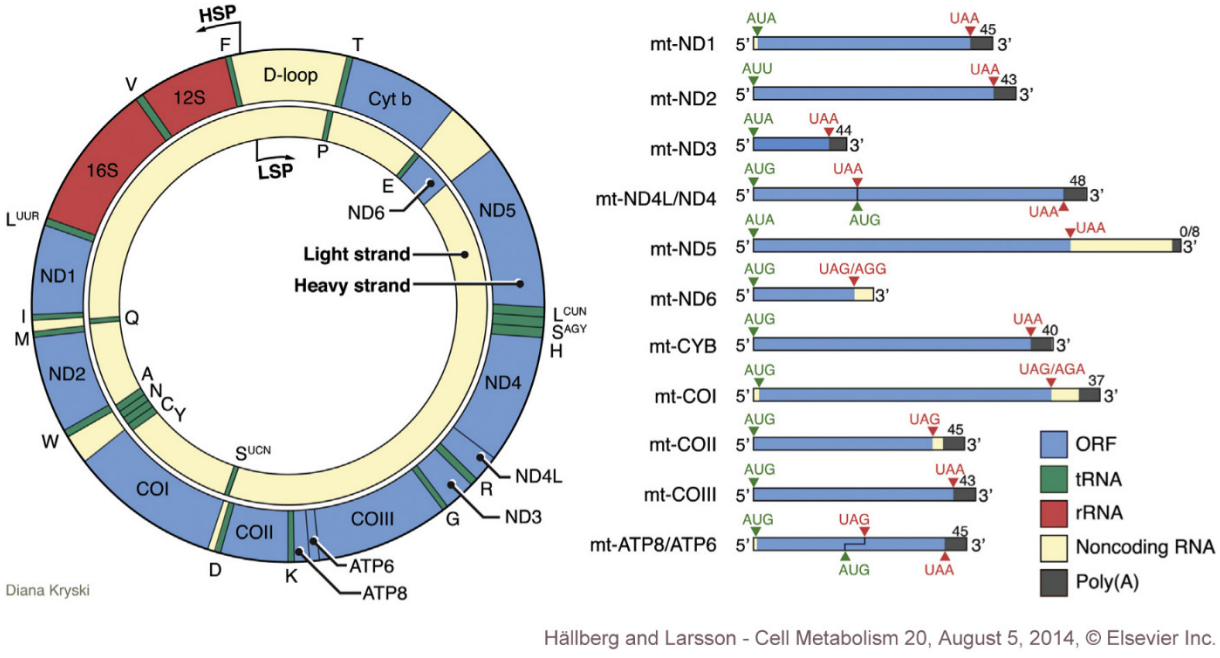

Figure 1.3 – Organization of mammalian mitochondrial DNA and architecture of encoded messenger RNAs. Two promoters for transcription, denoted HSP and LSP, are located in the non-coding regulatory control region (D-loop) to control the expression of mtDNA-encoded genes. The expression of mitochondrial ribosomal RNAs, 12S and 16S rRNA (red), is regulated by the HSP. The left panel highlights the structure of the 11 mtDNA-encoded messenger RNAs, encoding 13 OXPHOS proteins, with start codons (green letters), stop codons (red letters) and the polyadenine tail (poly(A), grey). Adapted from Hällberg and Larsson, Cell Metabolism 2014, Copyright © Elsevier Inc., Copyright clearance license ID: 4507760690000.

The previously mentioned NCR or D-loop is the only large non-coding mtDNA region harboring several functional sequences, the promoters historically denoted the heavy and light strand promoter (HSP and LSP), and the origin of replication of the heavy strand (O_H; figure 1.3; Gustafsson et al., 2016; Larsson, 2010). The origin of light strand replication (O_L) is located in a short non-coding region located in a cluster of mt-tRNA genes.

Interestingly, sequencing of human and mouse mtDNAs revealed that mt-rRNAs and mt-mRNAs are often interspersed by one or more mt-tRNA genes (figure 1.3; Gustafsson et al., 2016; Ojala et al., 1981). These tRNA punctuations are thought to be specifically recognized by mitochondrial RNase P (MRPP1 to 3) and RNAse Z (ElaC ribonuclease Z 2, ELAC2) hierarchically cleaving the 5' end and 3' ends (Lee et al., 2018; Ojala et al., 1981; Rackham et al., 2016).

1.3. Maintenance and expression of mitochondrial DNA

Each cell harbors hundreds to thousand mtDNA molecules, which can be expressed and maintained individually (Gustafsson et al., 2016; Kukat et al., 2011). mtDNA is fully coated by the mitochondrial transcription factor A (TFAM) into DNA-protein structures called nucleoids, which have an average diameter ~100 nm (Kukat et al., 2011; Larsson et al., 1998). Interestingly, the abundance or copy number of mtDNA is mostly linked to the levels of TFAM (Larsson et al., 1998).

mtDNA is exclusively maternally inherited and replicated in a cell cycle-independent manner (Larsson, 2010). A dedicated machinery, called the replisome, constituted of mtDNA polymerase γ, the mtDNA helicase TWINKLE, and the mitochondrial single-stranded binding protein (SSB), catalyzes mtDNA replication (Larsson, 2010). Interestingly, the mitochondrial RNA polymerase (POLRMT) is necessary for replication, namely for the primer synthesis (Fusté et al., 2010; Kühl et al., 2014, 2016; Larsson, 2010). It was shown that replication errors introduced by polymerase γ are the main source of mtDNA mutations (Larsson, 2010; Trifunovic et al., 2004; Zheng et al., 2006). Due to the multiple copies of mtDNA in each cell, mutations in can be present in all

(homoplasmy) or only in some molecules (heteroplasmy). Hence, segregation events during oogenesis can increase the level of pathogenic mtDNA mutations in mitochondria of oocytes and cause mitochondrial dysfunction during embryo development or disease in newborns and adults (Holt et al., 1988; Larsson, 2010; Wallace et al., 1988).

1.3.1. Transcription of mitochondrial DNA

Transcription from HSP or LSP synthesizes two almost full mtDNA-length polycistronic transcripts containing all mt-RNA species. The core machinery transcribing mtDNA consists of three proteins, TFAM, POLRMT and the mitochondrial transcription factor B2 (TFB2M; Gustafsson et al., 2016). Transcription initiation is likely promoted by binding of TFAM in proximity to HSP and LSP (Gustafsson et al., 2016). POLRMT is recruited to these sites and interacts with the mtDNA resulting in formation of ternary complex, which in turn induces conformational changes in the N-terminal domain of POLRMT (Gustafsson et al., 2016; Hillen et al., 2018; Posse et al., 2014). Subsequently, TFB2M joins to complete the mature initiation complex inducing further conformational changes to tighten the binding of POLRMT to the mtDNA (Gustafsson et al., 2016; Posse & Gustafsson, 2017). Next, TFAM and TFB2M dissociate from the complex, leading to the recruitment of the mitochondrial transcription elongation factor (TEFM), which promotes interaction of POLRMT with the DNA:RNA hybrid at the promoter to enable elongation and synthesis of the polycistronic transcripts (Gustafsson et al., 2016; Posse et al., 2015).

1.3.2. RNA processing in mammalian mitochondria

The polycistronic transcripts emerging from the mtDNA nucleoids are simultaneously, *i.e.* co-transcriptionally, processed by RNAse P and ELAC2 (Hällberg & Larsson, 2014; Lee et al., 2018). Initially, the 5’ ends and mt-tRNA boundaries are recognized by RNase P, a trimeric complex consisting of three subunits, MRPP1 a methyltransferase that modifies adenines or guanines of tRNAs, MRPP2 a short-chain dehydrogenase thought to contribute to the enzyme activity, and MRPP3 a pentatricopeptide repeat (PPR) RNA-

binding protein (Holzmann et al., 2008; Li et al., 2015; Reinhard et al., 2015; Vilardo et al., 2012a, 2012b). MRPP1 and MRPP2 bind to pre-5' ends of mt-tRNA substrates and recruit MRPP3 by an induced-fit mechanism to catalyze the endonucleolytic cleavage (figure 1.4; Reinhard et al., 2015; Reinhard et al., 2017). Interestingly, conditional *Mrpp3* knock-out mice were not only characterized by impaired 5' end processing but also diminished 3' end cleavage (Rackham et al., 2016). In contrast, 5' end tRNA processing could still occur in murine mitochondria in the absence of *Elac2*, (figure 1.4; Haack et al., 2013; Siira et al., 2018). These results indicate that 5' end processing proceeds 3' end cleavage *in vivo* (Rackham et al., 2016). *In vitro* experiments support this model, because it was shown that the 5' end-processed mt-tRNA transcripts remain bound to a MRPP1-2-only complex presenting it to ELAC2 and thereby enhancing the 3' end cleavage (Reinhard et al., 2017). The virtually mature mt-tRNAs remain bound to MRPP1-2 and are subsequently equipped with a trinucleotide cytosine-cytosine-adenine-linker (CCA) at the 3' end, catalyzed by the mitochondrial CCA-adding tRNA-nucleotidyltransferase (TRNT1; figure 1.4; Lee et al., 2018; Reinhard et al., 2017; Sasarman et al., 2015). The addition of the CCA-enables the loading of mt-RNAs with amino acids (Reichert et al., 2001; Rossmanith et al., 1995; Wende et al., 2015).

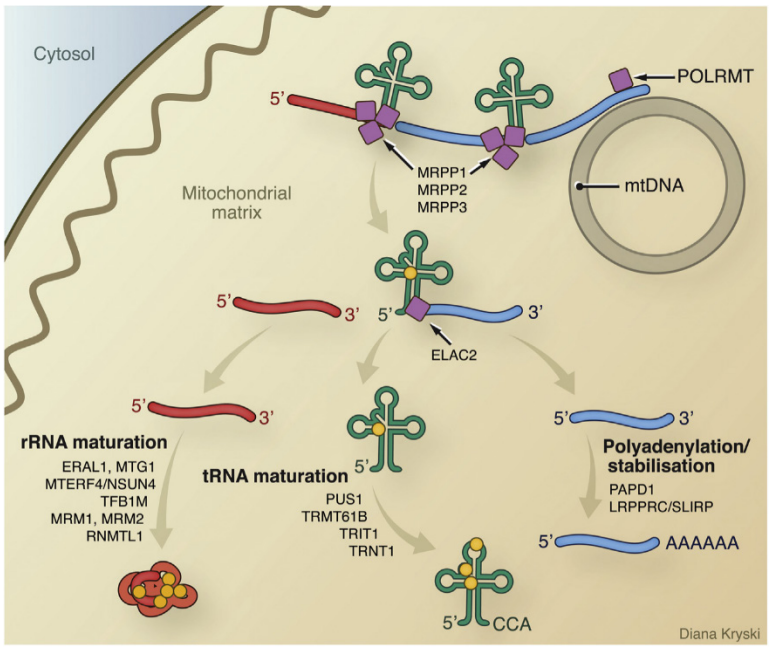

Hällberg and Larsson - Cell Metabolism 20, August 5, 2014, © Elsevier Inc.

Figure 1.4 – Transcription and co-transcriptional RNA processing occur in proximity to the mitochondrial DNA. Mitochondrial transcription driven by the mitochondrial RNA polymerase POLRMT produces almost full mtDNA-length polycistronic transcripts, containing rRNAs (red), tRNAs (green) and mRNAs (blue), which are cleaved in a hierarchical manner by the RNA processing complexes RNase P (MRPP1 to 3) at the 5' end and ELAC2 (RNase Z) at the 3' end. The mitochondrial rRNAs and tRNAs are matured by base modifications or sequence additions, *e.g.* CAA or polyadenylation, and stabilized by the LRPPRC-SLIRP complex. Adapted from Hällberg and Larsson, Cell Metabolism 2014, Copyright © Elsevier Inc., Copyright clearance license ID: 4507760690000.

Interestingly, the 5' ends of mt-*Co3* (complex IV subunit 3) and mt-*CytB* (cytochrome b of complex III) transcripts remained unchanged in the absence of MRPP3, indicating that another enzyme, likely to be PTCD2, is involved in their cleavage (Xu et al., 2008).

It was recently shown that the processing of tRNA-free junctions of the mt-*Nd5-CytB* and mt-*Atp8/6-Co3* transcripts is impaired in the absence of the mitochondrial FAST kinase domain-containing protein 5 (FASTKD5; Antonicka & Shoubridge, 2015). Recently, five FASTKD proteins were described in human mitochondria (Jourdain et al., 2015, 2017). Interestingly, these FASTKD proteins seem to fulfill various functions as they were found to promote stability of mt-*Nd6* (complex I subunit ND6), processing and modification of

mt-*Nd5-CytB* and the 16S mt-rRNA, as well as specific translational regulation of mt-*Co1* mRNA (Antonicka et al., 2017; Jourdain et al., 2017).

In addition to the concerted cleavage of mt-RNAs, all RNA species are further modified, including (di-)methylations, de- and polyadenylations, and pseudouridylations (ψ). Modifications are especially important for stabilizing mt-tRNAs as they often lack intramolecular loop interactions (Suzuki et al., 2011; Van Haute et al., 2015). Moreover, mitochondrial specific tRNA modifications including 5-formylcytidine and 5-taurinomethyl-(2-thio)uridine are described (Suzuki et al., 2011; Van Haute et al., 2015). Additionally, mt-mRNAs lack the canonical 7-methylguanosine cap at the 5' end (Grohmann et al., 1978). Hence, other mechanisms evolved to stabilize mitochondrial RNAs, which seems to be predominantly carried out by the Leucine-rich PPR motif-containing protein and SRA stem-loop-interacting RNA-binding protein complex (LRPPRC-SLIRP complex; figure 1.4; Baughman et al., 2009; Lagouge et al., 2015; Ruzzenente et al., 2012). LRPPRC belongs to the family of PPR domain-contain proteins and was initially identified in human patients suffering from a French-Canadian variant of the Leigh syndrome (Mootha et al., 2003). The stability of LRPPRC depends on the presence of SLIRP because LRPPRC steady-state levels are significantly reduced in *Slirp* knock-out mice (Lagouge et al., 2015).

Moreover, almost all mt-mRNAs, except mt-*Nd6*, are polyadenylated with ten – 55 adenines catalyzed by the mitochondrial poly-adenine polymerase (mtPAP; Hällberg & Larsson, 2014; Nagaike et al., 2005; Tomecki et al., 2004). Interestingly, LRPPRC seems to regulate the length of the polyadenine tails (Ruzzenente et al., 2012). A recent transcriptome analysis of *Lrpprc* knock-out mouse mitochondria suggested a chaperone-like function of the LRPPRC-SLIRP complex preventing formation of secondary structures within mt-mRNAs putatively enabling mitoribosome binding to exposed start codons (Siira et al., 2017). This is in agreement with an earlier *in vivo* study of *Lrpprc* knock-out mice, which show a deregulated mitochondrial translation, *i.e.* mtND1, mtND2 and mtND5 are synthesized more, whereas mtND3, mtND6, mtCOX1 and mtATP6 (complex V subunit 6) are produced less (Ruzzenente et al., 2012).

1.4. Unique features of mitochondrial translation

Mitochondrial translation is a multifaceted process and depends on post-transcriptional processing of mt-RNAs as well as on peptide bond synthesis catalyzed by mitochondrial-specific ribosomes (mitoribosomes) to synthesize mtDNA-encoded OXPHOS proteins. Due to the significant size reduction of the mtDNA the mitochondrial decoding system seems to be adapted. Human mtDNA encodes for only one methionine mt-tRNA, which can be formylated by the mitochondrial methionyl-tRNA formyltransferase (MTFMT) to incorporate formyl-methionine during initiation at AUA, AUG, AUU or AUC codons, and non-formylated methionine during elongation, whereas AUU and AUC additionally encode for isoleucine during elongation (figure 1.5; Hällberg & Larsson, 2014; Tucker et al., 2011). Furthermore, the mitochondrial decoding system deviates from universal genetic code, because UGA encodes tryptophan, and AGG, AGA, UAA and UAG are used as stop codons to induce translation termination (figure 1.5; Ott et al., 2016; Suzuki et al., 2011).

Codon	Amino acid (anticodon)	Codon	Amino acid (anticodon)	Codon	Amino acid (anticodon)	Codon	Amino acid (anticodon)
UUU	Phe	UCU		UAU	Tyr	UGU	Cys
UUC	(GAA)	UCC	Ser	UAC	(QUA)	UGC	(GCA)
UUA	Leu	UCA	(UGA)	UAA	stop	UGA	Trp
UUG	(τm^5UAA)	UCG		UAG		UGG	(τm^5UCA)
CUU		CCU		CAU	His	CGU	
CUC	Leu	CCC	Pro	CAC	(QUG)	CGC	Arg
CUA	(UAG)	CCA	(UGG)	CAA	Gln	CGA	(UCG)
CUG		CCG		CAG	($\tau m^5 s^2$UUG)	CGG	
AUU	Ile	ACU		AAU	Asn	AGU	Ser
AUC	(GAU)	ACC	Thr	AAC	(QUU)	AGC	(GCU)
AUA	Met	ACA	(UGU)	AAA	Lys	AGA	stop
AUG	(f^5CAU)	ACG		AAG	($\tau m^5 s^2$UUU)	AGG	
GUU		GCU		GAU	Asp	GGU	
GUC	Val	GCC	Ala	GAC	(QUC)	GGC	Gly
GUA	(UAC)	GCA	(UGC)	GAA	Glu	GGA	(UCC)
GUG		GCG		GAG	($\tau m^5 s^2$UUC)	GGG	

[a]Nonuniversal genetic codes are denoted in bold: AUA for Met, UGA for Trp, and AGA/G for stop. The anticodon sequence of each tRNA is shown in parentheses.

Suzuki et al., Annu. Rev. Genet. 2011. 45:299–329, Copyright © Annual Reviews

Figure 1.5. – Overview of the unique mammalian mitochondrial genetic code. Adapted from Suzuki et al. - Annu. Rev. Genet. 2011. 45:299–329, Copyright © Annual Reviews, Copyright clearance license ID: 4507770884764.

Interestingly, mammalian mitochondria do not harbor a glutamine (GLN, Q) aminoacyl-tRNA synthetase, the enzyme charging the tRNA with the corresponding amino acid, but instead the glutamate (GLU, E) tRNA synthetase was found to mis-aminoacylate the glutamine-mt-tRNA to form a glutamine-charged glutamate-mt-tRNA (Nagao et al., 2009). Furthermore, mtDNA harbors two tRNA genes encoding for leucine, 5-taurinomethyl-(2-thio)-UAA and UAG, and serine, UGA and GUC respectively (figure 1.5; Suzuki et al., 2011).

1.5. RNA modifications and mitoribosome assembly

The assembly of mitoribosomes is a highly complex multilayered process, which includes transcription as well as co- and post-transcriptional processing of mt-rRNAs and their hierarchical association with mitoribosome proteins (figure 1.6).

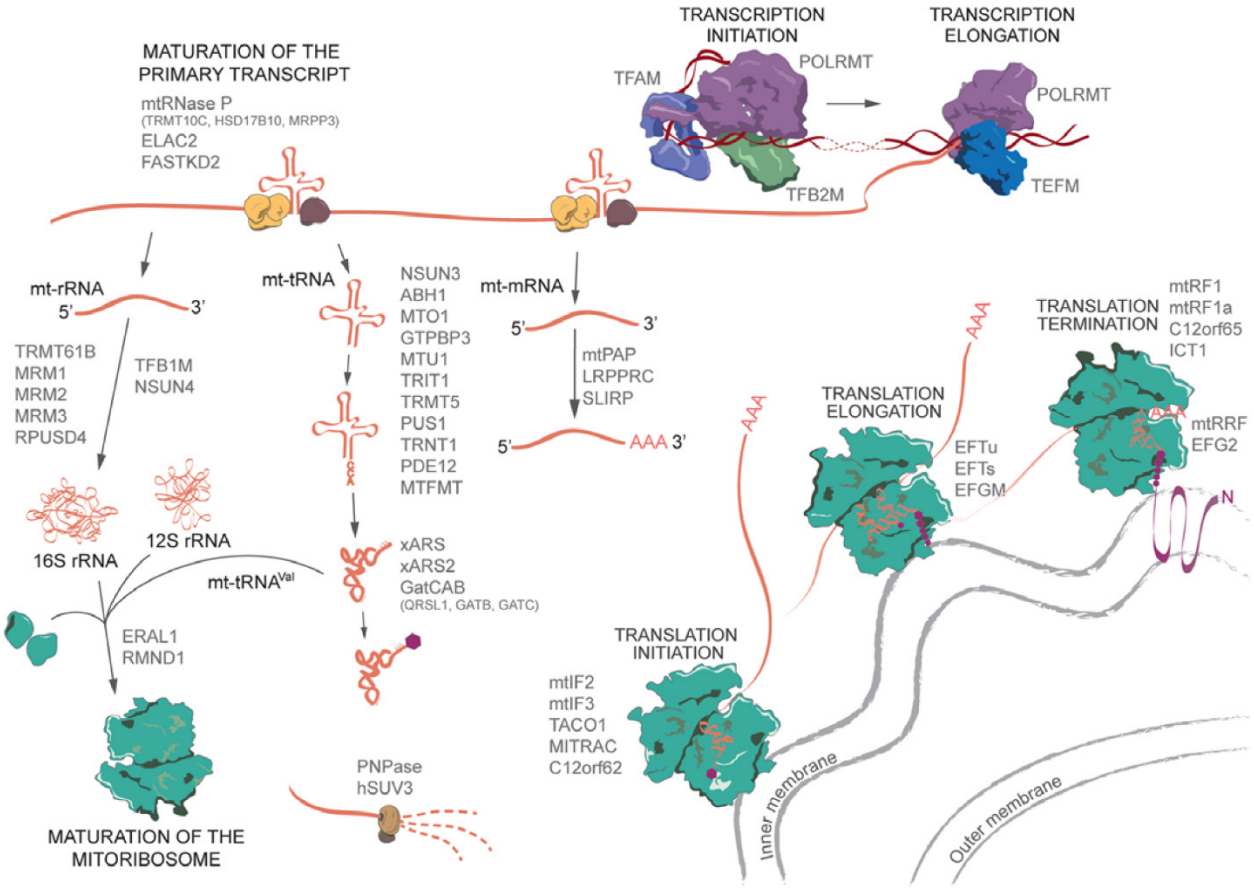

Figure 1.6 – Overview of proteins involved in RNA processing, mitoribosome assembly and translation in mammalian mitochondria. For details, please refer to chapters 1.5., 1.5.1., 1.5.2. and 1.5.3. Adapted from D'Souza A. R., Minczuk M., Mitochondrial transcription and translation: overview. Essays Biochem. 2018 Jul 20;62(3):309-320. doi: 10.1042/EBC20170102. Print 2018 Jul 20. Licensed by Creative Commons Attribution 4.0 International (CC BY 4.0, https://creativecommons.org/licenses/by/4.0/).

Mammalian mitochondrial ribosomes (mitoribosomes) are ~2.7 MDa complexes, consisting of three mitochondrial RNAs, two mt-rRNAs and an integrated mt-tRNA, and 82 nuclear-encoded proteins (Hällberg & Larsson, 2014). Mature 55S mitoribosomes are formed by two protein-RNA complexes, denoted the 28S small subunit (28S), composed of 30 proteins, and the 39S large subunit consisting of 52 proteins, named after their buoyant density in sucrose gradients (Amunts et al., 2015; Greber et al., 2015; O'Brien & Kalf, 1967a, 1967b). Mitoribosome-specific ribosomal proteins, not found in bacterial or cytoplasmic ribosomes, are denoted with mSx for small subunit proteins and mLx for large subunit proteins respectively, whereas x represents an integer (Ban et al., 2014). Moreover, bxx and uxx indicate homologs found in bacterial ribosomes or universally conserved ribosome proteins (Ban et al., 2014).

Ribosome assembly is mostly studied in bacteria and occurs through sequential rRNA conformational changes, induced by base modification, binding of ribosomal proteins or assembly factors (Davis & Williamson, 2017). Mitoribosome assembly is thought to be an order of magnitude more complex than canonical ribosome assembly because mitoribosomes have acquired additional protein constituents. It should be pointed out that assembly of cytosolic ribosomes assembly is estimated to require over 200 non-ribosomal proteins (Brown et al., 2017; Kressler et al., 2010).

Recent super-resolution microscopy and proteomic labeling experiments gave insights into the kinetics of mitoribosome assembly, which is initiated in proximity to the mtDNA in the mitochondrial nucleoid and appears to take two to three hours in cultured cells (Bogenhagen et al., 2014; Bogenhagen et al., 2018). Furthermore, it seems that the 28S subunit is first assembled and released from the vicinity of the nucleoid, which is in agreement with the position of the 12S mt-rRNA gene in mtDNA (figure 1.4; Bogenhagen et al., 2014; Bogenhagen et al., 2018). The sequential association of the 28S and 39S proteins can be divided into early, intermediate and late steps (Bogenhagen et al., 2018; Hällberg & Larsson, 2014).

1.5.1. Assembly and composition of the large 39S mitoribosome subunit

As previously mentioned, the assembly of ribosomes is mainly driven by modification and conformational changes of rRNA. The 39S subunit of the mitoribosome is composed of two RNA molecules and 52 proteins (figure 1.7; Amunts et al., 2015; Greber et al., 2015). In 1974 and 1978 the Dubin laboratory published two pioneering studies about the modifications of the mitochondrial large subunit rRNA, revealing the presence of three ribose methylations at guanine 1145 (1160), uridine 1369 (1388), and guanine 1370 (1389) in human and mouse ribosomes, respectively (Dubin & Taylor, 1978; Dubin, 1974).

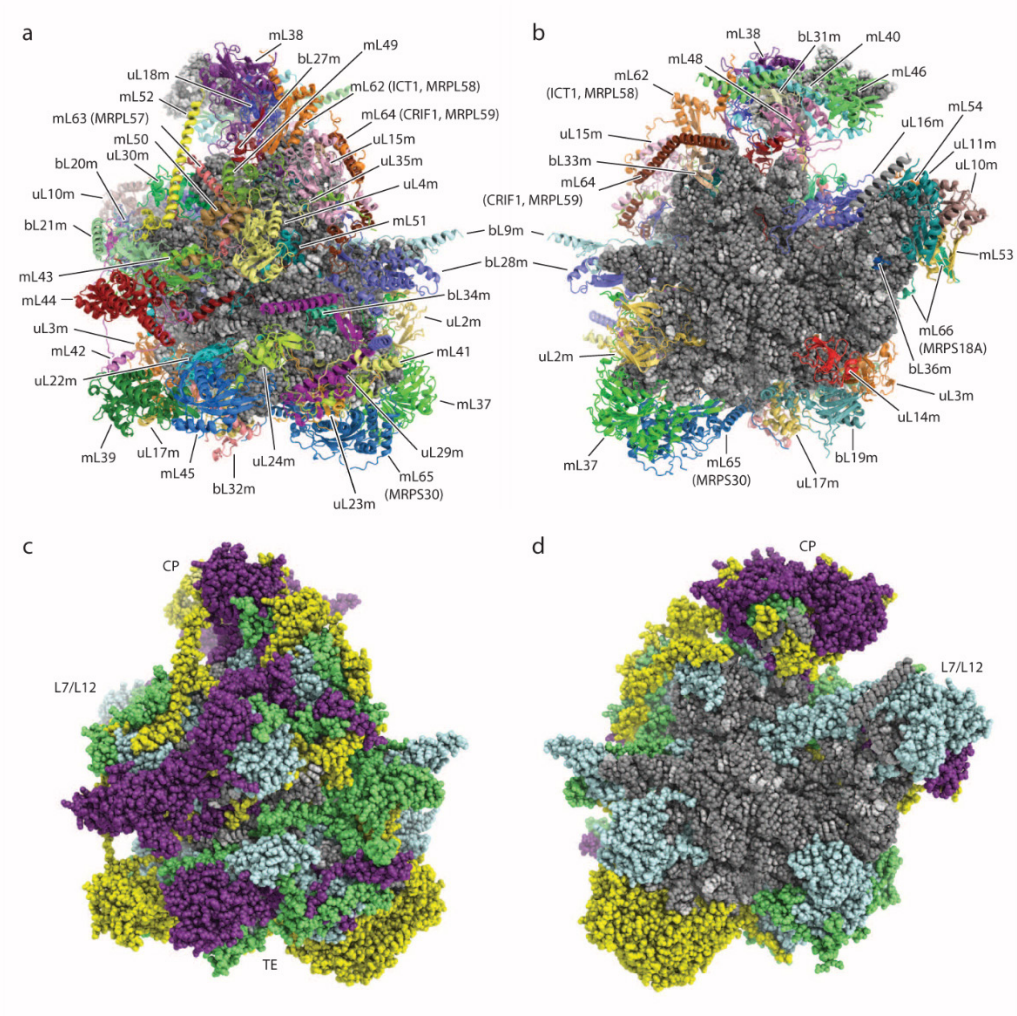

Greber et al., 284, Nature, Vol. 515, 13 November 2014,

Figure 1.7 – Cryo-EM structure of the mammalian 39S large mitoribosome subunit. **(a and b)** Organization of 39S subunit proteins binding the 16S mt-rRNA and the central protuberance (CP)-mt-tRNA in grey (**a** – solvent-exposed side, **b** – subunit interface). **(c and d)** Structure of the 39S subunit in the same orientation as in **a** and **b**, but colored according to the conserved and non-conserved elements. The following color code and abbreviations are used: 16S mt-rRNA and unassigned protein structures (grey), proteins conserved in bacteria (cyan), mitoribosome protein extensions (lime green), mitoribosome proteins found in yeast and mammals (purple), CP-mt-tRNA and mitoribosome proteins not present in yeast (yellow), L7/L12 stalk base (L7/L12) and polypeptide tunnel exit (TE). Adapted from Greber et al., 2014, Nature 284, Copyright © Macmillan Publishers Limited, Copyright clearance license ID: 4510130723037.

The mt-rRNA methyltransferases MRM1, MRM2 and MRM3 likely methylate the nascent 16S mt-rRNA co-transcriptionally as the enzymes are found in proximity to the mitochondrial nucleoid (Bogenhagen et al., 2014; Lee & Bogenhagen, 2014; Lee et al., 2013; Rorbach et al., 2014). Interestingly, knock-down of MRM2 or MRM3 in cultured cells caused severe ribosome assembly defects highlighting the importance of 16S mt-rRNA methylation for 39S assembly (Rorbach et al., 2014).

A pseudouridylation (ψ), which is an isomer of uridine connected to the ribose with a carbon bond instead of a nitrogen bond, was identified as the fourth 16S mt-rRNA modification (Ofengand & Bakin, 1997). Recently, the RNA pseudouridylate synthase domain-containing protein 4 (RPUSD4) was found to isomerize the uridine 1397 (human) and 1416 (mouse), respectively (figure 1.6; Antonicka et al., 2017; Perks et al., 2018; Zaganelli et al., 2017). Interestingly, the conditional knock-out of the RPUSD4-associated factor PTCD1 (Pentatricopeptide Repeat-containing protein 1, mitochondrial) in the mouse prevented the 16S mt-rRNA pseudouridylation, suggesting that RPUSD4 needs to be actively recruited to the 16S mt-rRNA (figure 1.6; Perks et al., 2018). In addition to modification of RNA bases, also the binding and conformational changes of proteins has a great impact on ribosome assembly (Davis & Williamson, 2017). RPUSD4 was also found to form a transient complex with a conserved GTP-binding protein GTPBP10 (Arroyo et al., 2016). GTPBP10 belongs to the Obg superfamily, structurally characterized by three characteristic glycine-rich regions inserted into a small eight-stranded beta-sandwich (Lavdovskaia et al., 2018; Maiti et al., 2018). It was recently shown that GTPBP10 binds the 16S mt-rRNA (Lavdovskaia et al., 2018; Maiti et al., 2018). Removal of *GTPBP10* from cultured human cells did surprisingly not affect 16S mt-rRNA levels, but strongly impaired mitoribosome assembly, whereas the underlying mechanism remains elusive (Lavdovskaia et al., 2018; Maiti et al., 2018).

A second member of the GTP-binding protein family called GTPBP7 (MTG1) was found to be involved in 39S biogenesis (Kim & Barrientos, 2018). GTPBP7 binds the 16S rRNA and seems to specifically interact with the 39S constituent bL19m and the 28S PPR-protein mS27 (figure 1.8; Kim & Barrientos, 2018). Based on the first structure of an mitoribosome intermediate, the authors propose a model in which GTPBP7 acts late during assembly to promote subunit association (figure 1.8; Brown et al., 2017; Kim &

Barrientos, 2018). Initially, GTP-bound GTPBP7 seems to bind the 39S subunit via uL19m, then GTP is hydrolyzed to remodel uL19m recruiting bL35m and bL36m to the premature 39S subunit (figure 1.8; Kim & Barrientos, 2018). Subsequently, mS27 of a mature 28S subunit might bind to GTPBP7 and promote its dissociation by regenerating GDP to GTP, thereby allowing association of 28S and 39S subunits by formation of an intersubunit bridge (figure 1.8; Kim & Barrientos, 2018).

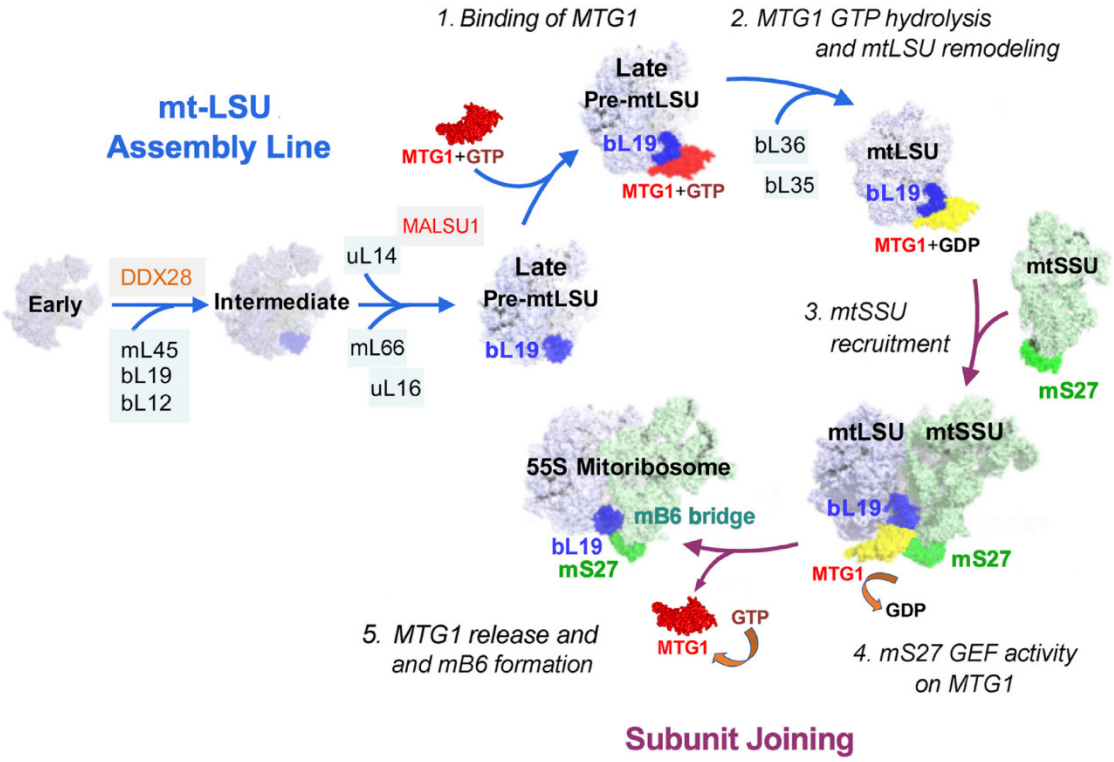

Figure 1.8 – Putative model of late steps in 39S biogenesis and formation of 55S monosomes mediated by GTPBP7 (MTG1) in mitochondria. For details, please refer to chapter 1.5.1. Adapted from Kim and Barrientos, Nucleic Acids Research, Vol. 46, Date 2018-07-31, Copyright © 2018, Oxford University Press, Copyright clearance license ID: 4510150341008.

Furthermore, the mentioned mitoribosome intermediate structure from human mitochondria revealed the presence of three additional assembly factors, mitochondrial

assembly of ribosomal large subunit 1 (MALSU1), mitochondrial acyl carrier protein (mt-ACP) and mitochondrial elongation factor 1 (MIEF1 or HsL0R8F8) bound on a nearly complete 39S subunit lacking only bL36m (Brown et al., 2017). The MALSU1-mt-ACP-HsL0R8F8 module seems to fulfil a ribosome anti-association activity guarding a quality control checkpoint to ensure that only mature 39S subunits assemble into 55S monosomes (Brown et al., 2017). Three earlier studies indicated that depletion of MALSU1 causes accumulation of 39S biogenesis intermediates (Fung et al., 2013; Rorbach et la., 2012; Wanschers et al., 2012). Surprisingly, two copies of mt-ACP are structurally integrated into complex I and also involved in fatty-acid and iron-sulfur cluster synthesis, indicating that these processes are interconnected with mitochondrial translation (Brown et al., 2017; Van Vranken et al., 2016; Zhu et al., Hirst, 2016).

Two members of the transcription termination factor family (MTERF) may also carry out a remodeling or quality control function during mitoribosome assembly, although they were initially identified as homologs to the mitochondrial transcription termination factor 1 (Hällberg & Larsson, 2014; Kruse et al., 1989). Loss of *Mterf3* in the mouse heart was found to cause mitochondrial dysfunction and to enhance transcription (Park et al., 2007). A subsequent study found that MTERF3 binds to the 16S mt-rRNA and is required for biogenesis of the 39S large subunit (Wredenberg et al., 2013). Upon loss of *Mterf3*, 16S mt-rRNA levels are severely reduced leading to destabilization of the 39S subunit, however the exact mechanism of this process remains enigmatic (Hällberg & Larsson, 2014; Wredenberg et al., 2013).

The second MTERF member involved in mitoribosome biogenesis is MTERF4, a factor that promotes association of 28S and 39S subunits (Cámara et al., 2011). MTERF4 forms a stoichiometric complex with the mitochondrial NOP2/Sun-RNA methyltransferase family member 4 (NSUN4), a homolog of bacterial m^5-Cytosine-methytransfereases (Cámara et al., 2011; Spahr et al., 2012). Removal of *Mterf4* from murine heart causes subunit dissociation accompanied by increased levels of 28S and 39S, which cannot, for a yet unknown reason, bind to each other (Cámara et al., 2011).

1.5.2. Assembly and composition of the small 28S mitoribosome subunit

The 28S small subunit is harbors the decoding center and is composed of the 12S mt-rRNA and 30 proteins (figure 1.9; Amunts et al., 2015; Greber et al., 2015). A second study from Baer & Dubin (1981) revealed the spectrum of 12S mt-rRNA modifications, which include two adenine dimethylations ($m^6{}_2A^{937}$ and $m^6{}_2A^{938}$), one uracil methylation (m^5U^{425}), and two cytosine methylations (m^4C^{840} and m^5C^{841} or m^5C^{842}) (Hällberg & Larsson, 2014).

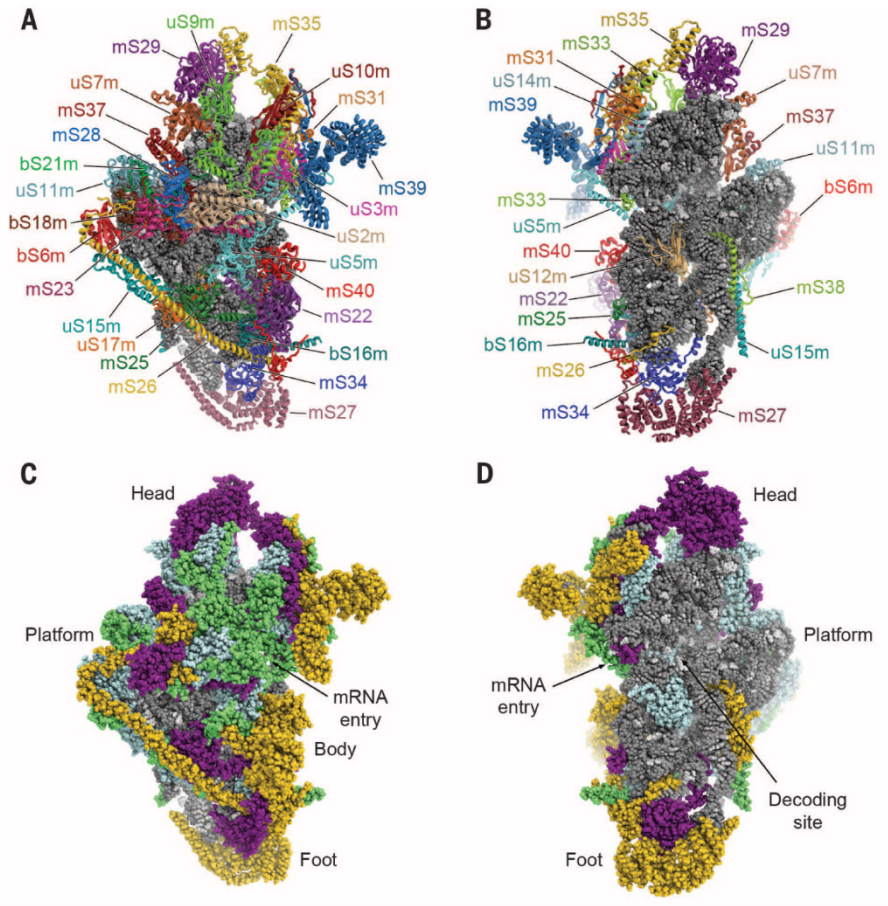

Figure 1.9 – Cryo-EM structure of the mammalian 28S small mitoribosome subunit. **(A and B)** Architecture of the 28S subunit folding binding the 12S mt-rRNA (grey; **A** – solvent-exposed side, **B** – subunit interface). **(C and D)** Structure of the 28S subunit in

the same orientation as in A and B, colored according to conserved and non-conserved elements. The color code is similar to figure 1.7 with 12S mt-rRNA and unassigned protein segments (grey), proteins conserved in bacteria (cyan), mitoribosome protein extensions (lime green), mitoribosome proteins found in yeast and mammals (purple), mitoribosome proteins not present in yeast (yellow). Adapted from Greber et al., Science, Apr 17, 2015, Copyright © The American Association for the Advancement of Science, Copyright clearance license ID: 4510160349484.

NSUN4, the interaction partner of MTERF4, was found to catalyze the m^5C^{842} methylation in mouse mitochondria (Metodiev et al., 2014). Upon loss of NSUN4, the steady-state levels of the 12S mt-rRNA are significantly increased but lacking the m^5C^{842} modification, indicating that a 28S maturation defect is causing 55S monosome loss (Metodiev et al., 2014). The aberrant phenotypes in *Nsun4* and *Mterf4* knock-out mice indicate that a free pool of NSUN4 methylates C^{842} of the 12S mt-rRNA to mark mature 28S subunits, whereas the MTERF4-NSUN4 complex actively promotes association of 39S and the mature 28S subunits to form 55S monosomes (Cámara et al., 2011; Hällberg & Larsson, 2014; Metodiev et al., 2014).

The 3' end adenine dimethylations at bases 936 and 937 (human) or 937 and 938 (mouse) are highly conserved in all domains of life (Hällberg & Larsson, 2014; Shutt & Gray, 2006). The latter adenines in 12S mt-rRNA are dimethylated by the mitochondrial transcription factor B1 (TFB1M), which is a methyltransferase despite its name (Metodiev et al., 2009). Conditional removal of *Tfb1m* in mice severely reduces the 12S mt-rRNA steady-state level consequently causing a 28S subunit assembly defect and loss of 55S monosomes (Metodiev et al., 2009). In the absence of NSUN4, A^{937} and A^{938} remain dimethylated indicating that TFB1M modifies the 12S mt-rRNA early during 28S biogenesis and before NSUN4 (Metodiev et al., 2009).

Two additional factors involved in 12S mt-rRNA maturation are the mitochondrial Era-like 12S rRNA chaperone 1 (ERAL1) and the mitochondrial ribosome-binding factor A (RBFA) (Dennerlein et al., 2010; Rozanska et al., 2017; Uchiumi et al., 2010). Similar to TFB1M, ERAL1 and RBFA bind the 12S mt-rRNA, whereas it was shown that the binding of RBFA improves the dimethylation efficiency of the 12S mt-rRNA by TFB1M (Rozanska et al., 2017). The role of ERAL1 is less clear, but the protein may fold the 12S mt-rRNA prior

binding of RBFA and TFB1M to dimethylate the adenines (Metodiev et al., 2009; Rozanska et al., 2017).

The Nitric oxide-associated protein 1 (NOA1, MTG3, C4ORF14) is a GTP-binding protein of the Obg family that is involved in the biogenesis of the 28S subunit (He et al., 2012; Kolanczyk et al., 2011). NOA1 descends from bacterial YqeH and was found to be required for embryonic development in mice and stability of 28S proteins (Kolanczyk et al., 2011; Loh et al., 2007). The yeast homolog of NOA1, Mtg3, is required for processing and stability of the small subunit mt-rRNA, suggesting that NOA1 may bind 12S mt-rRNA, however, the molecular mechanism remains to be determined (Paul et al. , 2012).

1.5.3. Regulatory mechanisms of mitoribosome assembly

The described assembly factors, GTPBP7 and GTPBP10, as well as the mitoribosome proteins bL32m and mL45, including its yeast homolog Mba1, are membrane-associated (see also figure 1.10; Lavdovskaia et al., 2018; Maiti et al., 2018; Nolden et al., 2005; Ott et al., 2006). This led to the hypothesis that mitoribosome large subunit assembly may occur, in parallel to the co-transcriptional processes in proximity to mtDNA nucleoids, on a platform of mitoribosome proteins bound to the inner membrane. Despite the clear evidence that mitoribosomes interact with protein complexes of the inner mitochondrial membrane, further biochemical and structural studies are needed to prove the membrane assembly platform-theory (Zeng et al., 2018).

A less well-studied area of mitoribosome assembly is the influence of post-translational processing of mitoribosome proteins by proteolytic cleavage and post-translational modification (Guo et al., 2017; Koc & Koc, 2012; Koc et al., 2017; Niemi et al., 2018; Nolden et al., 2005; Vögtle et al., 2009). It was shown that the mitochondrial AAA protease (*m*-AAA) in yeast and mouse mitochondria removes an N-terminal segment of bL32m to enable its incorporation into the large mitoribosome subunit (Nolden et al., 2005). Interestingly, disruption of the *m*-AAA function led to accumulation of a bL32m precursor and impaired mitochondrial translation (Nolden et al., 2005).

Moreover, the stability of the 28S constituent uS10m (MRPS10) was found to partly depend on conserved twin cysteine motifs, which are oxidized to cysteine-cysteine bonds during import through the inter-membrane space (Jin et al., 1997; Longen et al., 2014). It was suggested that uS10m regulates mitochondrial translation, because deletion or mutation-induced destabilization of uS10m reduced the *de novo* translation in yeast mitochondria (Longen et al., 2014).

Furthermore, recent proteomic studies indicate that the steady-state levels of the mitoribosome proteins uL30m, mL41 and mS26 are actively regulated by dephosphorylation catalyzed by the mitochondrial PTC7 protein phosphatase homolog (PPTC7; Guo et al., 2017; Niemi et al., 2018).

Hence, it will be interesting in the future to investigate how maturation of mitoribosome proteins influences assembly and translation.

1.6. Structural and functional adaptations of mitoribosomes

The structures of mitoribosomes strongly diverge from the bacterial or cytosolic ribosomes (Greber & Ban, 2016; Sharma et al., 2003). The stepwise compaction of mtDNA led to a reduction of the nucleotide length of 12S (962 nt) and 16S mt-rRNAs (1569 nt) by ~50 %, resulting in a 2:1 protein RNA ratio (Greber & Ban, 2016). During evolution mitoribosomes acquired 36 additional proteins, which do not structurally replace positions of the deleted mt-rRNA sequences (figures 1.7, 1.9 and 1.10; (Amunts et al., 2015; Greber et al., 2015; Petrov et al., 2018; Sharma et al., 2003). In contrast to their bacterial or cytoplasmic counterparts, mitoribosome proteins are often harbor large N- or C-terminal extensions, which may serve new functions in membrane attachment and mt-mRNA recruitment (Amunts et al., 2015; Greber et al., 2015; Suzuki et al., 2001a, 2001b). The protein acquisition was also accompanied by increased contacts between neighboring mitoribosome proteins, likely contributing to subunit interaction due to the reduced mt-rRNA content (Greber & Ban, 2016).

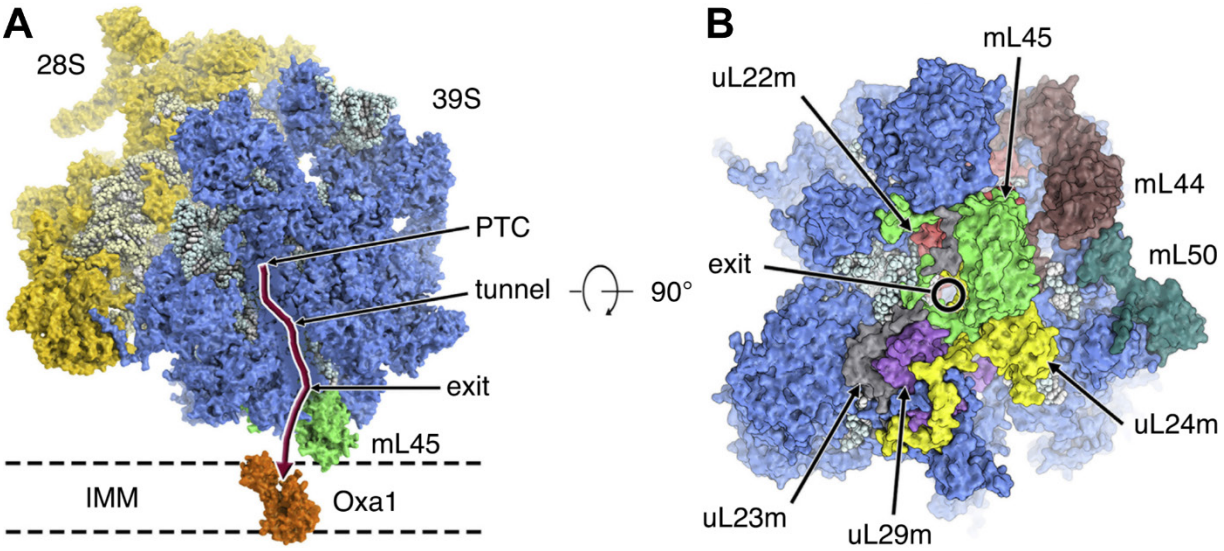

Figure 1.10 – Structure of the mammalian 55S mitoribosome. (A) Putative model and orientation of translating mitoribosomes, composed of 28S small subunit (yellow), 39S

large subunit (blue), mt-rRNAs (grey), associating with the inner mitochondrial membrane. The mitoribosome-membrane interaction could be mediated by mL45, located at the end the polypeptide exit site, binding to the the inner membrane (IMM) protein OXA1L to allow insertion of the nascent polypeptide. **(B)** Close-up view of mitoribosome proteins forming the polypeptide tunnel and exit. Adapted from Bieri et al., Current Opinion in Structural Biology, Vol. 49, Apr 1, 2018, Copyright © 2018 Elsevier Ltd. All rights reserved. Copyright clearance license ID: 4510170635971.

Evolution of mitoribosomes resulted in several structural adaptations, besides rRNA reduction and protein expansion, which include structural elements to recruit leaderless mt-mRNAs, remodeling of the central protuberance (CP) and remodeling of the polypeptide exit tunnel to allow it to associate with the inner mitochondrial membrane (Amunts et al., 2015; Greber et al., 2015; Kummer et al., 2018; Liu & Spremulli, 2000).
A unique structural adaptation of the 28S subunit is the acquisition of a PPR domain-containing protein called mS39 (PTCD3) to the mt-mRNA entry (figure 1.9; or PTCD3, Amunts et al., 2015; Greber et al., 2015). As previously mentioned, mt-mRNAs lack the canonical 7-methylguanosine caps, moreover, they also do not harbor a 5' Shine-Dalgarno-sequence, which together direct positioning of the start codon on the small subunit in canonical ribosomes (Hällberg & Larsson, 2014; Ott et al., 2016). Hence, the ability of mS39 to bind mt-mRNA may facilitate recruitment of the leaderless mt-mRNAs (Amunts et al., 2015; Greber et al., 2015). Moreover, the recent structural determination of the mitoribosome initiation complex demonstrated that the small subunit protein uS5m seems to guide the mt-mRNA towards the decoding center to align the start codon into an in-frame position (Kummer et al., 2018). Furthermore, the mitochondrial initiation factor $IF2_{mt}$ was found to lock the mt-mRNA entry tunnel and to stabilize the interaction between the mt-mRNA start codon and the decoding center (Kummer et al., 2018).
In addition to the greatly increased number of protein constituents and the two mt-rRNAs, mitoribosomes harbor a structurally integrated mt-tRNA located within the CP (figure 1.9; Greber & Ban, 2016). The denoted CP-mt-tRNA is mt-tRNA phenylalanine in porcine mitochondria and mt-tRNA valine in human mitochondria (Amunts et al., 2015; Greber et al., 2015). Interestingly, the phenylalanine and valine mt-tRNA genes flank the mt-rRNAs genes (figure 1.3). The CP-mt-tRNA appears to partially substitute a domain fold of the

bacterial 5S rRNA (figure 1.7; Brown et al., 2014; Greber et al., 2014; Ott et al., 2016). It has been proposed that the CP, including the CP-mt-tRNA, coordinates movements between the 39S subunit and the 28S subunit during translation elongation by connecting to the head of the small subunit and bound mt-tRNAs (Brown et al., 2014; Greber et al., 2014). In contrast to this, yeast, *Saccharomyces cerevisiae* (baker's yeast) mitoribosomes lack a CP-tRNA and are composed of only two mt-rRNAs and 75 proteins (Desai et al., Ramakrishnan, 2017).

Furthermore, the mitoribosome L7/L12 stalk on the large 39S subunit, built by bL7m and bL12m, which is required for recruitment of elongation factors, also appears to be greatly remodeled, but the due to the large variability in conformation an atomic resolution was not achieved (figure 1.7; Brown et al., 2014).

The most intriguing structural changes may occurred within and in vicinity to the polypeptide exit tunnel through which the nascent polypeptide emerges during translation (figure 1.10; Brown et al., 2014; Greber et al., 2014). In mitoribosomes this tunnel is covered with hydrophobic amino acid residues of the mitoribosome protein uL22m likely as an adaption to the hydrophobicity of mtDNA-encoded proteins (figure 1.10; Brown et al., 2014). Another specific feature of the exit region is the recruitment of mL45 juxtapose to the exit site (Englmeier et al., 2017; Greber et al., 2014). mL45 is structurally homologous to translocase of inner mitochondrial membrane 44 (TIM44), a peripheral inner membrane protein, and Mba1 a well-studied membrane-associated mitoribosome receptor from yeast (figures 1.7 and 1.10; Greber et al., 2014; Ott et al., 2006). In initiating mitoribosomes, the 80 N-terminal amino acids of mL45 were found to be folded into the exit tunnel, putatively to assist translation or folding of the synthesized peptide (Kummer et al., 2018). The location of mL45 is similar to the Mba1 binding site on yeast mitoribosomes, indicating that mL45, if not folded into the exit tunnel, associates with the inner membrane or with the inner membrane protein oxidase (cytochrome *c*) assembly 1-like (OXA1L) to insert polypeptides into the inner membrane (figure 1.10; Greber et al., 2014; Kummer et al., 2018; Ott et al., 2016).

1.7. Protein synthesis in mitochondria

The unique function of ribosomes is to decode mRNAs and to catalyze peptide bond formation to synthesize proteins. This highly complex process can be divided into three major steps: initiation, elongation and termination (figure 1.11). Essentially, the 28S subunit binds mt-mRNAs and translates the triplet code, within in the mt-mRNA, into a corresponding amino acid sequence by promoting selection of a cognate mt-tRNA (Ott et al., 2016). If a stable mRNA codon-tRNA anti-codon complex is formed, the peptidyl transferase center in the core of the 16S mt-rRNA, within the 39S subunit, catalyzes peptide bond formation by promoting a condensation reaction between two neighboring amino acids (Ban et al., 2000; Greber & Ban, 2016; Petrov et al., 2015).

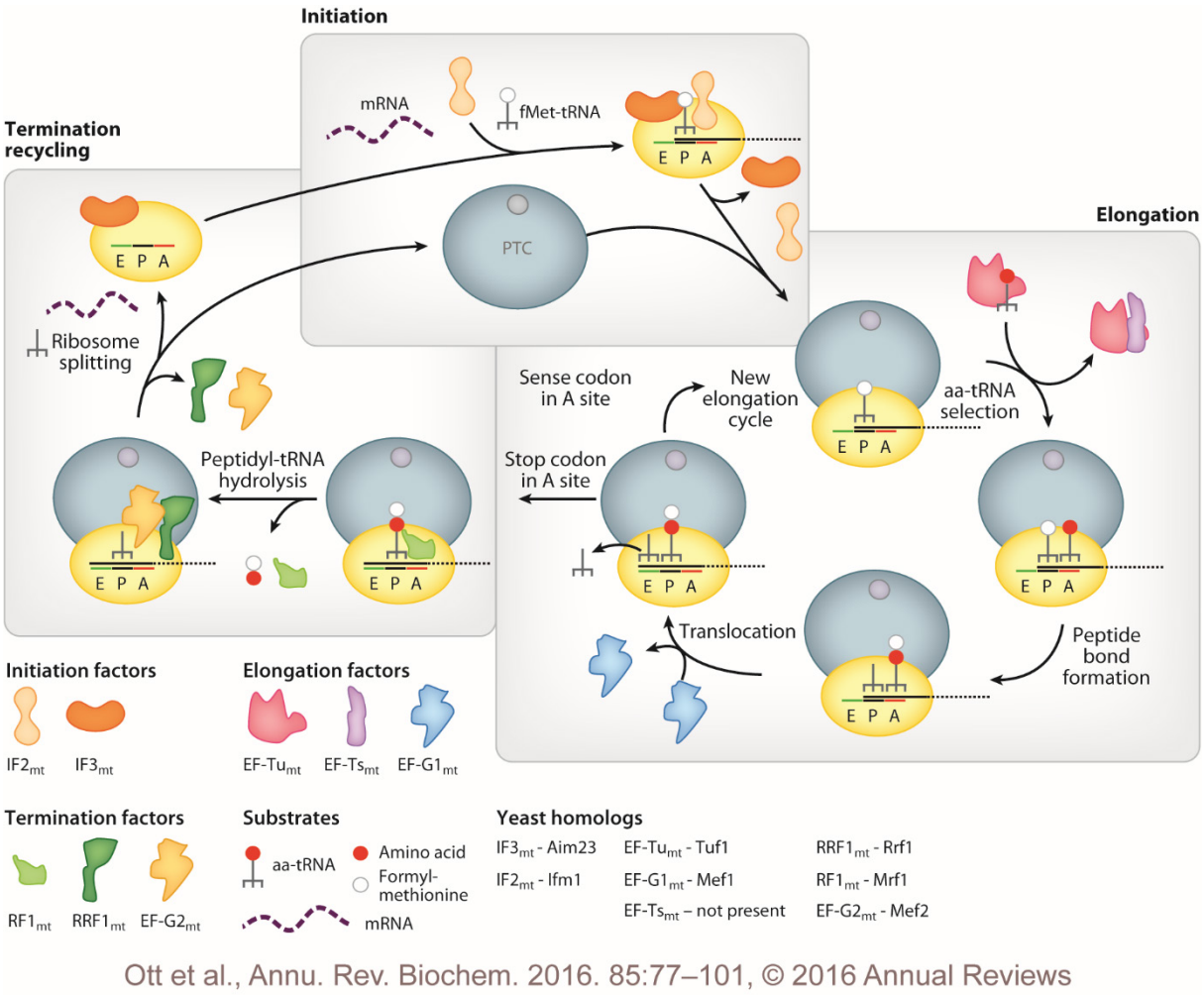

Ott et al., Annu. Rev. Biochem. 2016. 85:77–101, © 2016 Annual Reviews

Figure 1.11 – The cycle of protein synthesis by mitoribosomes and associated translation factors in mitochondria. For details, please refer to chapter 1.7. Adapted from Ott et al., Annu. Rev. Biochem. 2016. 85:77–101, © 2016 Annual Reviews, Copyright clearance license ID: 4510191098502.

The 28S subunit initially scans mt-mRNAs for a 5' end start codon, mostly AUG encoding formyl-methionine, and positions it on the peptidyl transfer site (P-site) supported by mS39, uS5m and two initiation factors denoted $IF2_{mt}$ and $IF3_{mt}$ (Kummer et al., 2018; Ott et al., 2016). Interestingly, mitochondria lack a homolog of bacterial IF1 and instead harbor an extension segment within $IF2_{mt}$ (Gaur et al., 2008; Kummer et al., 2018). Once, a stable pre-initiation complex is formed the 39S subunit is recruited, leading to dissociation of $IF2_{mt}$ and $IF3_{mt}$ (figure 1.11; Ott et al., 2016). The subsequent codon is

recognized and guanosine triphosphate (GTP)-bound mitochondrial elongation factor EF-Tu_{mt} delivers the amino acid-charged mt-tRNA to the aminoacyl site (A-site). EF-Tu_{mt} dissociates from the complex and is recharged with GTP by elongation factor EF-Ts_{mt} (figure 1.11; Ott et al., 2016; Ramakrishnan, 2002).

Next, the peptide bond is formed between the mt-tRNA-bound amino acids, at P- and A-site, catalyzed by the 16S mt-rRNA peptidyl transferase center (Ban et al., 2000; Ramakrishnan, 2002). This transient complex is recognized by GTP-bound mitochondrial elongation factor G1 (EF-$G1_{mt}$), which catalyzes the transfer of the peptide from the A- to the P-site mt-tRNA by hydrolysis of GTP (figure 1.11; Ott et al., 2016; Ramakrishnan, 2002).

Elongation continues until a stop codon, UAA, UAG, UGA, or possibly also AGA and AGG, reaches the A-site to initiate termination (Ott et al., 2016). The empty A-site recruits release factors, which catalyze hydrolysis reactions to split the ester bond between the mt-tRNA and the polypeptide to release the latter from the mitoribosome (figure 1.11). The exact mechanisms of mitochondrial translation termination are debated intensively, because a -1 frameshift has been proposed for AGA and AGG triplets to produce a UAG codon at the A-site, however, that does not seem to account for all vertebrate mtDNA genomes (Akabane et al., 2014; Ott et al., 2016; Richter et al., 2010; Temperley et al., 2010). Hence, the exact roles of the mitochondrial release factors (RF), namely RF1mt, mL62 and C12ORF65, have to be studied in more detail in the future (figure 1.11; Ott et al., 2016).

A less well studied process is the recycling of mitoribosomes, which are thought to dissociate into 28S and 39S complexes following the concerted action of the mitochondrial ribosome recycling factor ($RRF1_{mt}$) and EF-$G2_{mt}$ (figure 1.11; Ott et al., 2016; Rorbach et al., 2008).

1.7.1. Mitoribosome-associated proteins

Despite the recent insights into atomic structures of mitoribosomes, the proteins and mechanisms regulating engagement of the leaderless mt-mRNAs and membrane interaction in mammalian mitochondria remain elusive (Hällberg & Larsson, 2014; Ott et al., 2016). The concept of proteins mediating the selective recruitment of mt-mRNAs to mitoribosomes, denoted translational activators, is well-studied in yeast (Ott et al., 2016). These proteins often belong to the PPR family and are thought to bind the 5' UTR region, present in yeast mt-mRNAs to direct the mt-mRNA to the small mitoribosome subunit (Ott et al., 2016). The interaction of the translational activator with the mt-mRNA and the OXPHOS biogenesis intermediate allows precise regulation of the synthesis of a certain mtDNA-encoded protein by the mitoribosome in a feedback loop mechanism (Ott et al., 2016). More specifically, the synthesis of mtCox1 in yeast is coupled to the availability the complex IV co-factor *heme b* (Ott et al., 2016; Perez-Martinez et al., 2003). If *heme b* is present at a sufficient concentration it is incorporated into the mitochondrial splicing suppressor 51 (Mss51) protein, which in turn binds to the mitoribosome to promote mtCOX1 synthesis together with petite colonies 309 (Pet309) and mitochondrial acidic matrix protein 33 (MAM33; Ott et al., 2016; Perez-Martinez et al., 2003). Once, the newly synthesized mtCox1 is inserted into the membrane, additional complex IV assembly factors are recruited to the mtCox1 biogenesis intermediate leading to dissociation of Mss51 to further promote mtCox1 synthesis (Ott et al., 2016; Perez-Martinez et al., 2003). If the *heme b* levels decrease to a certain threshold, Mss51 is inactivated and mtCox1 synthesis is repressed (Ott et al., 2016; Perez-Martinez et al., 2003). Similar mechanisms exist in yeast to regulate the synthesis of mtCox2, mtCox3, mtCytB, mtAtp6 and mtAtp8 (Gruschke et al., 2011; Kuzmenko et al., 2016; Rak & Tzagoloff, 2009).

In contrast to the well-studied translational control mechanisms in yeast mitochondria, to date only two proteins actively involved in translation of the mtCOX1 in mitochondria of mammals are known (figure 1.12; Richter-Dennerlein et al., 2016; Weraarpachai et al., 2009). Initially, a mutant variant of TACO1 (translation activator of COX1) was identified in a patient suffering from an isolated complex IV deficiency due to a specific translational impairment of mtCOX1 synthesis (Weraarpachai et al., 2009). This pioneering study was

corroborated by generation of *Taco1* mutant mice, which were also characterized by a mtCOX1-specific synthesis defect (Richman et al., 2016). Moreover, the study of Richman et al. (2016) demonstrated that TACO1 indeed binds predominantly to the *Cox1* mt-mRNA and the 28S subunit indicating a mt-mRNA recruitment-based mechanism.

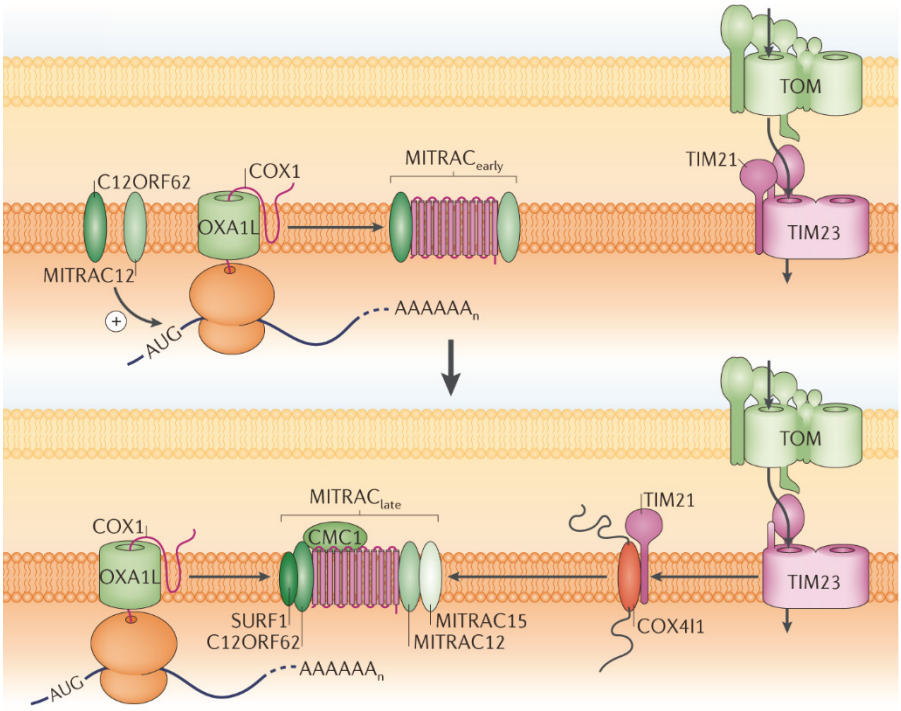

Richter-Dennerlein et al., 2015 Nature Reviews Molecular Cell Biology, Sep 16, 2015, Copyright © 2015, Springer Nature

Figure 1.12 – mtCOX1-translating mitoribosomes associate with inner membrane-embedded proteins to promote complex IV biogenesis. The mitoribosome and nascent polypeptide chain of mtCOX1, emerging from the exit site, are recruited to OXA1L. Upon insertion of a few transmembrane domains of mtCOX1, into the inner membrane, additional complex IV assembly factors (including C12ORF62 and MITRAC12) are recruited to promote folding of mtCOX1 and thereby contributing to complex IV biogenesis in the inner mitochondrial membrane. Adapted from Richter-Dennerlein et al., 2015 Nature Reviews Molecular Cell Biology, Sep 16, 2015, Copyright © 2015 Springer Nature, Copyright clearance license ID: 4510200443082.

Furthermore, proteomic analysis of complex IV intermediates in human cultured cells revealed the existence of a conglomerate of intermediate complexes, composed of the

mtDNA and nuclear encoded complex IV subunits, protein import machineries and mitoribosomes, denoted mitochondrial translation regulation assembly intermediate of cytochrome *c* oxidase (MITRAC; figure 1.12; Mick et al., 2012; Richter-Dennerlein et al., 2016). A component of these complexes denoted C12ORF62 (or COX14) specifically interacts with mitoribosomes harboring and translating the *COX1* mt-mRNA (figure 1.12; Richter-Dennerlein et al., 2016). Similar to yeast, the nascent mtCOX1 is sequentially recognized by two additional complex IV assembly factors, MITRAC12 and COX4, to promote a stepwise insertion of the mtCOX1 transmembrane domains (Richter-Dennerlein et al., 2016). Furthermore, MITRAC complexes also associate to some extent with OXA1L, which probably assists in membrane insertion of mtDNA-encoded proteins (figure 1.12; Mick et al., 2012). Surprisingly, patients suffering from a mutation destabilizing OXA1L are characterized by severely reduced levels of complex I, IV and V, but not complex III (Thompson et al., 2018). Moreover, it is known that the C-terminus of OXA1L binds specifically to proteins of the mitoribosome exit tunnel (Haque et al., 2010; Liu & Spremulli, 2000).

In summary, the interaction of mitoribosomes with OXPHOS subunits and assembly factors, import and insertion machineries suggest that several layers of translation regulation exist in mammalian mitochondria, possibly represented by dynamically-formed protein complexes at the inner mitochondrial membrane (Richter-Dennerlein et al., 2015).

1.8. Mitochondrial translation-associated human diseases

A faithful mitochondrial translation is essential for proper mitochondrial function and thus mutations in mt-RNAs species or proteins involved in mitoribosome assembly and translation can cause severe human diseases (Hällberg & Larsson, 2014; Suzuki et al., 2011; Van Haute et al., 2015). Translation-associated diseases are mostly caused by mutations in mt-tRNA genes that prevent 5' or 3' end processing, modifications or aminoacylation causing mt-tRNA destabilization and impaired mitochondrial translation (Suzuki et al., 2011; Van Haute et al., 2015). These patients suffer from multisystem or tissue-specific disorders including diabetes, kidney and pancreas failure, sideroblastic anemia (impaired hemoglobin biosynthesis), neuromuscular dysfunction including ataxia (movement disorders), myopathy and ophthalmoplegia (weakness of (eye) muscles), as well as and deafness (Hällberg & Larsson, 2014). Moreover, mutations in the mt-rRNAs genes are known to cause deafness or predispose for aminoglycoside-induced ototoxicity (antibiotic-induced hearing loss) due to increased translational misreading, as exemplified the m.1555A.G transition in the 12S mt-rRNA gene (Khatami et al., 2018; O'Sullivan et al., 2015; Prezant et al., 1993; Yang-hao et al., 2018; Zhu et al., 2015).

The use of DNA sequencing as a diagnostic tool has also unraveled several rare disease-causing mutations in nuclear genes encoding assembly factors and mitoribosome proteins (Jackson et al., 2018; Van Haute et al., 2015). Mitoribosome-associated diseases often appear early in childhood and are frequently accompanied by hypertrophic cardiomyopathy (enlarged and dysfunctional heart muscle; Jackson et al., 2018). To date, disease-causing mutations have been identified in uL3m (MRPL3), bL12m (MRPL12), mL44 (MRPL44), uS2m (MRPS2), uS7m (MRPS7), uS14m (MRPS14), bS16m (MRPS16), mS22 (MRPS22), mS23 (MRPS23), bS1m (MRPS28), mS34m (MRPS34) and mS39m (MRPS39; Borna et al., 2019; Carroll et al., 2013; Distelmaier et al., 2015; Galmiche et al., 2011; Gardeitchik et al., 2018; Jackson et al., 2018; Kohda et al., 2016; Lake et al., 2017; Menezes et al., 2015; Miller et al., 2004; Pulman et al., 2018; Saada et al., 2007; Serre et al., 2013; Smits et al., 2011).

1.9. Research aims

Despite recent advances in cryo-electron microscopy and *in vitro* characterization of a few known mitoribosome maturation factors, proteins promoting assembly and selective engagement of mitochondrial mRNAs as well as recruiting mitoribosomes to the sites of OXPHOS biogenesis are poorly studied in mammals, mostly due to the lack of appropriate *in vivo* models. Therefore, this PhD thesis focused on the characterization of three mitoribosome-associated protein factors and the generation of MitoRibo-Tag mouse strains as a novel tool to define the mitoribosome interactome in differentiated tissues. Specifically, the research aims were:

1.) To investigate the molecular consequences on the mitoribosome upon removal of RNA-binding proteins MRPP3, PTCD1 and SLIRP.

2.) To generate MitoRibo-Tag mice to efficiently purify mitoribosomes and determine their interactome in differentiated tissues.

3.) To define the composition of putative mitoribosome biogenesis intermediates formed under the conditions of defective mitoribosome assembly.

4.) To detect novel mitoribosome-interacting proteins and understand their role in mitoribosome biogenesis and mitochondrial translation.

2. Results

2.1. Mitochondrial transcription and translation are hierarchically coupled

The chapters about MRPP3 and PTCD1 include partial results from Perks et al. (2018) and Rackham et al. (2016) published in Cell Reports. The data are based on collaborative research from the laboratories of Prof. Dr. Aleksandra Filipovska, Prof. Dr. Oliver Rackham (both located at the Harry Perkins Institute of Medical Research at the University of Western Australia, Nedlands, WA 6009, Australia) and Prof. Dr. Nils-Göran Larsson (at the Max Planck Institute for Biology of Ageing, Joseph-Stelzmann-Str. 9b, D-50931 Cologne, Germany, and Karolinska Institutet - Division of Molecular Metabolism, Biomedicum, floor 9D, Solnavägen 9, 171 65 Stockholm). The experiments and data were prepared in partial fulfilment of the PhD and doctoral theses of Kara L. Perks (Harry Perkins Institute of Medical Research at the University of Western Australia) and myself (at the Max Planck Institute for Biology of Ageing, Cologne, Germany).

Transcription of mtDNA results in nearly genome-length polycistronic transcripts harboring mt-rRNAs, mt-mRNAs and mt-tRNAs. These precursor transcripts are processed and chemically modified by proteins to obtain functional RNAs. Mutations in genes encoding RNA processing proteins can cause severe human diseases, but the molecular mechanisms causing those phenotypes are not understood. To study the *in vivo* consequences of altered mt-RNA processing and stability we generated conditional knock-out mouse models of two different RNA-binding proteins which are involved in RNA processing and modification.

2.1.1. RNA cleavage by MRPP3 is required for mitoribosome assembly

As described above, one of the protein complexes involved in the 5' end cleavage of tRNAs is the RNAse P complex. Mammalian RNAse P is composed of three subunits, MRPP1, MRPP2, and the pentatricopeptide repeat (PPR) RNA-binding protein MRPP3 (figure 2.1.A; Rackham et al., 2016). To assess the functional importance of MRPP3 for mtDNA expression, exon three of murine *Mrpp3* gene was deleted using homologous recombination and Cre-LoxP system (Rackham et al., 2016).

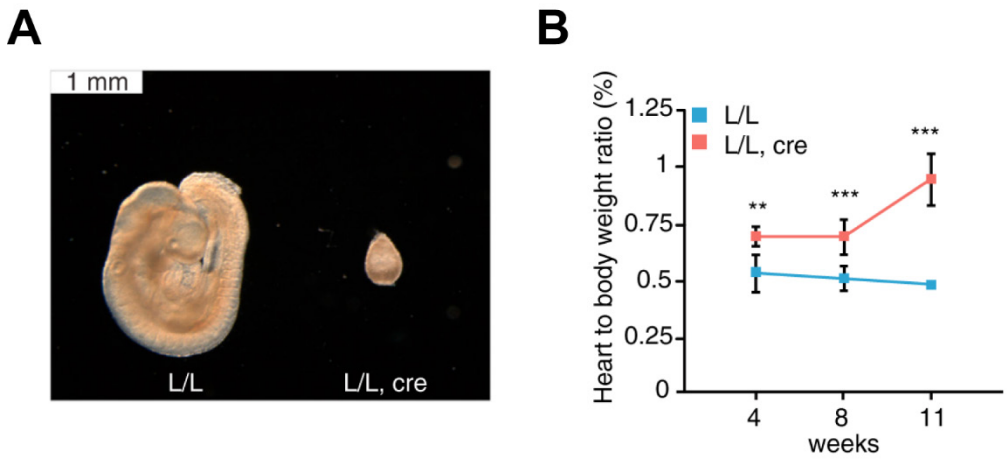

Figure 2.1 – Mrpp3 is essential for embryonic development and conditional removal causes cardiomyopathy in mice. (A) Embryos of *Mrpp3*$^{+/+}$ (loxP/loxP, L/L) control and whole-body *Mrpp3*$^{-/-}$ (L/L; *βCre)* knock-out animals at embryonic day E8.5. **(B)** Heart-to-body weight ratio of *Mrpp3*$^{L/L}$ control and *Mrpp3*$^{L/L}$*; +/Cre* conditional heart knock-outs between an age of four (n = 8), eight (n = 12) to eleven weeks (n = 12). Error bars indicate SEM with **p < 0.01; ***p < 0.001 using the Student's t test. Adapted with Elsevier © author permission from Rackham et al., 2016 Cell Reports http://dx.doi.org/10.1016/j.celrep.2016.07.031.

Animals with heterozygous (*Mrpp3*$^{+/L}$ *and Mrpp3*$^{+/L}$*; +/βCre*) and homozygous loxP-flanked *Mrpp3*-allleles (*Mrpp3*$^{L/L}$) as well as wild-type animals were obtained according to expected Mendelian ratios, but no whole-body *Mrpp3* knock-out mice (*Mrpp3*$^{L/L}$*; +/βCre*) were born (Rackham et al., 2016). Morphological assessment of embryos at day E8.5

revealed that the *Mrpp3$^{L/L}$; +/βCre* knock-out embryos were small and not developing normally compared to control embryos, indicating that *Mrpp3* is essential for embryonic development and required for animal survival (figure 2.1.A; Rackham et al., 2016). To understand the molecular function of *Mrpp3*, the *Mrpp3$^{L/L}$* mice were crossed with mice expressing the Cre recombinase under the control of muscle creatinine kinase promoter (*Ckmm-cre, Cre*) to obtain conditional heart- and skeletal muscle homozygous *Mrpp3* knock-out mice (Rackham et al., 2016). In contrast to the whole-body *Mrpp3* knock-out animals, conditional heart knock-out (*Mrpp3$^{L/L}$; +/Cre*) were viable but developed a progressive cardiomyopathy resulting in a shortened lifespan and premature death at an age of ~11 weeks (figure 2.1.B; Rackham et al., 2016).

Several molecular biology and biochemical assays were applied to investigate the precise molecular effects of *Mrpp3* loss on mitochondrial function (Rackham et al., 2016). Western blots revealed a progressive loss of respiratory chain complexes and biochemical assays demonstrated severely decreased enzyme activities. Transcriptome-wide analyses of 5' tRNA cleavage sites by parallel analyses of RNA ends (PARE) and RNA-sequencing showed that 5' tRNA cleavage precedes 3' end processing *in vivo.* Lastly, northern blot analyses demonstrated accumulation of unprocessed polycistronic RNA transcripts, which are described in detail in Rackham et al. (2016).

Interestingly, loss of *Mrpp3* had differential effects on mitoribosome protein steady-state levels as determined by western blots, whereas some proteins were upregulated for instance mS34 and mL44, and others downregulated such as mS35 and mL37 (Rackham et al., 2016). To assess the molecular consequences of impaired RNA processing by loss of *Mrpp3* on mitochondrial translation, isolated mitochondria from 11-week-old *Mrpp3$^{L/L}$* (control) animals and homozygous *Mrpp3$^{L/L}$; +/Cre* (L/L, Cre) knock-out animals were incubated and radiolabeled [^{35}S]-methionine and [^{35}S]-cysteine to follow the incorporation into newly synthesized mtDNA-encoded proteins (figure 2.2.A; Rackham et al., 2016). Deletion of *Mrpp3* completely abolished *de novo* mitochondrial translation as no radioactive amino acids were incorporated (figure 2.2.A; Rackham et al., 2016).

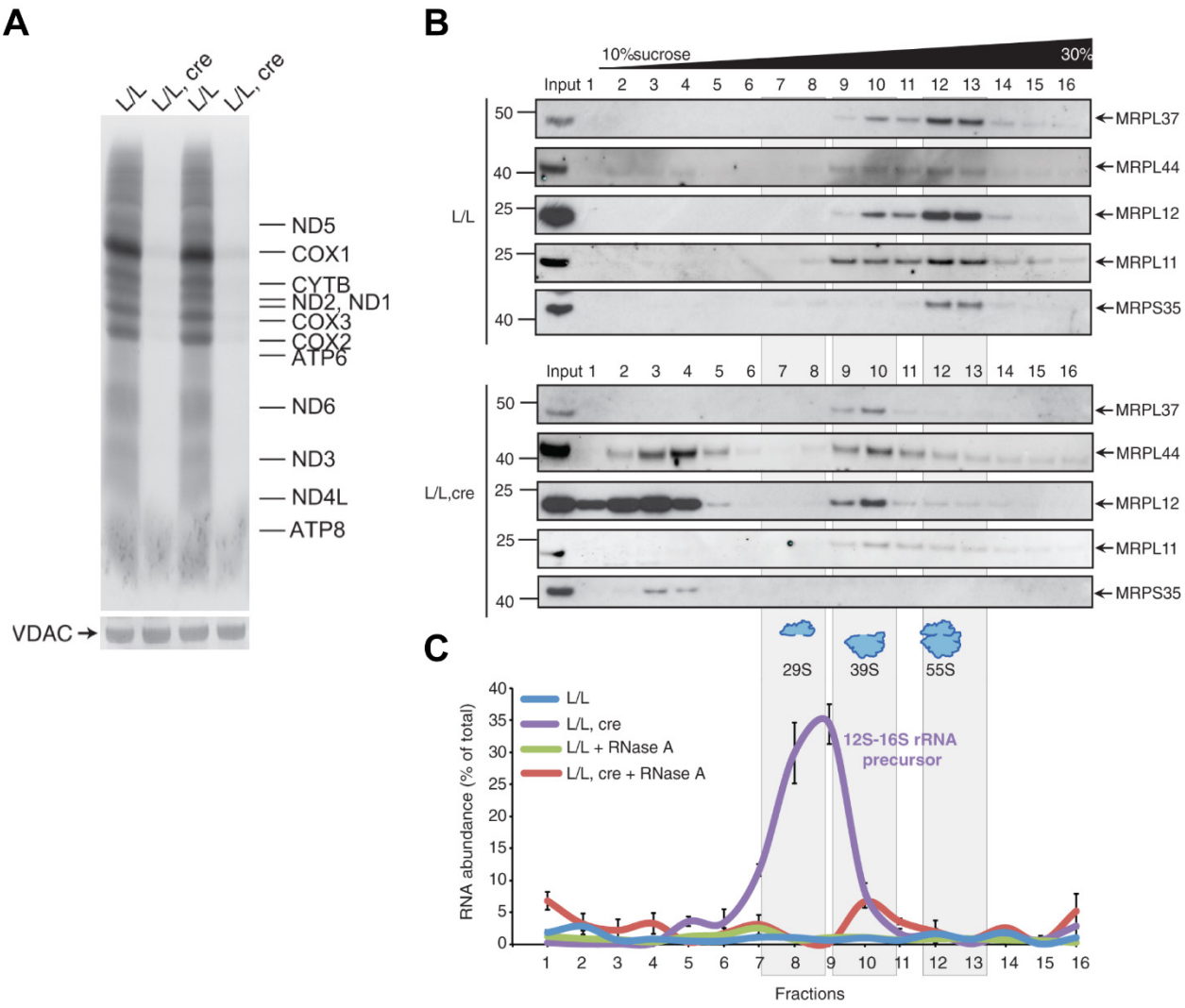

Adapted from Rackham et al., 2016 Cell Reports, Copyright © Elsevier Inc., http://dx.doi.org/10.1016/j.celrep.2016.07.031

Figure 2.2 – *Mrpp3* is essential for mitochondrial translation and its loss leads to accumulation of a mitoribosome biogenesis intermediate in mouse mitochondria. **(A)** *In organello* pulse-labeling translation by incorporation of [^{35}S]-methionine and [^{35}S]-cysteine in isolated heart mitochondria from 11-week-old *Mrpp3*$^{L/L}$ control and cardiac-specific *Mrpp3*$^{L/L}$ *+/Cre* knock-out mice. A western blot decorated against VDAC is shown as loading control. The result is representative for three biological independent experiments. **(B)** Sucrose density gradient analysis of mitoribosomes in heart mitochondria from 11-week-old *Mrpp3*$^{L/L}$ control and *Mrpp3*$^{L/L}$*; +/Cre* knock-out mice. **(C)** qRT-PCR analysis of the mitochondrial 12S-16S rRNA-junction distributed among the sucrose density gradient fractions shown in (B) of *Mrpp3*$^{L/L}$ control and *Mrpp3*$^{L/L}$*; +/Cre* knock-out mitochondria in presence or absence of RNase A. Data are represented as percentage of total RNA abundance based on four independent biological replicates.

Adapted with Elsevier© author permission from Rackham et al., 2016 Cell Reports http://dx.doi.org/10.1016/j.celrep.2016.07.031.

To elucidate the molecular effects of altered RNA processing and imbalanced mitoribosome protein levels on the mitoribosome, its assembly was analyzed using 10 – 30 % linear sucrose density gradient centrifugation and western blot against mitoribosome proteins of the 28S and the 39S subunits (figure 2.2.B and C; Rackham et al., 2016). In comparison to *Mrpp3*$^{L/L}$ mice, cardiac-specific knock-out animals (*Mrpp3*$^{L/L}$*; +/Cre*) have only negligible levels of 55S monosomes (figure 2.2.B fractions 12 and 13; Rackham et al., 2016). This loss seems accompanied by vastly increased levels of remaining large subunit proteins bL12m and mL44, appearing in two different pools, *i.e.* fractions two to four and fraction ten. Moreover, the density gradient analyses indicate that the 28S constituent mS35 is redistributed to fractions three and four. These results suggest that loss of *Mrpp3* impairs mitoribosome assembly (figure 2.2.B fractions 12 and 13; Rackham et al., 2016). Furthermore, the improperly processed *12S-16S* junction RNA transcript, identified by northern blot (data not shown), was also found to be enriched in gradient fractions seven to ten, likely as a consequence of binding of remaining mitoribosome proteins to the *12S-16S* precursor (figure 2.2.C; Rackham et al., 2016).

The density gradient analysis indicated differential effects on certain mitoribosome proteins upon *Mrpp3* removal. To gain further insights, we analyzed the composition of the putative mitoribosome biogenesis intermediate(s) in an unbiased manner by label-free quantitative mass spectrometry (LFQ-MS/MS). To this end, the gradient-separated mitoribosome subunits were precipitated according to Wessel & Flügge (1984) by methanol-chloroform extraction to remove sucrose, which is known to disturb downstream sample preparation and proteomic analysis (Rackham et al., 2016).

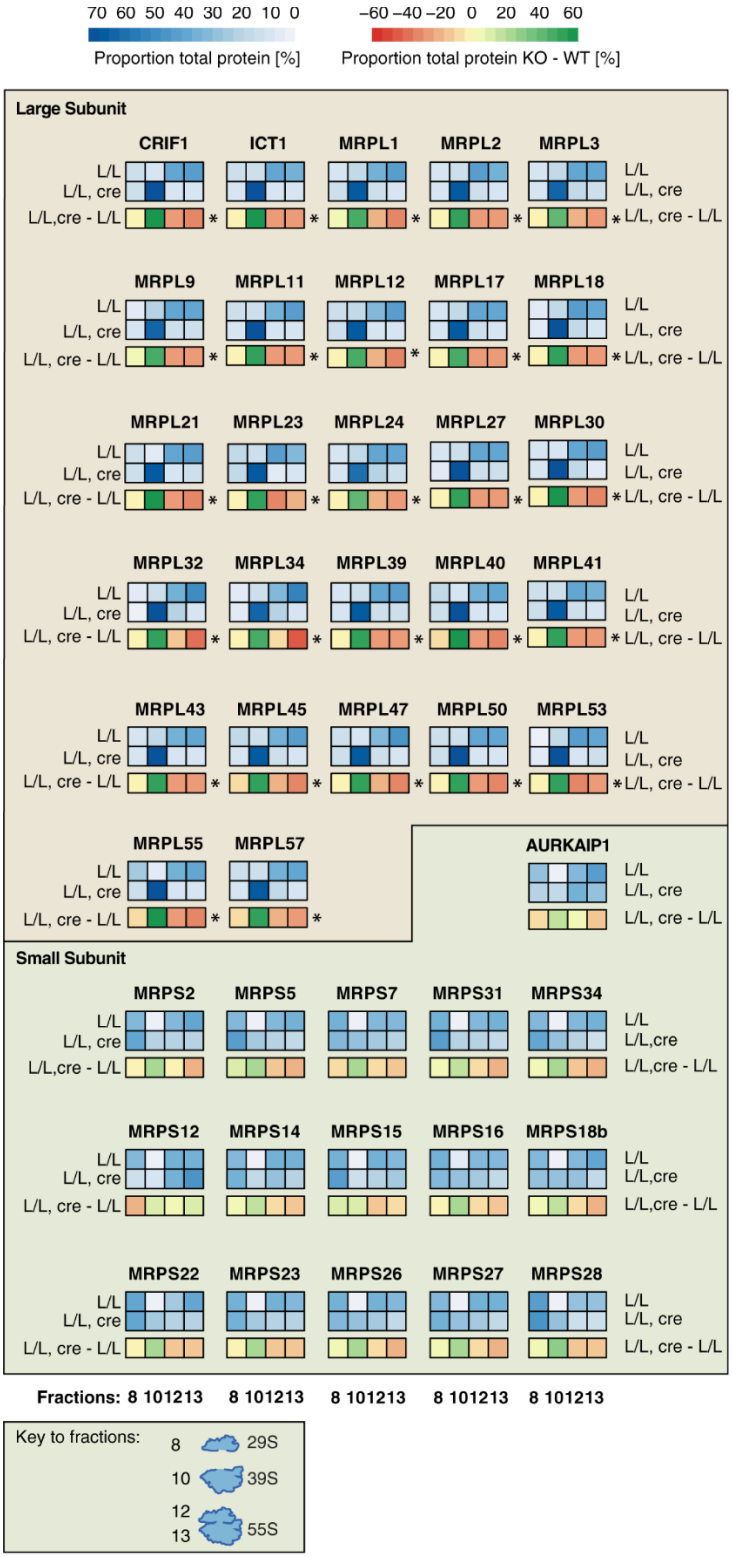

Adapted from Rackham et al., 2016 Cell Reports, Copyright © Elsevier Inc., http://dx.doi.org/10.1016/j.celrep.2016.07.031

Figure 2.3 – Mitoribosome proteins are differentially re-distributed in *Mrpp3* conditional heart knock-out mice. Proteins from 10 – 30 % sucrose density gradient

fractions, shown in figure 2.2 panel B, harboring majorities of 28S (fraction 8), 39S (fraction 10) subunits and the 55S monosome (fraction 12 and 13) were analyzed by label-free quantitative mass spectrometry. The result is based on three independent biological replicates of 11-week-old *Mrpp3*$^{L/L}$ (L/L) control and conditional heart knock-out *Mrpp3*$^{L/L}$*; +/Cre* mice (L/L, cre) and were adjusted for multiple testing using the Benjamini-Hochberg procedure, whereas only proteins with an adjusted p-value of less than 0.01 (with a false discovery rate of 1 %) were termed significant and marked with an asterisk (*). Adapted with Elsevier© author permission from Rackham et al., 2016 Cell Reports http://dx.doi.org/10.1016/j.celrep.2016.07.031.

The MS-based protein quantification confirmed the absence of 55S monosomes (fraction 12 and 13) and the simultaneous accumulation of subassembled biogenesis intermediates in fraction ten of *Mrpp3* knock-out heart mitochondria compared to controls, which is consistent with the enrichment of the *12S-16S* precursor (figure 2.3; Rackham et al., 2016).

2.1.2. Ribosomal RNA modification depends on PTCD1

Another PPR domain-containing protein with an enigmatic function in mitochondrial RNA metabolism is the mitochondrial pentatricopeptide repeat-containing protein 1 (PTCD1). Initially, PTCD1 was identified as a mitochondrial matrix protein to regulate levels of mt-tRNAs encoding leucine and mt-tRNA leucine-containing precursor transcripts (Rackham et al., 2009). A subsequent study found that PTCD1 is essential for embryonic development and animal survival as homozygous whole-body *Ptcd1* gene knock-outs are not viable (Perks et al., 2017). Interestingly, PTCD1 haploinsufficiency causes adult-onset obesity, imbalanced mt-RNA levels and a marked decrease of mitochondrial *de novo* translation in mice, whereas the exact function of the protein for mitochondrial RNA metabolism remained elusive (Perks et al., 2017). To understand the precise role of PTCD1, the genomic locus of *Ptcd1* was targeted with CRISPR/Cas9, which allowed the generation of conditional *Ptcd1* knock-out mice, explained in detail in Perks et al. (2018). Similar to other mtDNA expression knock-out mouse models, conditional heart *Ptcd1* knock-out mice (*Ptcd1*$^{L/L}$*; +/Cre*) develop a severe cardiomyopathy and die around 10

weeks of age (Perks et al., 2018). Furthermore, *Ptcd1*$^{L/L}$*; +/Cre* mice are characterized by altered steady-state levels of 28S and 39S mitoribosome subunits and strongly decreased rate of mitochondrial *de novo* translation (figure 2.4.B to C; Perks et al., 2017, 2018).

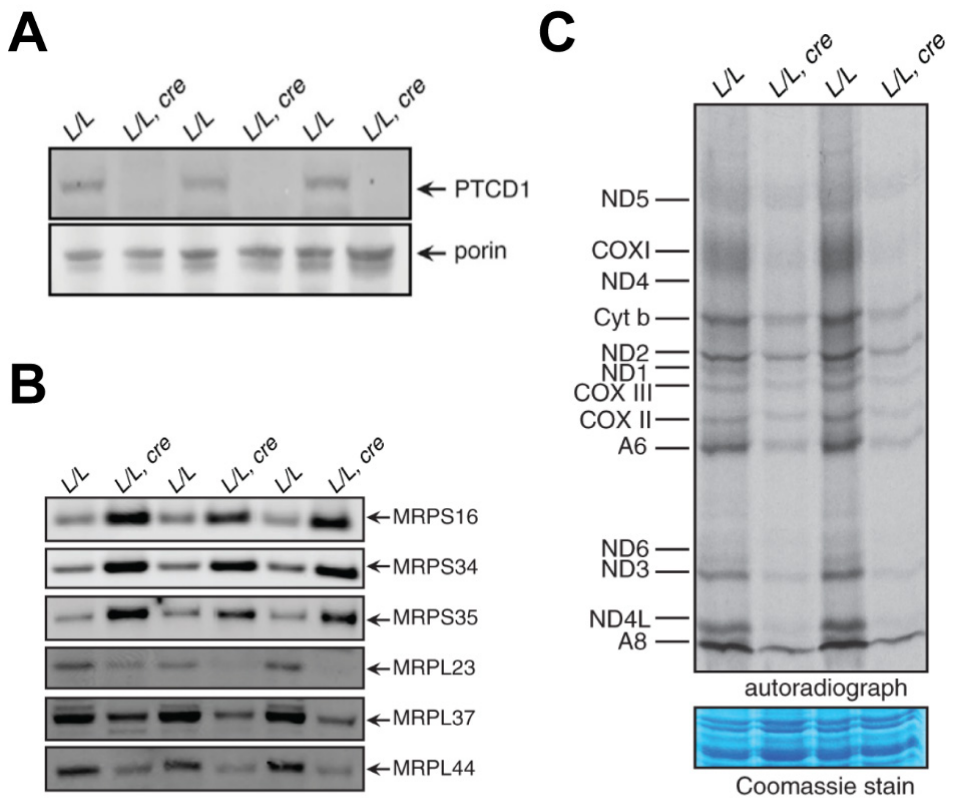

Figure 2.4 – Loss of *Ptcd1* in the mouse heart affects mitoribosome protein steady-state levels and decreases mitochondrial translation. Protein steady-state levels of PTCD1 **(A)** and mitoribosome proteins **(B)** in *Ptcd1*$^{L/L}$ (L/L) control and cardiac-specific *Ptcd1*$^{L/L}$*; +/Cre* (L/L, cre) knock-out mice determined by western blot. A Porin western blot is used as loading control. **(C)** *In organello* pulse-labeling translation by incorporation of [^{35}S]-methionine and [^{35}S]-cysteine in isolated mitochondria from 10-week-old *Ptcd1*$^{L/L}$ control and *Ptcd1*$^{L/L}$*; +/Cre* knock-out mice. 50 µg of mitochondrial protein of each approach were separated on a SDS-PAGE gel. Experiments are representative for three biological replicates per genotype. Adapted with Elsevier© author permission from Perks et al., 2018 Cell Reports https://doi.org/10.1016/j.celrep.2018.03.033.

Consistent with the western blot experiments, proteomic analysis of the protein steady-state levels in heart mitochondria revealed that the large 39S mitoribosome subunit constituents in contrast to the 28S small subunit proteins are significantly downregulated, indicating a 39S subunit assembly defect upon loss of *Ptcd1* (figures 2.4.B and 2.5; Perks et al., 2018).

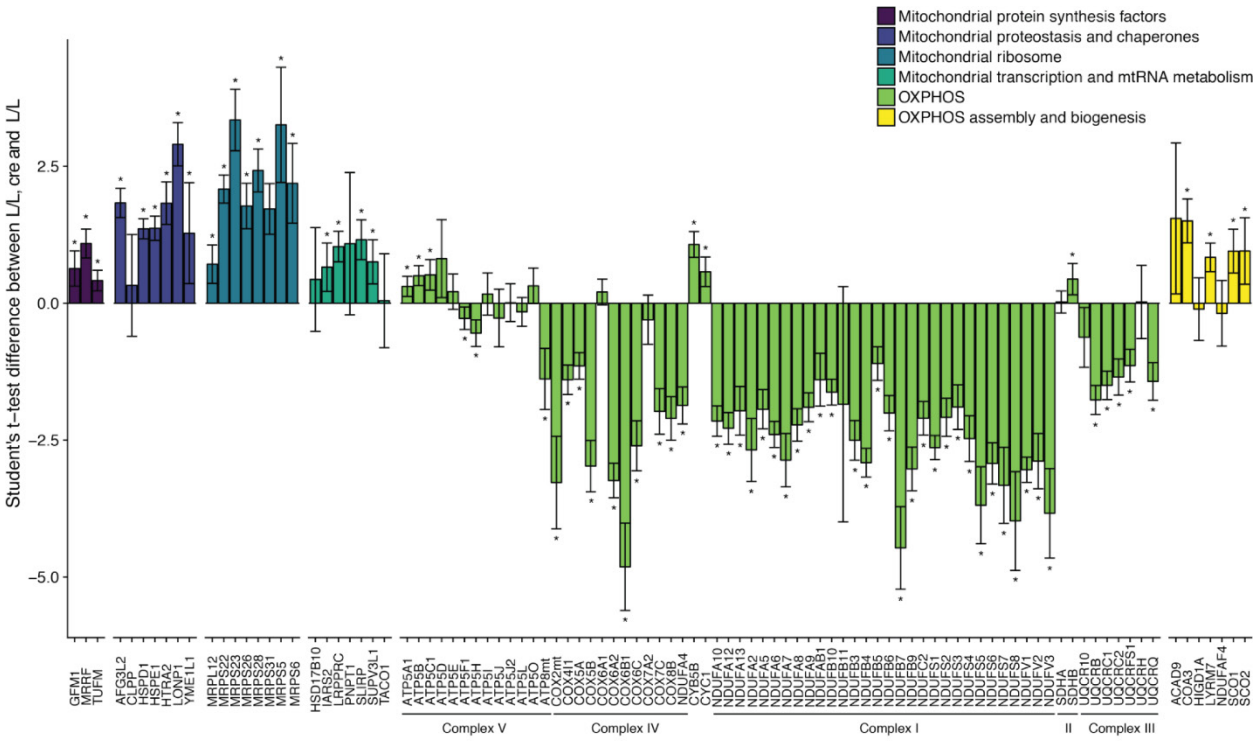

Figure 2.5 – Proteomics of conditional heart *Ptcd1* knock-out mitochondria reveals alterations of mitoribosome and OXPHOS steady-state levels. The figure represents five biological replicates of 10-week-old *Ptcd1*$^{L/L}$ control and *Ptcd1*$^{L/L}$ *+/Cre* knock-out mice. P-values were adjusted according to the Benjamini-Hochberg procedure, whereas proteins with an adjusted p-value less than 0.05 were designated as differentially expressed and marked with asterisk (*). Proteins involved in mitochondrial RNA metabolism, translation, OXPHOS biogenesis and proteostasis are highlighted. Adapted with Elsevier© author permission from Perks et al., 2018 Cell Reports, https://doi.org/10.1016/j.celrep.2018.03.033.

The altered mitochondrial *de novo* translation together with the proteomic analysis indicated that the mitochondrial translation machinery is specifically affected in *Ptcd1*

knock-out animals (figures 2.4.B and 2.5; Perks et al., 2018). Hence, a mitochondrial transcriptome analysis was performed, which revealed that the steady-state levels of the 16S mt-rRNA were markedly reduced, corroborating earlier observations (Perks et al., 2017, 2018). Regarding the latter, pseudouridine sequencing was performed revealing that PTCD1 is required for the ψ formation in the 16S mt-rRNA at position 1416, which was found earlier to be catalyzed by RPUSD4 (Antonicka et al., 2017; Perks et al., 2018; Zaganelli et al., 2017). Moreover, co-immunoprecipitation of PTCD1-FLAG from mouse tissues and human cells revealed that PTCD1 associates with the 16S mt-rRNA module components FASTKD2 and RPUSD4 (Perks et al., 2018).

2.1.3. The LRPPRC-SLIRP complex fine-tunes mitochondrial translation

The following chapter includes partial results from Lagouge et al. (2015) been published in PLOS Genetics. The data are based on collaborative efforts between members of the laboratory of Prof. Dr. Nils-Göran Larsson (at the Max Planck Institute for Biology of Ageing, Joseph-Stelzmann-Str. 9b, D-50931 Cologne, Germany, and Karolinska Institutet - Division of Molecular Metabolism, Biomedicum, floor 9D, Solnavägen 9, 171 65 Stockholm). Experiments and data were prepared in partial fulfilment of my PhD thesis (at the Max Planck Institute for Biology of Ageing, Cologne, Germany).

Another important layer of mtDNA expression is the regulation of mt-RNA stability by the LRPPRC-SLIRP complex. LRPPRC was identified to be mutated in patients with French-Canadian variant of the Leigh syndrome, and SLIRP to be required for mitochondrial RNA maintenance (Baughman et al., 2009; Mootha et al., 2003). Two additional studies found that LRPPRC and SLIRP form a stoichiometric complex (Ruzzenente et al., 2012; Sasarman et al., 2010). Conditional *Lrpprc* knock-out mice were found to have significantly reduced mt-mRNA polyadenylation and deregulated translation as some proteins were found to be synthesized at a much higher rate than others (Ruzzenente et al., 2012).

To investigate *in vivo* role of SLIRP and its involvement in RNA stability, *Slirp* knock-out mice were generated by flanking exon 2 of the *Slirp* locus in the mouse germline using the Cre-LoxP system as explained above (Lagouge et al., 2015). Surprisingly, homozygous *Slirp* knock-out mice (*Slirp*$^{-/-}$) were born at mendelian ratios, showing that SLIRP is not essential for embryonic and animal development (figure 2.6.A; Lagouge et al., 2015).

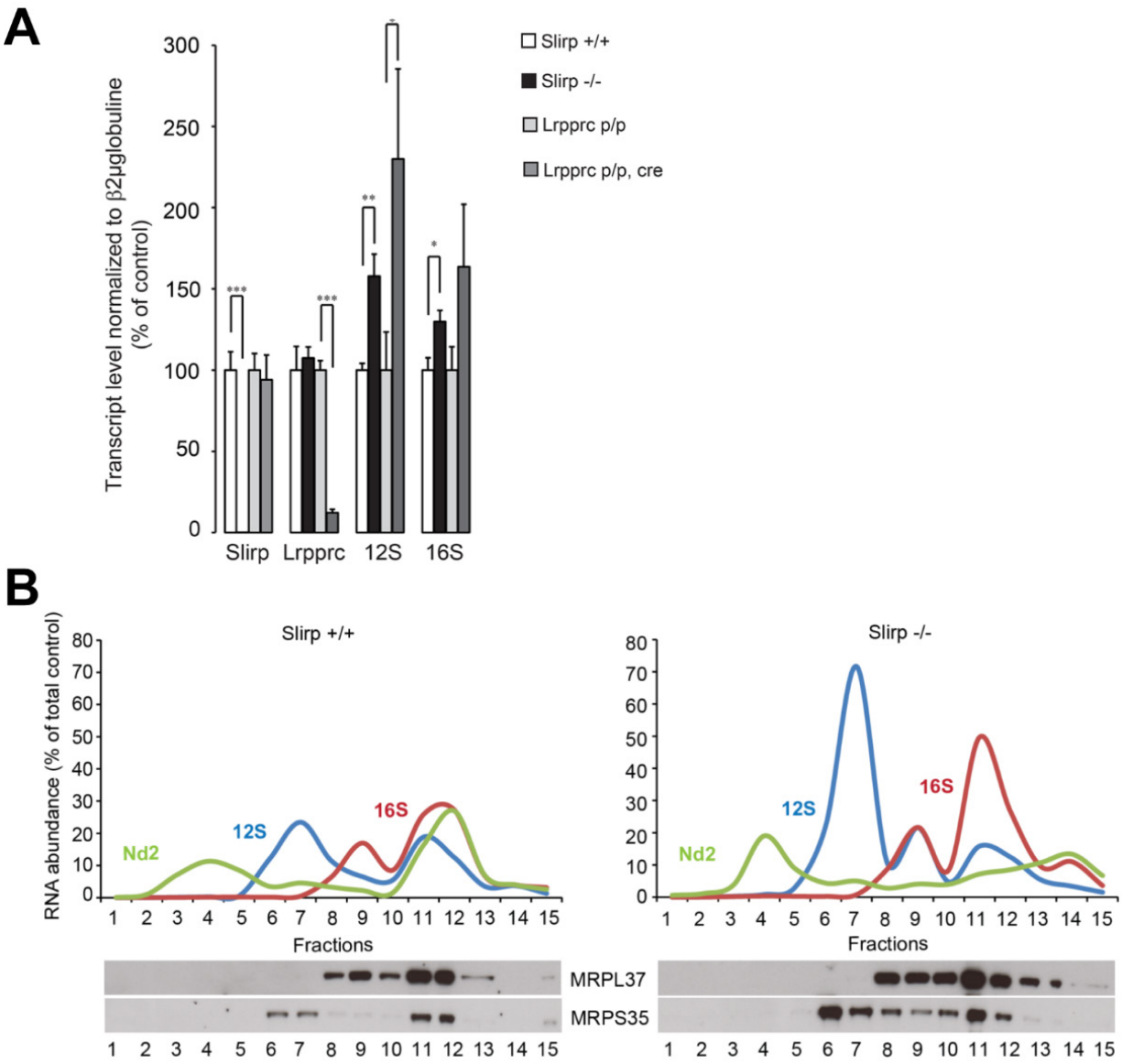

Figure 2.6 – SLIRP has regulatory role in fine-tuning translation. (A) qRT-PCR transcript analysis in hearts of *Slirp*$^{+/+}$ (wild type), *Slirp*$^{-/-}$ (knock-out), *Lrpprc* LoxP control (*Lrpprc*$^{p/p}$), and conditional *Lrpprc*$^{p/p}$*; +/Cre* knock-out mice at an age of 12 weeks. The result is representative for five biological genotypes per genotype and error bars show SEM. * p-value < 0.05. ** p-value < 0.01. *** p-value < 0.001. **(B)** 10 to 30 % sucrose density gradient analysis of mitoribosomes in liver mitochondria from 12-week-old *Slirp*$^{+/+}$ wild type and *Slirp*$^{-/-}$ knock-out mice by qRT-PCR and western blot against mitoribosome proteins of the 28S subunit protein MRPS35 (mS35) and the 39S subunit protein MRPL37 (mL37).

Slirp$^{-/-}$ mice have a mildly reduced bodyweight, but do not show canonical mitochondrial dysfunction-like symptoms despite severely reduced mt-mRNA levels of ~50 to 70 % (Lagouge et al., 2015). Western blot analysis of revealed that LRPPRC steady-state levels are reduced by approximately 50 % upon loss of SLIRP (Lagouge et al., 2015). The 12S and 16S mt-rRNA and corresponding 28S and 39S mitoribosome proteins were found to be significantly upregulated in liver mitochondria determined by qRT-PCR and western blot analysis of sucrose density gradients (figure 2.6.A and B; Lagouge et al., 2015). qRT-PCR analysis of relative mt-*Nd2* mRNA levels comigrating with the mitoribosomes indicated that mt-mRNAs are less engaged with the 55S mitoribosome in liver mitochondria in the absence of *Slirp* (figure 2.6.B; Lagouge et al., 2015). Interestingly, an opposite molecular phenotype was observed in heart mitochondria of *Slirp*$^{-/-}$ mice, in which mt-mRNAs were more associated with 55S monosomes (Lagouge et al., 2015). Those tissue-specific *Slirp* knock-out responses were independently proven by *in organello* translation experiments, finding that *Slirp*$^{-/-}$ heart mitochondria seem to more rapidly initiate mitochondrial translation than liver mitochondria, which seem to have a slightly reduced incorporation capacity (Lagouge et al., 2015). Taken together these data indicate that SLIRP stabilizes LRPPRC and that mitochondria of differentiated organs respond diversely to disturbed mt-RNA levels or translation by yet unknown mechanisms.

2.2. Generation and characterization of MitoRibo-Tag mice

The following chapter includes results from Busch et al. (2019) published in Cell Reports (Volume 29, ISSUE 6, P1728-1738.e9, November 05, 2019). Experiments and data were prepared in partial fulfilment of my PhD thesis (at the Max Planck Institute for Biology of Ageing, Cologne, Germany).

After dissecting important steps in mitochondrial RNA maturation and regulatory mechanisms of the mitochondrial RNA metabolism, we sought out to generate a tool to study mitoribosomes in different tissues and under diverse physiological states. Previously, mitoribosome composition and biogenesis was mostly studied in yeast and

mammalian cell culture, whereas cultured cells are characterized by very high growth rates accompanied by a fast protein turnover. Those conditions might not accurately resemble the situation *in vivo* and in differentiated tissues. Hence, the idea was to engineer an experimental model to purify mitoribosomes from different tissues and determine their exact composition and interactome by mass spectrometry (figure 2.7).

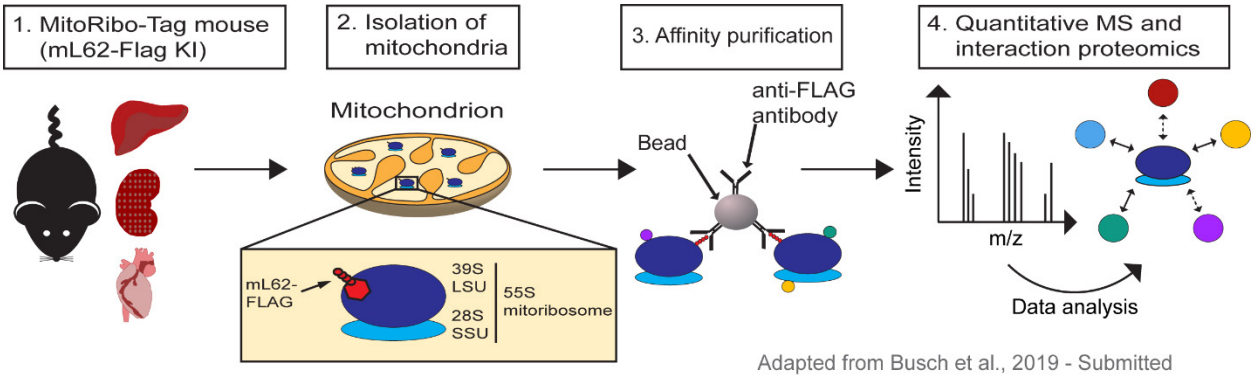

Figure 2.7 – Concept of mitoribosome purification from MitoRibo-Tag mice.

Initial literature research revealed the recent identification of the mitoribosome protein mL62 (also known as ICT1, Immature colon transcript 1) by Richter et al. (2010). The study revealed that mL62 is a constituent of the 39S mitoribosome subunit and may act as peptidyl transfer ribonucleic acid tRNA hydrolase. This characteristic activity involves the amino acid GGQ-motif to break the ester bond between the nascent polypeptide and the retained tRNA at the P-site to release the nascent protein from the ribosome during termination of translation. The codon-independent release factor activity of mL62 was questioned by a study from Akabane et al. (2014) showing that mitoribosome-integrated mL62 does not exert hydrolysis activity. Even though none of the abovementioned studies used an *in vivo* model to study mL62 function, both reports indicated that the mitoribosome-integrated mL62 is a good candidate protein for mitoribosome purification (62 mitoribosome proteins co-purified with mL62-FLAG; Richter et al., 2010). Moreover, mL62 was recently shown to be an integral constituent 39S subunit and part of the 55S monosome in human and porcine mitochondria (Amunts et al., 2015; Greber et al., 2015).

To generate MitoRibo-Tag mice, the genomic locus of the mouse gene encoding mL62 (Ensembl gene ID: ENSMUSG00000018858 and NCBI gene ID: 6857) was engineered by homologous recombination (figure 2.8).

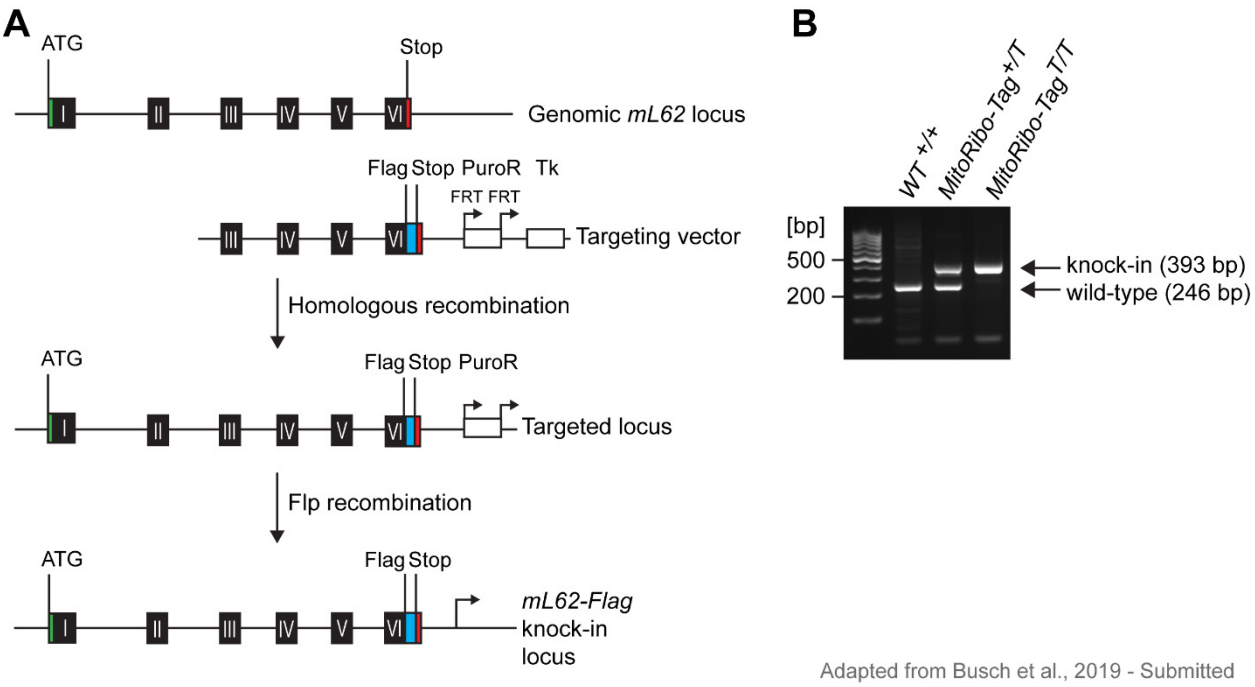

Figure 2.8 – Generation of MitoRibo-Tag mice by homologous recombination. (A) Applied targeting strategy for construction of conditional *mL62-Flag* knock-in mice (Flag-tag sequence in blue, stop codon in red). **(B)** Integration of the *mL62-Flag* locus was verified by PCR as the knock-in leads to a 146 bp-size shift compared to the wild type allele (wild type (+/+), transgenic heterozygous (+/T) and homozygous (T/T) mice).

Essentially, the targeting vector, harboring the homologous sequences of exon three to six with an additional sequence encoding the FLAG-tag at the 3' end before the stop codon, was transfected into mouse embryonic stem cells. Homologous recombination integrated the *mL62-Flag* sequence into the *mL62* locus of the mouse genome (figure 2.8). The recombined genome of the mouse embryonic mouse stem cells allowed selection of transfected clones with puromycin. Afterwards, the puromycin-resistant clones transferred into the mouse germline to generate heterozygous *mL62-Flag* knock-in mice, which were still harboring the PuroR cassette. The puromycin cassette was

removed by breeding the heterozygous *mL62-Flag* mice with animals expressing the *FLP* recombinase. Animals harboring the *mL62-Flag* allele, devoid of the PuroR, were intercrossed for several generations to obtain homozygous MitoRibo-Tag mice with a defined C57/BL6N genetic background (figure 2.8.A). The knock-in of *mL62-Flag* was verified by PCR, as the engineered transgenic allele leads to a size-shift of 146 bp compared to the wild type allele (figure 2.8.B).

2.2.1. MitoRibo-Tag stably express mL62-FLAG

The *mL62-Flag* allele should induce the expression of a mL62-FLAG fusion protein controlled by the endogenous promotor. To assess the expression of the fusion protein, mitochondria from heart, liver and kidney of MitoRibo-Tag were isolated and analyzed by western blot (figure 2.9).

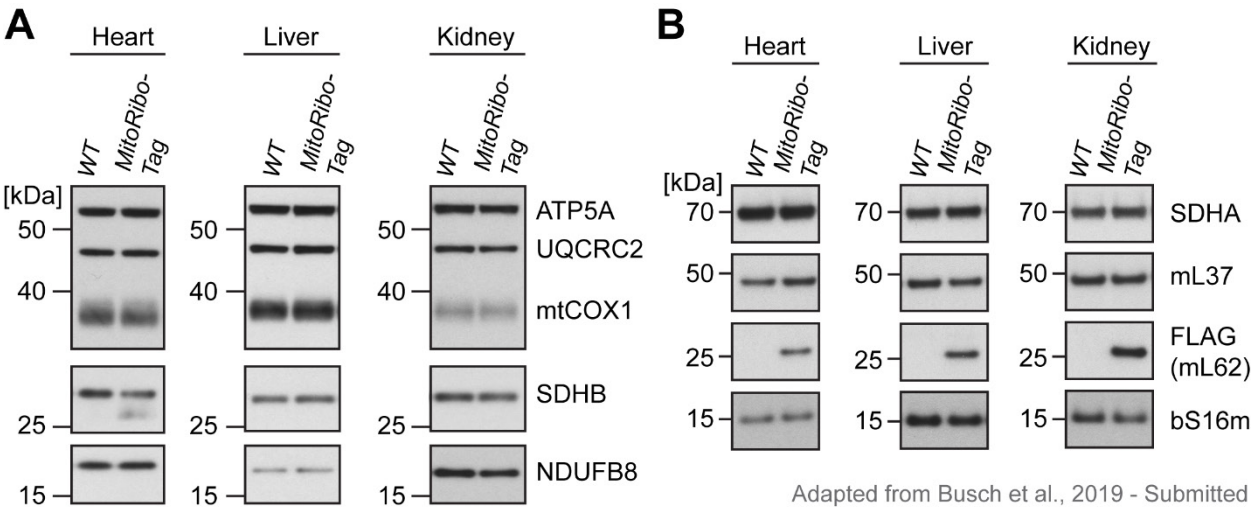

Figure 2.9 – Western blot analysis of protein steady-state levels heart, liver and kidney mitochondria. (A) Steady-state levels of mitoribosome proteins from 39S large subunit (mL37 and mL62-FLAG) and 28S small subunit (bS16m) in homozygous MitoRibo-Tag and wild type (WT) mice. SDHA was used as a loading control. **(B)** Analyses were performed as in (A) except that the levels of OXPHOS proteins CI (NDUFB8), CII (SDHB, loading control), CIII (UQCRC2), CIV (mtCOX1) and CV (ATP5A)

were analyzed. Experiments are representative of four biological replicates per genotype and tissue.

mL62-FLAG is stably expressed in heart, liver and kidney mitochondria and its expression does not alter the levels of other mitoribosomal or nuclear and mtDNA-encoded OXPHOS proteins (figure 2.9.A and B). To look at the possible mL62-FLAG-induced consequences systematically, the isolated mitochondria of MitoRibo-Tag mice were solubilized, proteins extracted and peptides analyzed by LFQ-MS/MS (figure 2.10).

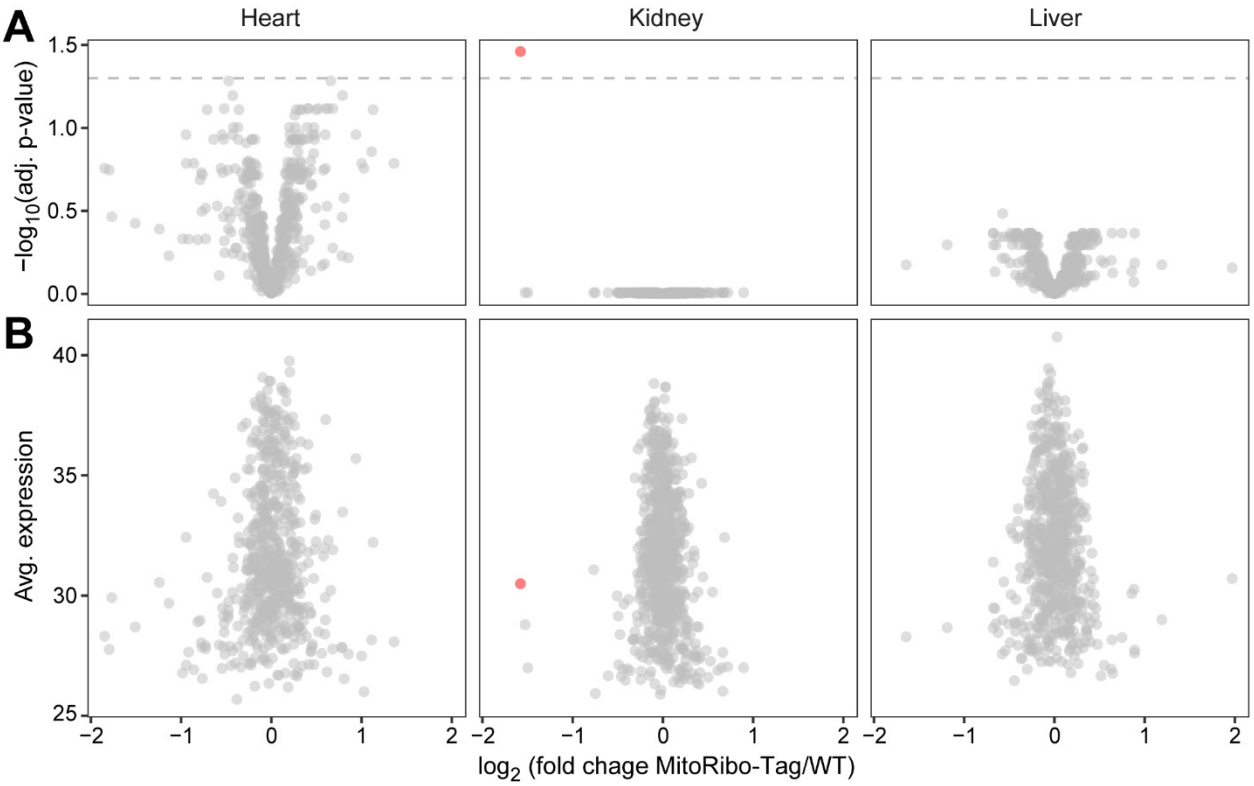

Figure 2.10 – Endogenous expression of mL62-FLAG does not influence protein steady-state levels mitochondria isolated from different tissues MitoRibo-Tag mice. (A) shows non-significantly changed (grey) and significantly changed (mitochondrial carbamoyl-phosphate synthase, red) proteins quantified in heart, liver and kidney mitochondria of MitoRibo-Tag mice vs. WT. **(B)** indicates the relative average expression of proteins. Proteins with an adjusted p-value of less than 0.05 (5 % false

discovery rate, dashed line) were termed significant. The result represents five biological replicates per genotype and tissue.

The heart, liver and kidney mitochondrial proteome analyses of homozygous MitoRibo-Tag mice are consistent with the western blot results, as the proteome composition remains unaffected despite the expression of mL62-FLAG in comparison with wild type (figure 2.10). The only protein identified that appears slightly less expressed in kidney mitochondria is the carbamoyl-phosphate synthase (figure 2.10, red dot). The adjusted p-value of the carbamoyl-phosphate synthase is low and not indicative of a mL62-FLAG expression induced regulation, suggesting an experimental or technical artifact. Moreover, the obtained data are also in good agreement with previous studies on the mouse mitochondrial proteome from the Mootha laboratory, as 30 to 40 % of mitochondrial proteins are found to be ubiquitously expressed whereas the majority of the mitochondrial proteins show a tissue-specific expression pattern (Calvo et al., 2016; Mootha et al., 2003; Pagliarini et al., 2008).

2.2.2. MitoRibo-Tag mice have wild type mitoribosome assembly

To ensure that the mitoribosome is fully functional in MitoRibo-Tag mice, mitoribosome assembly in heart, liver and kidney mitochondria was biochemically assessed using linear sucrose density gradient analysis. This technique was originally applied by Matthews et al. (1982) to determine the protein composition of mitoribosomes from bovine heart. The protocol of Matthews et al. (1982) was modified according to Rackham et al. (2016), to analyze mitoribosome assembly in heart, liver and kidney mitochondria.

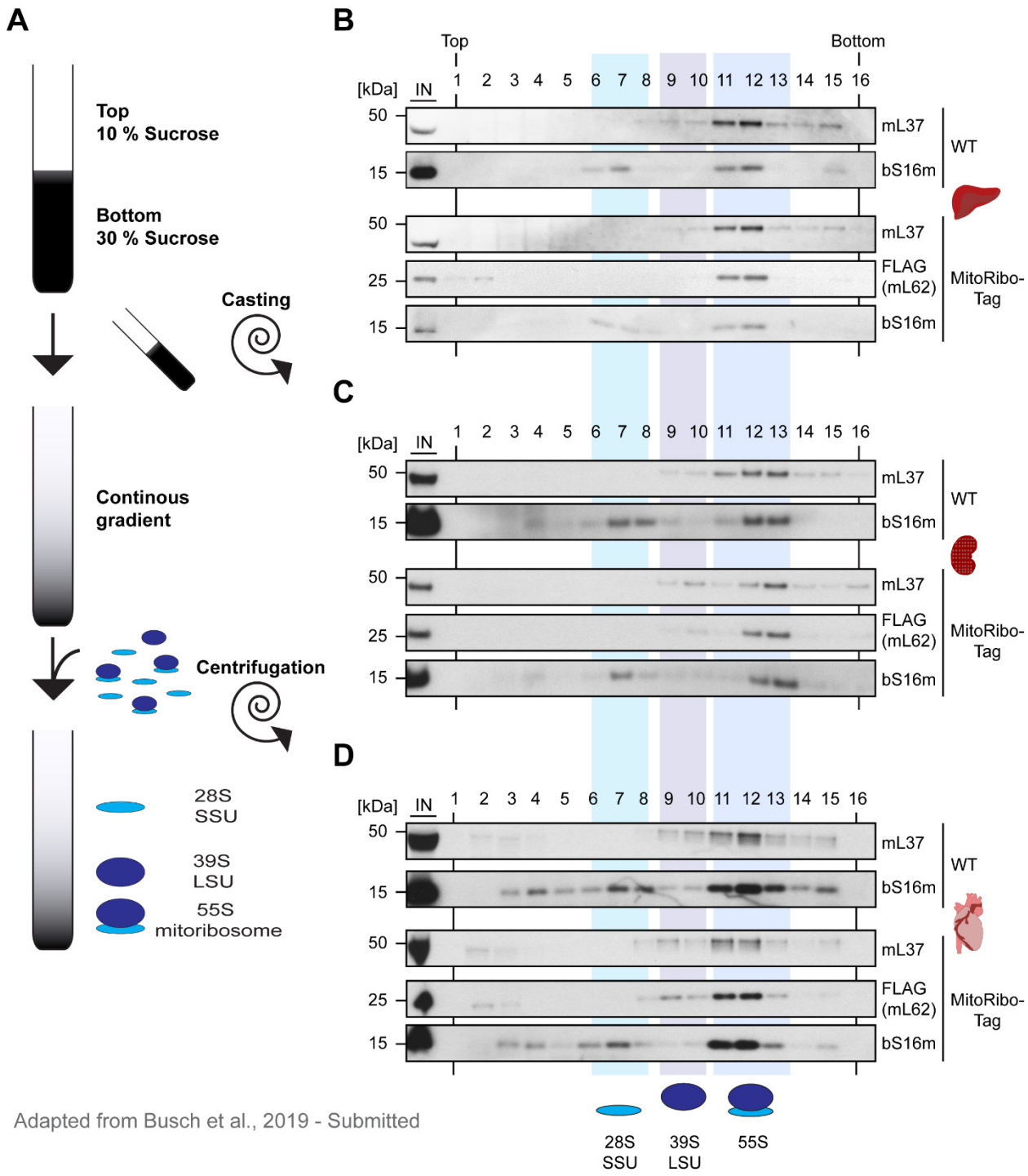

Figure 2.11 – Sucrose density gradient analysis of mitoribosomes by western blot. **(A)** Schematic representation of gradient casting and mitoribosome subunit separation in a 10 to 30 % linear sucrose gradient from liver **(B)**, kidney **(C)** and heart **(D)** mitochondria of homozygous MitoRibo-Tag (T/T) and wild type (WT) mice. Isolated mitochondria were lyzed in a digitonin-containing buffer and centrifuged on continuous sucrose gradients. Fractions were collected from the top and analyzed by western blot. The input fractions

correspond to ~30% of loaded mitochondrial lysate. The experiments are representative for at least four biological replicates per genotype and tissue.

As depicted in figure 2.11 mitoribosomes from differentiated tissues mostly are present as 55S complexes also known as monosomes (figure 2.11.B to D). It is interesting to note that the majority mL62-FLAG comigrates with the 55S monosome in all analyzed tissues. Our *in vivo* findings are thus in good agreement with previous molecular biology and cryo-EM studies showing that mL62 is integrated into the 55S monosome complex under basal conditions (Amunts et al., 2015; Greber et al., 2015; Richter et al., 2010). Furthermore, the data indicate that the addition of a C-terminal FLAG-tag to mL62 does not perturb mitoribosome assembly in homozygous MitoRibo-Tag mice, as the migration patterns are similar to those of wild type animals (figure 2.11.B to D).

2.2.3. MitoRibo-Tag mice can be used to purify mitoribosomes from tissues

Next, we optimized the purification conditions for mL62-FLAG for mitoribosome co-immunoprecipitation. Many different purification conditions were previously tested to obtain assembled mitoribosomes from mitochondria of mouse tissues, but the detailed explanation of all of them would exceed the scale of the current thesis. In summary, different salts were titrated including sodium, magnesium or potassium chloride or acetate, the polyamine spermidine was added, the binding capacities of different affinity gels, *e.g.* magnetic or agarose beads, were determined and the conditions used to elute purified protein complexes, including glycine, urea, FLAG peptide or partial digest-trypsin elution were compared (data not shown). High concentration of sodium chloride, Tris or potassium chloride significantly reduced the amounts of co-enriched mitoribosome proteins (data not shown). Unexpectedly, addition of the polyamine spermidine led to unspecific purification of mitoribosomes from wild type samples, contrasting with the purification conditions for bacterial or yeast mitoribosomes (Kehrein et al., 2015; Turncock, 1971).

To purify assembled mitoribosomes, we hypothesized that a purification condition is needed with a sufficient amount of salt for efficient washing, which is at same time mild enough to avoid loss of mitoribosome proteins. Besides preservation of 55S monosomes, also putative interactions with membrane-associated proteins or membrane-bound complexes should be maintained. Following the pioneering work of many laboratories a mild biochemical condition including 10 mM Tris-HCl pH 7.5, 20 mM magnesium chloride, 100 mM potassium chloride and digitonin was chosen (Liu & Spremulli, 2000; Matthews et al., 1982; Spremulli & Kraus, 1987).

In comparison with the sucrose gradient conditions, few adaptations had to be made for the co-immunoprecipitation experiments. Firstly, all co-immunoprecipitation buffers were prepared without sucrose, to avoid interference with subsequent mass spectrometry. Moreover, no RNase inhibitor was added as it is dissolved in a buffer containing a reducing agent, which would possibly reduce the cysteine-cysteine bonds of the FLAG-tag antibodies bound to the beads. A representative result of the established mL62-FLAG co-immunoprecipitation experiment is shown in figure 2.12.

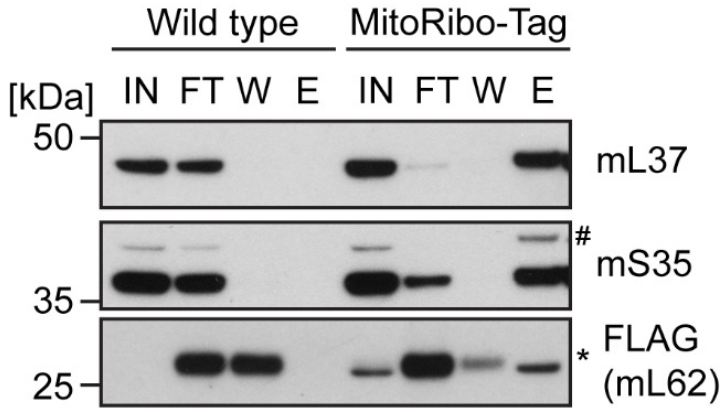

Adapted from Busch et al., 2019 - Submitted

Figure 2.12 – mL62-FLAG co-immunoprecipitation from liver mitochondria of wild type and MitoRibo-Tag animals analyzed by western blot. The input (IN), flow-through (FT) and wash (W) fractions correspond to 10 % of the respective total fraction volume, and the eluate fraction (E) is 100 %. The hash (#) indicates a remaining signal from mL37 on the mS35 decoration and the asterisk (*) a cross-reacting band produced from

detached antibody light chain of the cross-linked beads. The result is representative for at least three biological replicates.

The western blot analysis of the mL62-FLAG co-immunoprecipitation from liver mitochondria of wild type and MitoRibo-Tag animals indicates that the applied biochemical conditions allow a very efficient purification of mitoribosomes as the majority of the mL62-FLAG signal specifically appears in the eluate fraction of proteins purified from MitoRibo-Tag mitochondria (figure 2.12). The specificity of the experiment is supported by the exclusive co-purification of mL62-FLAG with the 28S subunit protein mS35 and the 39S subunit protein mL37 from mitochondria of MitoRibo-Tag mice, which is not observed with wild type mitochondria. Nevertheless, minor amounts of mS35 and mL37 remain in the flow-through fraction of the FLAG approach (figure 2.12). The purification experiment seems also to be very specific as no mitoribosome proteins are enriched from wild type mitochondria.

As mitoribosomes are RNA:protein complexes, it was important to investigate if and which RNA species are co-purified with mL62-FLAG and the mitoribosome proteins using the established mitoribosome purification procedure. To this end, the mL62-FLAG co-immunoprecipitations were repeated, whereas the elution was carried for 1 hour out at 4°C to protect putatively co-purifying RNAs from degradation, subsequently followed by isolation of RNAs from the purified fractions.

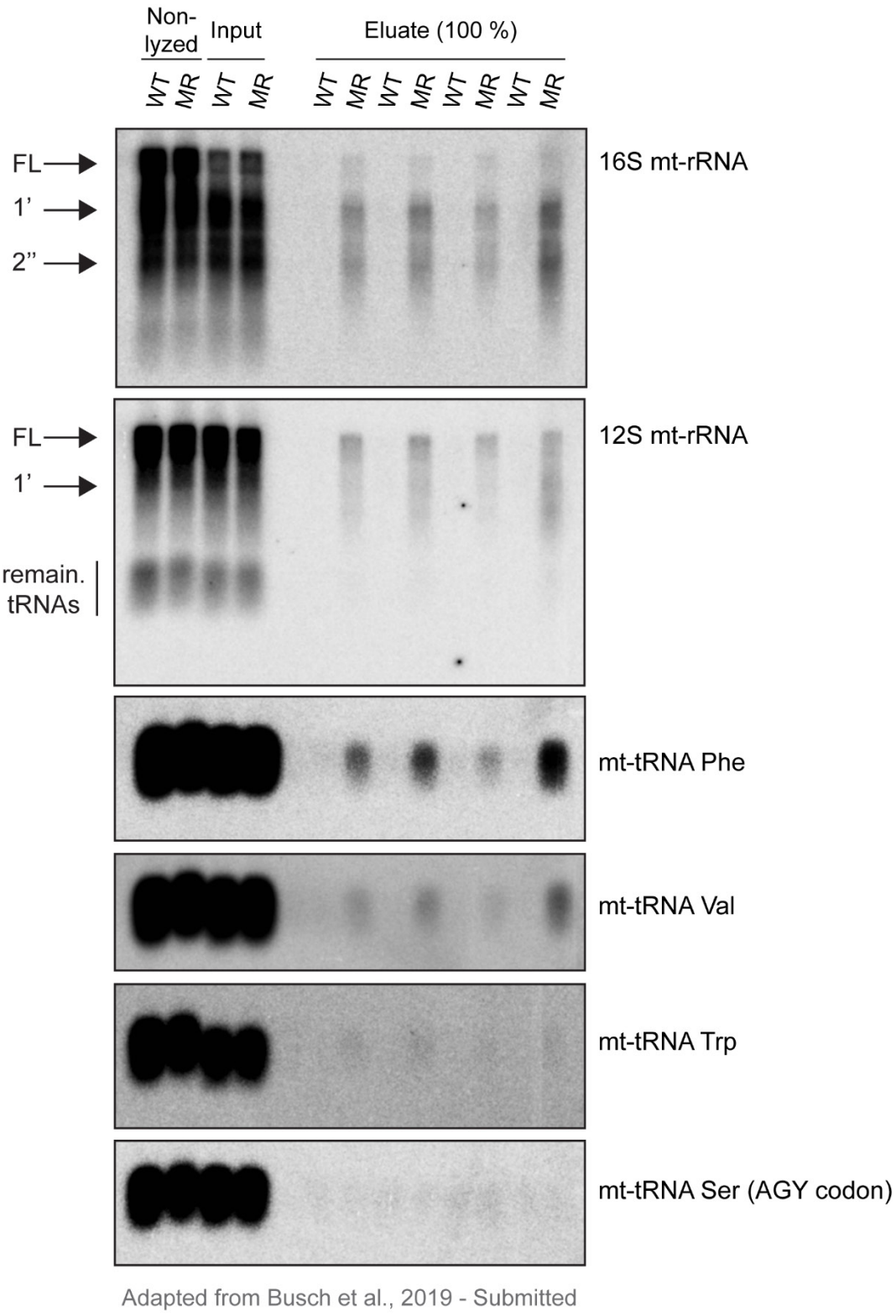

Figure 2.13 – Northern blot of mL62-FLAG co-immunoprecipitations from liver mitochondria of wild type and homozygous MitoRibo-Tag animals. Non-lyzed and input RNA was prepared before or after protein solubilization and corresponds to 10 % of

the total RNA obtained from 100 µg total mitochondrial protein. The eluate fractions from wild type (WT) and MitoRibo-Tag mice (MR) correspond to 100 % of the total RNA obtained after the mL62-FLAG co-immunoprecipitation. Full-length (FL) and cleaved transcripts (one and two prime) are indicated by the arrows. The northern blot was decorated with radioactive probes recognizing the mitochondrial 12S and 16S mt-rRNAs, and the phenylalanine (Phe), valine (Val), tryptophan (Trp) and serine (AGY codon) mt-tRNAs.

Similar to the protein analysis of the mL62-FLAG co-immunoprecipitation, the northern blot analysis shown in figure 2.13 demonstrates an efficient and specific co-purification of ribosomal mt-rRNAs and tRNAs. The northern blot further indicates that upon solubilization of mitochondria ribosomal RNAs are accessible for cleavage by an unknown RNase despite careful handling. Although not in the focus of the current study, the northern blot reveals that MitoRibo-Tag mice can also be used as a tool to study the mitoribosome RNA content.

2.2.4. Mitoribosome interactomes from different tissues reveal putative novel interacting proteins

The co-immunoprecipitation and western blot experiments demonstrated an efficient and specific purification of mitoribosomes from mitochondria of homozygous MitoRibo-Tag mice. Hence, mitochondria from different tissues of wild type and transgenic mice were prepared and applied to co-immunoprecipitation-coupled label-free quantitative mass spectrometry experiments (LFQ-MS/MS) as described in material and methods chapter 4.2.4. The comparison of different tissues is especially intriguing as the mitochondrial proteome composition strongly varies between tissues (Calvo et al., 2016; Mootha, Bunkenborg, et al., 2003; Pagliarini et al., 2008). Moreover, these compositional differences might contribute to the formation or increased detection probability of tissue-specifically enriched or exclusively formed complexes of mitoribosomes and associated factors, which will be denoted as mitoribosome-interacting proteins abbreviated MIPs in the following chapters of this thesis.

We initially aimed to investigate the mitoribosome interactome by proteomics in various tissues, including skeletal muscle, brain, heart, liver and kidney, which are among the tissues with the highest concentration of mitochondria according to the ratio of cytochrome *c* per gram of tissue (Pagliarini et al., 2008). During pilot experiments, only small amounts of mitochondria were obtained from brain and skeletal muscle tissue for gradient and co-immunoprecipitation experiments. In fact, brain tissue contains large amounts of fat and many hundreds of different cell types, such as glia and neuronal cells, which would make the sufficient and pure isolation of mitochondria from a certain cell type very laborious. Hence, preparation of mitochondria from brain for given purposes would have required pooling mitochondria from several dozen animals. Although very abundant skeletal muscle is usually treated mildly with trypsin to release interfibrillar mitochondria and obtain larger amounts of mitochondria. The treatment of muscle tissue with trypsin did not allow an efficient purification of mitoribosomes, despite addition of trypsin and protease inhibitors (data not shown). Hence, the analyses focused on the purification of mitoribosomes from heart, liver and kidney mitochondria. As mentioned earlier, mitochondria from heart, liver and kidney of wild type and homozygous MitoRibo-Tag mice were isolated by differential centrifugation and applied to the established mL62-FLAG co-immunoprecipitation. In contrast to the above shown co-immunoprecipitation in figure 2.12, proteins were eluted from the beads by partial on-beads digest using Trypsin prior mass spectrometry (Keilhauer et al., 2015). Changing the elution procedure was necessary as an excess of FLAG peptide necessary to elute proteins interfered and prevented the detection and identification of peptide spectra from many proteins, especially low abundant proteins (data not shown).

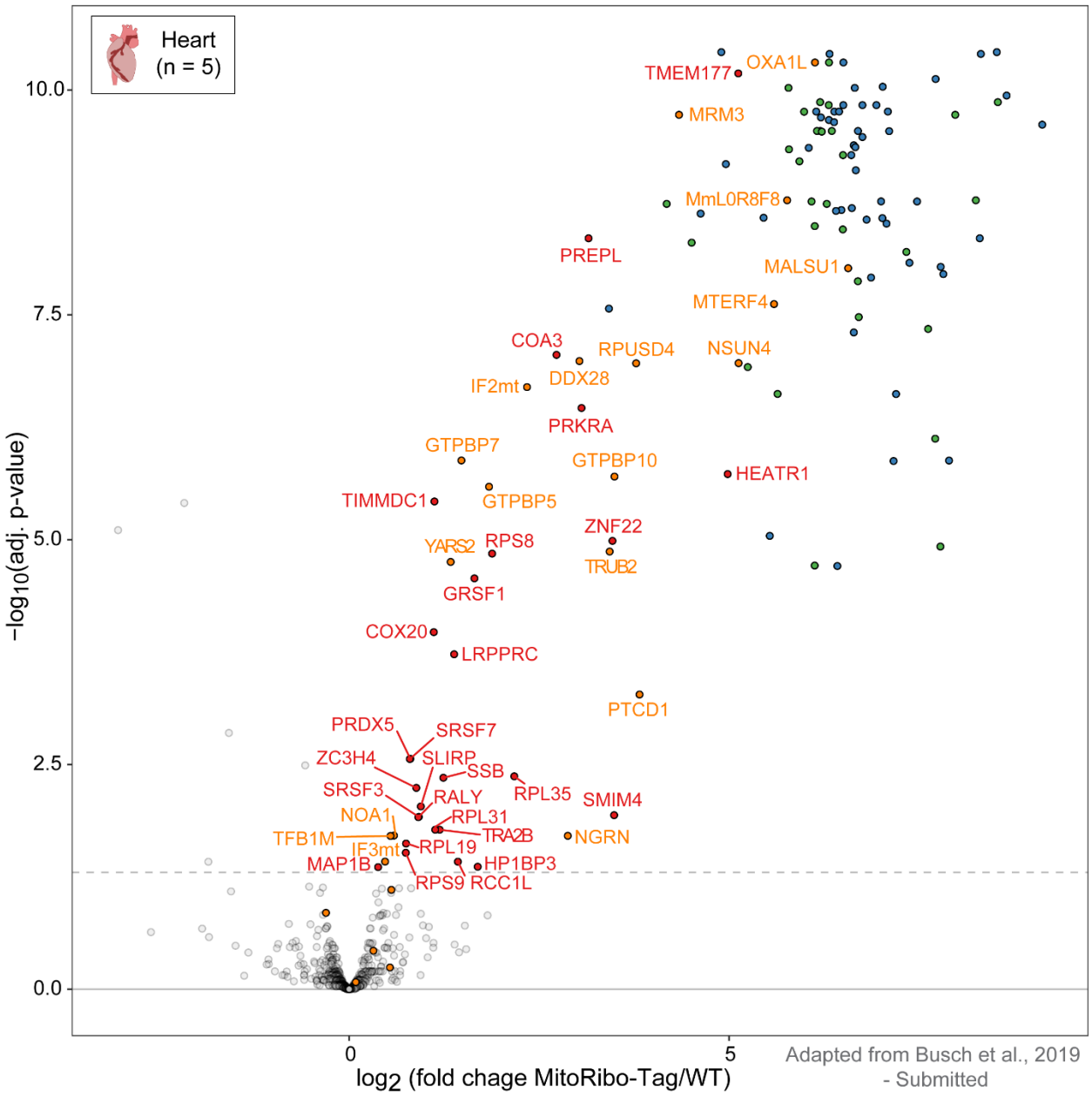

Figure 2.14 – Mitoribosome interactome in heart mitochondria using MitoRibo-Tag mice and proteomics. Crude mitochondria were isolated from homozygous mL62-FLAG MitoRibo-Tag and wild type (WT, negative control) mouse tissues and applied to co-immunoprecipitation-coupled LFQ-MS/MS. Dots represent mitoribosome 39S (blue), 28S (green), translation-associated (orange) and significantly enriched proteins (red). The x-axis indicates the enrichment expressed as $\log_2$ (fold change of MitoRibo-Tag/WT) and the y-axis shows the $-\log_{10}$(adjusted p-value). Proteins with an adjusted p-value of less than 0.05 (5 % false discovery rate, dashed line) were termed significant. The result represents five biological independent replicate experiments.

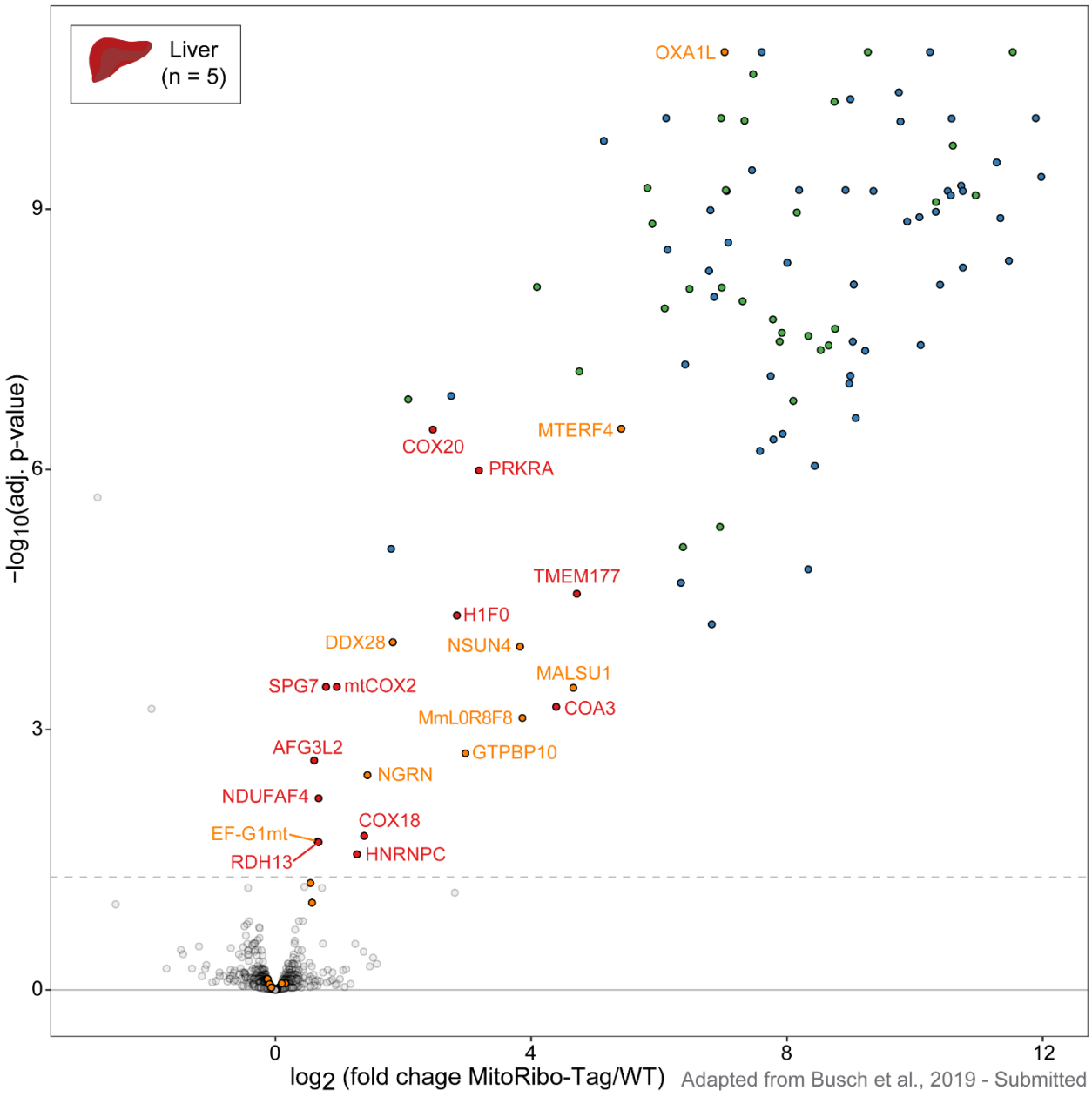

Figure 2.15 – Mitoribosome interactome in liver mitochondria using MitoRibo-Tag mice and proteomics. Crude mitochondria were isolated from homozygous mL62-FLAG MitoRibo-Tag and wild type (WT, negative control) mouse tissues and applied to co-immunoprecipitation-coupled LFQ-MS/MS. Dots represent mitoribosome 39S (blue), 28S (green), translation-associated (orange) and significantly enriched proteins (red). The x-axis indicates the enrichment expressed as $\log_2$ (fold change of MitoRibo-Tag/WT) and the y-axis shows the $-\log_{10}$(adjusted p-value). Proteins with an adjusted p-value of less than 0.05 (5 % false discovery rate, dashed line) were termed significant. The result represents five biological independent replicate experiments.

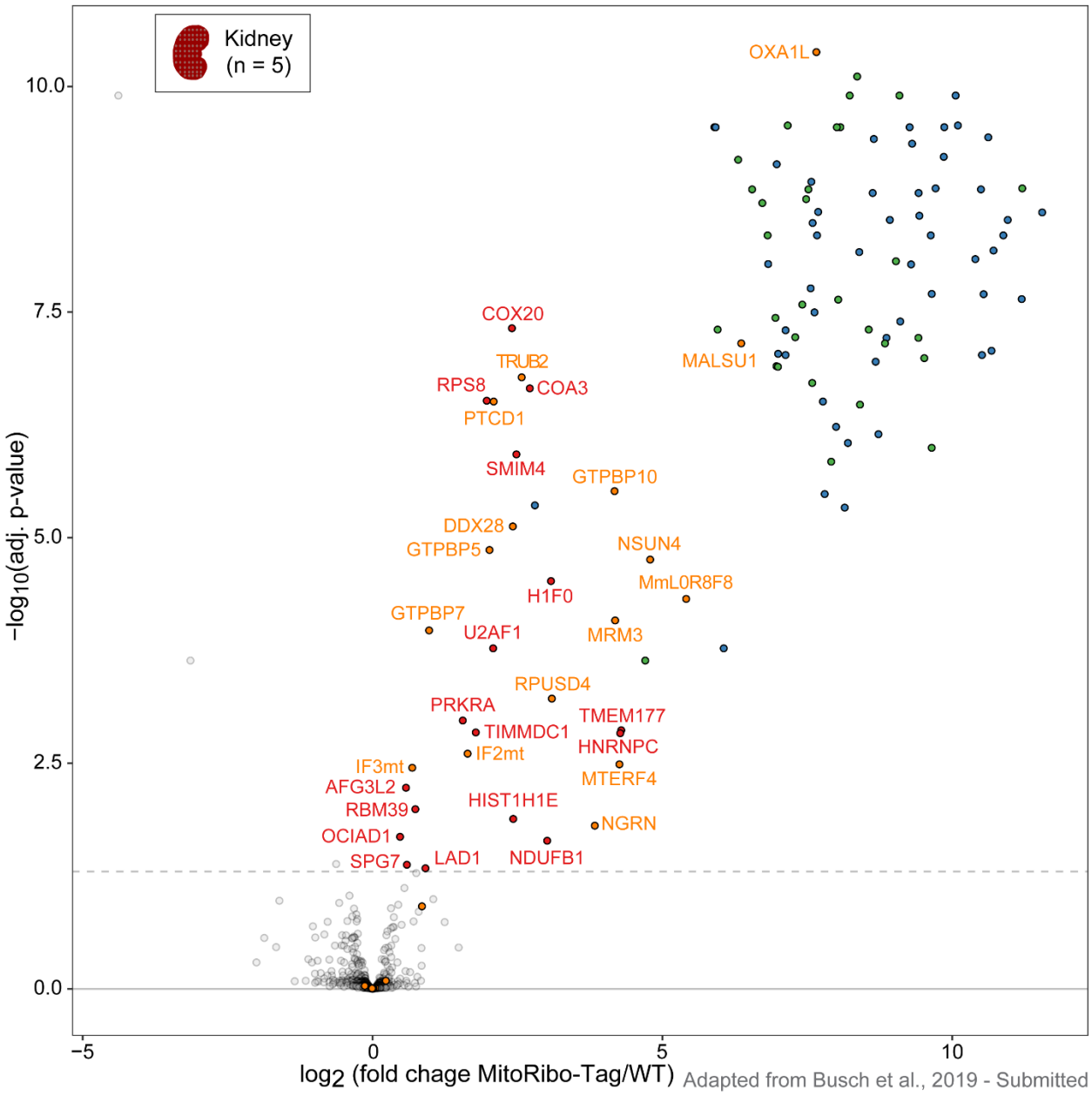

Figure 2.16 – Mitoribosome interactome in kidney mitochondria using MitoRibo-Tag mice and proteomics. Crude mitochondria were isolated from homozygous mL62-FLAG MitoRibo-Tag and wild type (WT, negative control) mouse tissues and applied to co-immunoprecipitation-coupled LFQ-MS/MS. Dots represent mitoribosome 39S (blue), 28S (green), translation-associated (orange) and significantly enriched proteins (red). The x-axis indicates the enrichment expressed as $\log_2$ (fold change of MitoRibo-Tag/WT) and the y-axis shows the $-\log_{10}$(adjusted p-value). Proteins with an adjusted p-value of less than 0.05 (5 % false discovery rate, dashed line) were termed significant. The result represents five biological independent replicate experiments.

The figures 2.14 to 2.16 illustrate and summarize the mL62-FLAG co-immunoprecipitation-coupled LFQ-MS/MS experiments from heart, liver and kidney mitochondria of MitoRibo-Tag mice. Our established mitoribosome purification procedure using MitoRibo-Tag mice allows the identification and quantification of 98.8 % of all mitoribosome proteins from heart, liver and kidney, representing in average 22 % improvement as 18 additional mitoribosome proteins are identified and quantified compared to the previously published procedures (Amunts et al., 2015; Greber et al., 2015; Richter et al., 2010). The mitoribosome proteins appear as a discrete protein cloud as they belong to the same complex. Surprisingly, bL36m, a protein joining late during assembly, was not quantified as the corresponding peptides rarely were detected in mitochondria of different tissues (figures 2.14 to 2.16; Brown et al., 2017). The MitoRibo-Tag mitoribosome composition data are in agreement with the published literature as wrongly annotated proteins like the α-ketoglutarate dehydrogenase subunit KGD4, formerly known as MRPS36, are not co-purified (Amunts et al., 2015; Brown et al., 2014; Heublein et al., 2014). In summary, the LFQ-MS/MS proteomic analysis of mitoribosomes purified from MitoRibo-Tag mouse tissues supports this model as a valuable tool to study mitoribosomes *in vivo*.

Our major interest in creating and using MitoRibo-Tag mice was to discover and characterize novel proteins related to the mitoribosome and translation. Hence, the LFQ-MS/MS data obtained from mitoribosome co-immunoprecipitations of heart, liver and kidney mitochondria were explored for novel proteins, not previously annotated to the mitoribosome, which are characterized by high enrichment and confidence values (figures 2.14 to 2.16). Strikingly, these analyses suggest tissue-specific compositional differences in the mitoribosome interactomes among heart, liver and kidney mitochondria, which may be explained to some extent by the large protein compositional differences between tissues (Mootha et al., 2003; Pagliarini et al., 2008). Mitoribosomes from heart co-purify with the largest number of putative MIPs, whereas mitoribosomes from liver seem to interact with much less MIPs despite the same purification procedure (figures 2.14 to 2.16). The mitoribosome interactome from kidney mitochondria share characteristics from heart and liver preparations and presents a medium number of identified MIPs. The data from MitoRibo-Tag mice verify several previously published *in vitro* studies, as for

example OXA1L, MALSU1 and MmL0R8F8 are the most co-enriched MIPs (Haque et al., 2010a; Haque et al., 2010b; Rorbach et al., 2012; Wanschers et al., 2012). Furthermore, the data demonstrate that the MTERF4:NSUN4 complex and the 16S mt-rRNA-protein module, consisting of NGRN and the pseudouridine synthases RPUSD4 and TRUB2, strongly interact with mitoribosomes under basal physiological conditions in mouse mitochondria (Antonicka et al., 2017; Arroyo et al., 2016; Cámara et al., 2011; Metodiev et al., 2014; Zaganelli et al., 2017). Moreover, the mitoribosome interactome from liver also allowed quantification of the mtDNA-encoded complex IV subunit mtCOX2, which indicates that the established purification procedure preserves mitoribosomes in a translationally-active state (figures 2.14 to 2.16). This assumption is also supported by co-enrichment and quantification of the translation initiation factors $IF2_{mt}$ and $IF3_{mt}$, which likely indicate the presence of mitoribosomes at the initiation phase (figures 2.14 to 2.16). Our data additionally indicate that several proteins of the mitochondrial RNA metabolism interact with mitoribosomes, *e.g.* PTCD1, MRM3, the RNA helicase DEAD-box helicase 28 (DDX28), the RNA-binding protein G-rich RNA sequence binding factor 1 (GRSF1), the LRPPRC:SLIRP complex and the tyrosyl-tRNA synthetase YARS2 (Antonicka et al., 2017; Jourdain et al., 2013; Perks et al., 2018; Ruzzenente et al., 2012; Tu & Barrientos, 2015). Furthermore, the MitoRibo-Tag *in vivo* data corroborate recent studies finding that the GTP-binding proteins GTPBP5, GTPBP7, GTPBP10, and NOA1 interact with mitoribosomes and are heavily involved in mitochondrial translation in differentiated tissues (Kim & Barrientos, 2018; Kolanczyk et al., 2011; Lavdovskaia et al., 2018; Maiti et al., 2018).

The comparison of interactomes from different tissues also shows that mitoribosomes dynamically interact with several inner mitochondrial membrane-associated or -integrated proteins, in addition to OXA1L (figures 2.14 to 2.16). This group of membrane-bound proteins includes regulators of respiratory chain assembly, such as the NADH:ubiquinone oxidoreductase assembly factor TIMM domain-containing protein 1 (TIMMDC1), the NADH:Ubiquinone oxidoreductase complex assembly factor 4 (NDUFAF4), as well as the cytochrome *c* oxidase assembly factors COA3/MITRAC12, COX20 and the transmembrane protein 177 (TMEM177; Guarani et al., 2014; Lorenzi et al., 2018; Richter-Dennerlein et al., 2016).

Additionally, our data reveal several novel (orphan) proteins as putative MIPs with unknown function to be involved in mitochondrial translation by binding to mitoribosomes, including the prolyl endopeptidase-like protein (PREPL), the retinol dehydrogenase 13 (RDH13), the small integral membrane protein 4 (SMIM4), and the zinc finger protein 22 (ZNF22; figures 2.14 to 2.16). Interestingly, some of these proteins reproducibly co-enrich with mitoribosomes in a tissue-specific manner, as RDH13 is exclusively quantified in liver and SMIM4 in heart and kidney, but not in liver mitoribosome preparations (figures 2.14 to 2.16). The co-enrichment of SMIM4 and ZNF22 with mitoribosomes is intriguing as these proteins are not predicted to be imported to mitochondria or identified in commonly used mitochondrial proteome databases (Calvo et al., 2016; Pagliarini et al., 2008). Surprisingly, the cytosolic ribosome constituent RPS8 was reproducibly co-enriched with mitoribosomes from heart and kidney mitochondria (figures 2.14 to 2.16). However, a transient expression of a FLAG-tagged RPS8 in human HeLa cells did not indicate that it has a mitochondrial localization (data not shown).

In summary, our data support previously proposed models in which mitochondrial transcription and RNA metabolism are hierarchically and spatially organized to regulate mitoribosome assembly and translation (Bogenhagen et al., 2014; Perks et al., 2018; Rackham et al., 2016). Regarding the latter, it was recently shown that yeast mitochondria harbor dynamically-formed RNA metabolism-mitoribosome and mitoribosome-respiratory chain assembly-complexes (Kehrein et al., 2015; Stoldt et al., 2018). The interactome analyses of mitoribosomes under basal physiological conditions in tissues of MitoRibo-Tag mice unravels several known proteins to dynamically link mitochondrial translation with respiratory chain assembly.

2.3. Generation and characterization of MitoRibo-Tag mice lacking MTERF4

To experimentally explore a condition of defective mitochondrial translation and to identify additional MIPs involved in mitoribosome assembly, MitoRibo-Tag mouse models with defective mitoribosome biogenesis, potentially accumulating subassembled intermediates, were generated. Initially, the idea was to target a late mitoribosome assembly stage at which the 28S and 39S mitoribosome subunits are stably formed but still bound to putative maturation factors. The conditional heart *Mterf4* knock-out mouse was chosen as an appropriate model system. The *Mterf4* knock-out mouse model is characterized by loss of monosomes and elevated levels of 28S and 39S mitoribosome subunits (Cámara et al., 2011). Accordingly, homozygous MitoRibo-Tag mice were bred with mice carrying a LoxP-flanked *Mterf4* gene to ultimately generate mice expressing mL62-FLAG but not MTERF4 (figure 2.17).

It should be stated that during the course of this work, several other knock-out mouse models lacking factors required for RNA stability or mitoribosome assembly, were generated in the MitoRibo-Tag background. Namely, we combined MitoRibo-Tag with MTERF3 (39S biogenesis impairment), TFB1M and NSUN4 (defective early and a late steps of 28S biogenesis), as well as conditions mirroring misbalanced mitochondrial RNA levels by removal of LRPPRC or SLIRP (data not shown; Lagouge et al., 2015; Metodiev et al., 2009; Metodiev et al., 2014; Park et al., 2007; Ruzzenente et al., 2012; Wredenberg et al., 2013). Due to the time limitation, the analyses presented in this thesis were focused on *Mterf4* knock-out MitoRibo-Tag mice (Cámara et al., 2011).

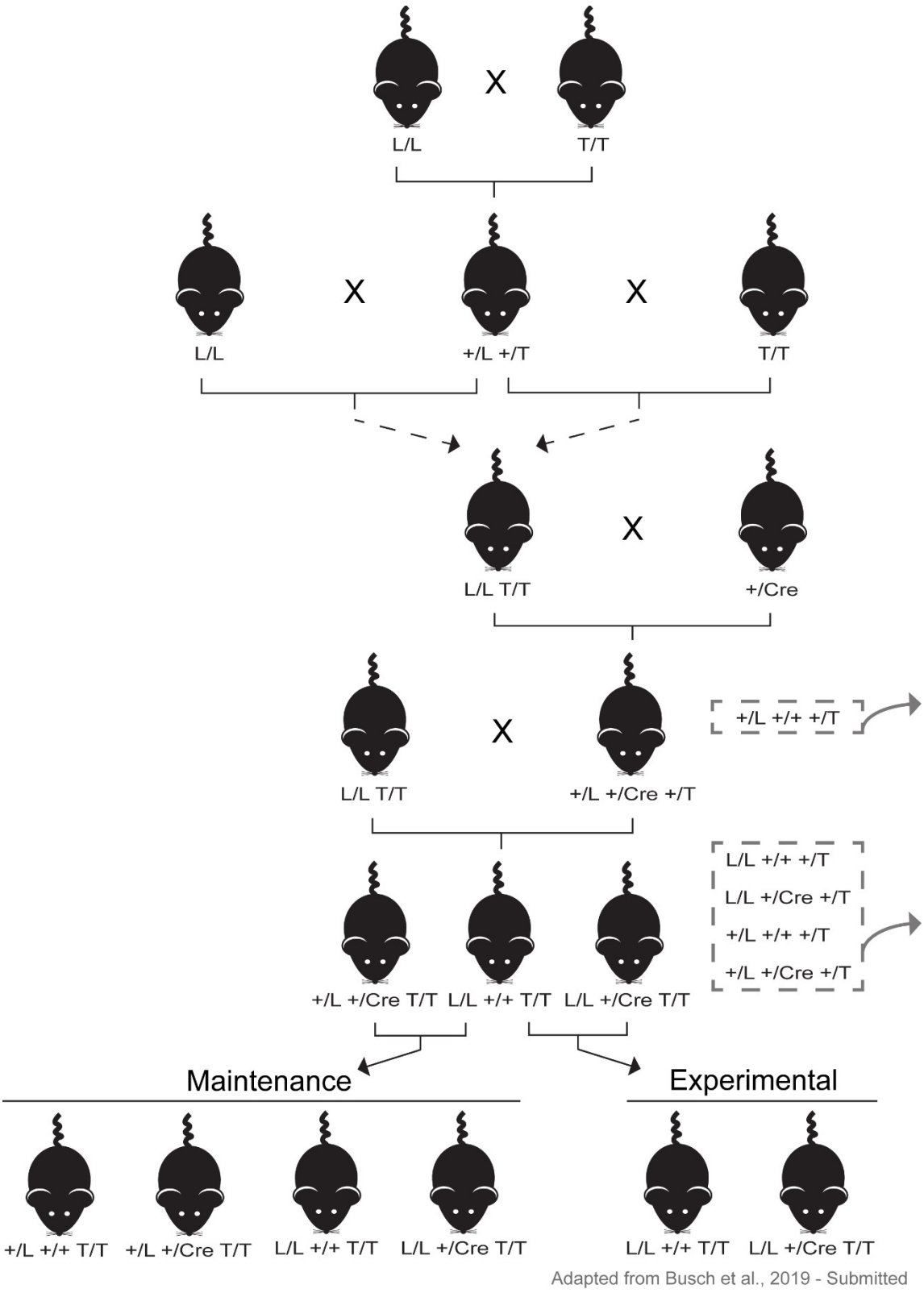

Figure 2.17 – Breeding strategy to generate MitoRibo-Tag *Mterf4* knock-out mice. Genotypes of LoxP-flanked (L), *mL62-Flag* (T) MitoRibo-Tag knock-in and *Ckmm-Cre*

(*Cre*) alleles are indicated. (X) indicates animal breeding. The dashed boxes highlight animal genotypes not further used during breeding.

As illustrated in figure 2.17, several breeding steps were required to generate animals of the genotypes L/L; +/+; T/T and +/L; +/*Cre*; T/T, which were further bred to obtain conditional heart and skeletal muscle specific *Mterf4* knock-out animals carrying homozygous alleles of *mL62-Flag* (L/L; +/*Cre*; T/T) and controls (L/L; +/+; T/T). It should be mentioned that for the matings denoted as experimental matings only knock-out male mice were bred with control females, because knock-out females would not survive the pregnancy due to the progressive cardiomyopathy. In agreement to Cámara et al. (2011), MitoRibo-Tag mice lacking *Mterf4* have increased steady-state levels of 28S and 39S proteins and die around an age of 20 weeks due to severe mitochondrial cardiomyopathy (figure 2.18; Cámara et al., 2011).

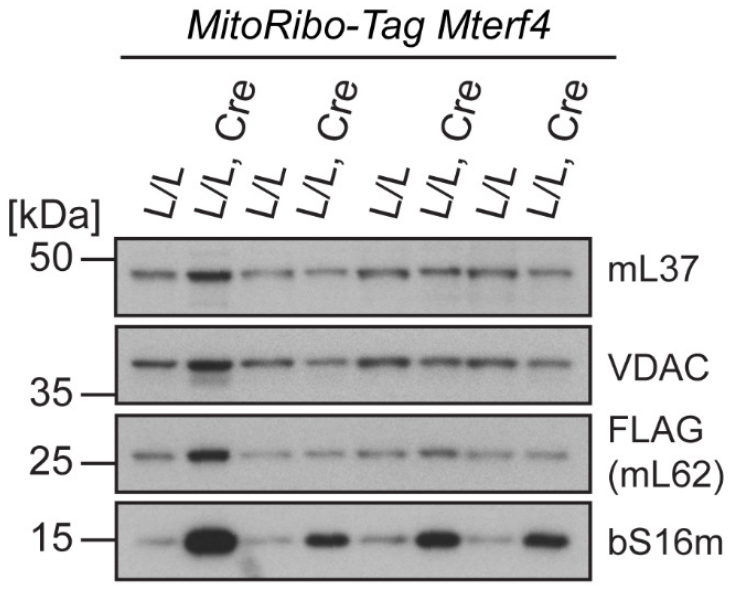

Figure 2.18 – Mitoribosome protein steady-state levels are increased in *Mterf4* knock-out MitoRibo-Tag mice. Mitochondria were prepared by differential centrifugation from *Mterf4* control (L/L; +/+; T/T abbreviated L/L) and knock-out (L/L; +/Cre; T/T abbreviated L/L, Cre) mice followed by western blot against mL37, mL62-FLAG (39S large subunit), bS16m (28S small subunit) and VDAC as a loading control.

2.3.1. *Mterf4* knock-out MitoRibo-Tag mice accumulate a mitoribosome biogenesis intermediate

The interactome analysis was focused on older knock-out animals, because we assumed that these animals would have a homogenous population of mitoribosome biogenesis intermediates contrary to younger knock-out animals. The reason for that lays within the relatively long half-life and stability of mitochondrial protein complexes, *i.e.* younger knock-out animals at an early stage might harbor a mixed population of functional mitoribosomes and putatively non-functional intermediate complexes (Bogenhagen et al., 2018; McShane et al., 2016). The heterogeneous mixtures of different complexes in different biological replicates or animals might introduce variable experimental results. Hence, mitochondria from knockout (L/L; +/*Cre*; T/T) and control (L/L; +/+; T/T) *Mterf4* MitoRibo-Tag mice animals between 18 and 20 weeks of age were isolated and applied to co-immunoprecipitation-coupled proteomics.

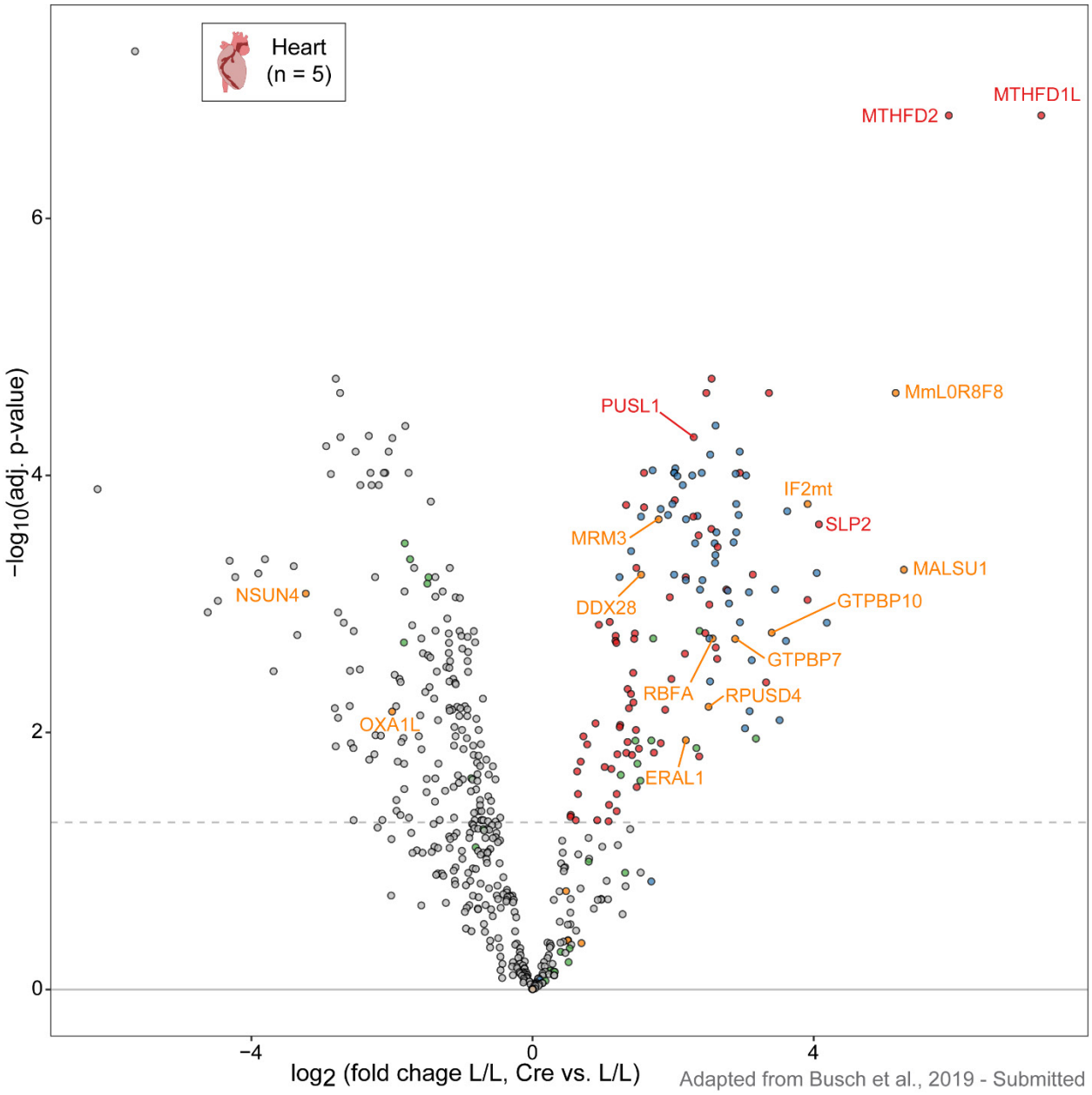

Figure 2.19 – Purification and LFQ-MS/MS analysis of the mitoribosome biogenesis intermediate formed in the absence of *Mterf4* in MitoRibo-Tag mice. Crude mitochondria were isolated from *Mter4$^{L/L}$; +/Cre; T/T* (L/L, Cre; knock-out) and *Mterf4$^{L/L}$; +/+; T/T* (L/L; control) MitoRibo-Tag mice and applied to FLAG-co-immunoprecipitation-coupled LFQ-MS/MS. Dots represent mitoribosome 39S (blue), 28S (green), translation-associated (orange) and significantly enriched proteins (red). The x-axis indicates the enrichment expressed as $\log_2$ (fold change of MitoRibo-Tag/WT) and the y-axis shows the $-\log_{10}$(adjusted p-value). Proteins with an adjusted p-value of less than 0.05 (5 % false discovery rate, dashed line) were termed significant. The result represents five biological independent replicate experiments.

As expected the mass spectrometry-based determination of the *Mterf4* knock-out biogenesis intermediate reveals that mostly 39S constituents are co-enriched with mL62-FLAG, which is in agreement with the study from Cámara et al. (2011), showing dissociation of 28S and 39S subunits. Interestingly, besides the 39S constituents a large number of known and putative mitoribosome assembly factors are co-enriched with the 39S biogenesis intermediate in MitoRibo-Tag *Mterf4* knock-out animals including DDX28, ERAL1, GTPBP7, GTPBP10, MALSU1, MmL0R8F8, MRM3, RBFA and RPUSD4 (figure 2.19). The result further indicates that the initiation factor $IF2_{mt}$, similar to MALSU1, tightly binds to the mitoribosome intermediate complex formed in the absence of *Mterf4* (figure 2.19). We also found several other mitochondrial proteins co-enriched, including the respiratory chain subunits NDUFB5 and NDUFB6 of complex I, UQCRH and UQCR10 of complex III and ATP5C1 and ATP5D of complex V, the Stomatin-like protein 2 (SLP2), and the tetrahydrofolate metabolism enzymes methylenetetrahydrofolate dehydrogenase 1-like (MTHFD1L) and methylenetetrahydrofolate dehydrogenase 2 (MTHFD2; figure 2.19). The latter seem highly enriched but probably do not directly bind to the mitoribosomes, as they are highly upregulated due to strong secondary responses caused by the loss of *Mterf4* also observed in other mouse models of mitochondrial dysfunction (Kühl et al., 2017). These cellular responses likely contribute to increased mitochondrial biogenesis and the cardiac phenotype, which also coincide with a plethora of secondary effects and changes in the cytosolic proteome as observed by putatively false-positive co-enrichment of cytosolic ribosome subunits RPL31, RPL26, RPL35, RPL32, RPL18A, RPL27 and RPS8 due to their increased steady-state levels (figure 2.19; Kühl et al., 2017).

Surprisingly, among the most co-enriched proteins, an uncharacterized protein called pseudouridylate synthase-like 1 (PUSL1) was identified with very high confidence (figure 2.19). It is interesting to note that PUSL1 was not identified as a putative MIP in our previous co-immunoprecipitation analyses from heart mitochondria under basal conditions, which may suggest that the protein binds either transiently to an mitoribosome biogenesis intermediate or specifically before MTERF4 promotes mitoribosome subunit joining (figures 2.14 to 2.16 and figure 2.19; Cámara et al., 2011). Furthermore, PUSL1

seems to be specifically upregulated in models with defective translation or mitoribosome assembly, *e.g. Lrpprc* and *Mterf4* knock-out mice (data not shown; Kühl et al., 2017).

2.4. PUSL1 is a novel mitochondrial matrix protein

As mentioned above PUSL1 was specifically identified as a putative MIP binding to a mitoribosome biogenesis intermediate formed in the absence of *Mterf4*. PUSL1 was recently shown to localize to mitochondria in two high-throughput studies (Calvo et al., 2016; Pagliarini et al., 2008; Zaganelli et al., 2017). Despite the general mitochondrial localization of PUSL1, detailed insights into the submitochondrial localization are lacking. Initially, data about the amino acid sequences of human and mouse PUSL1 from the UniProt database were extracted and *in silico* analyzed with MitoProtII v1.101 and the alignment tool Clustal omega (summarized in figure 2.20; Bateman et al., 2017; Claros & Vincens, 1996; Mitchell et al., 2018; Sievers et al., 2011). The *in silico* analyses revealed that PUSL1 is conserved among metazoans and that the amino acid sequences of mouse and human PUSL1 are highly similar (figure 2.20).

A

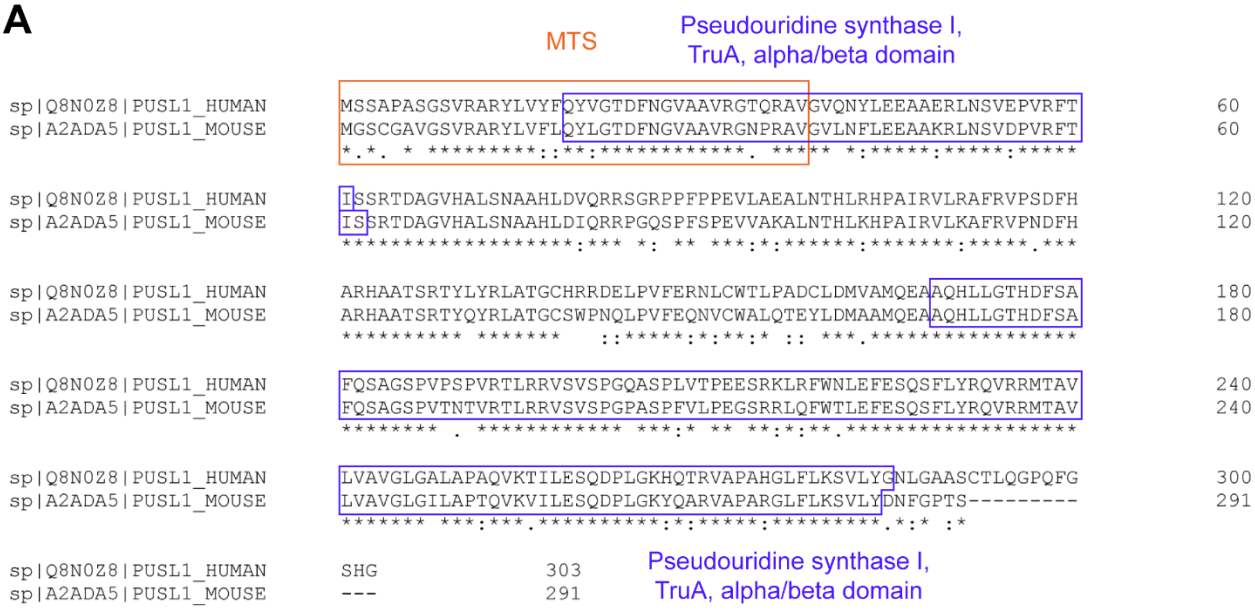

B

Amino acid position	MTS (1 -38)	TruA domain I	TruA domain II
Human PUSL1	*40.56 %*	19 - 121	168 - 284
Mouse PUSL1	*29.45 %*	19 - 122	168 - 285

Adapted from Busch et al., 2019 - Submitted

Figure 2.20 – Amino acid sequence alignment of human and mouse PUSL1. (A) The amino acid alignment was carried out with the CLUSTAL omega (1.2.4) and the domain predictions for the mitochondrial targeting signal (MTS, orange) and TruA-like pseudouridine synthase domains (blue) were made with MitoProtII and InterPro. The *in silico* predictions are summarized in **(B)**.

The amino acid sequence alignment of human (Ensembl ID: ENST00000379031.9 and NCBI gene ID: 126789) and mouse (Ensembl ID: ENSMUSG00000051557 and NCBI gene ID: 433813) PUSL1 shown above indicates that human and mouse PUSL1 harbor very similar predicted mitochondrial targeting sequences within the first 38 amino acids with a putative mitochondrial processing peptidase-cleavage site after amino acid 38 (figure 2.20.A and B). Moreover, both PUSL1 variants share two highly conserved pseudouridine synthase domains at the N- and the C-termini, which are homologous to the bacterial pseudouridine synthase TruA (tRNA pseudouridine synthase A) from *E. coli*. The only obvious difference between human and mouse PUSL1 is that the mouse variant

has a truncated C-terminus being 12 amino acids shorter than human PUSL1 (figure 2.20). Since human and mouse PUSL1 are very similar, the further biochemical characterization was focused on human PUSL1 (figures 2.21 and 2.23). Unfortunately, commercial antibodies were not reproducibly working and accompanied by many cross-reacting bands, not allowing an adequate biochemical localization (figure 2.25). To this end, the cDNA encoding human *PUSL1* harboring additionally a sequence encoding the FLAG-tag at C-terminus was cloned into the pcDNA5/FRT/TO vector. To verify the localization of PUSL1 and to assess if the construct can be used to express PUSL1-FLAG, human HeLa cells were transiently transfected and applied to immunofluorescence imaging analyses.

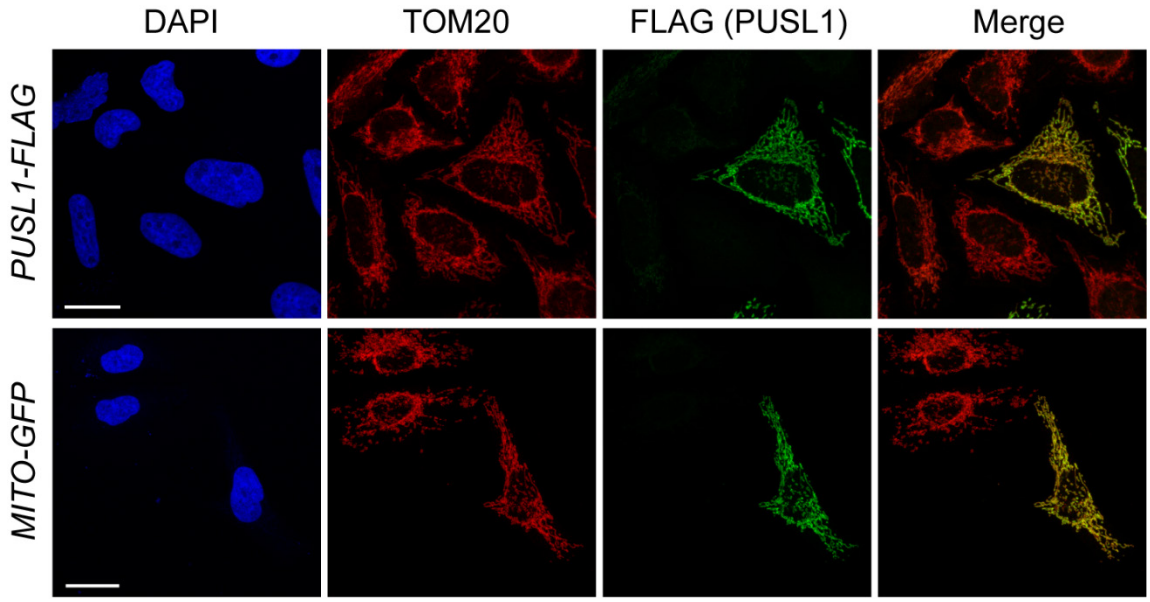

Figure 2.21 – Immunofluorescence analysis of human HeLa cells transiently transfected with a pcDNA5/FRT/TO vector harboring *PUSL1-FLAG* or mitochondrial-targeted GFP. The cover slips were decorated with anti-TOM20, as mitochondrial marker, and anti-FLAG tag antibodies. DNA was stained with DAPI. The scale bars correspond to 20 µm. The result is representative of three replicates.

The immunofluorescence experiments verify earlier observations finding that PUSL1 is a mitochondrial protein (Calvo et al., 2016; Pagliarini et al., 2008; Zaganelli et al., 2017).

To elucidate the exact submitochondrial localization of PUSL1 and to circumvent the lack of an appropriate antibody, we used the pcDNA5/FRT/TO-*PUSL1-FLAG* vector to generate human cells that inducibly and stably can express FLAG-tagged PUSL1. Essentially, the pcDNA5/FRT/TO-*PUSL1-FLAG* vector was transfected into human Flp-In TREx HEK293 cells (HEK293T), which harbor a genome-integrated FLP recombination site as schematically illustrated in figure 2.22. Co-transfection of pcDNA5/FRT/TO-*PUSL1-FLAG* with a vector called *pOG44*, harboring the FLP recombinase gene, should induce the stable integration the engineered *PUSL1-FLAG* into the cell genome by a homologous recombination event. Moreover, the integrated locus would be controlled by the tetracycline repressor, *i.e.* addition of tetracycline to the culture media induces the expression of the protein-of-interest. Initially, transfected cells were selected by incubation in culture media containing the antibiotics blasticidin S and hygromycin B, which should eradicate all non-transfected cells by inhibiting the cytosolic translation. Following selection of transfected clones and expansion of the putative PUSL1-FLAG cell line, tetracycline was titrated to determine the minimal concentration needed to induce the expression of PUSL1-FLAG (figure 2.22.B).

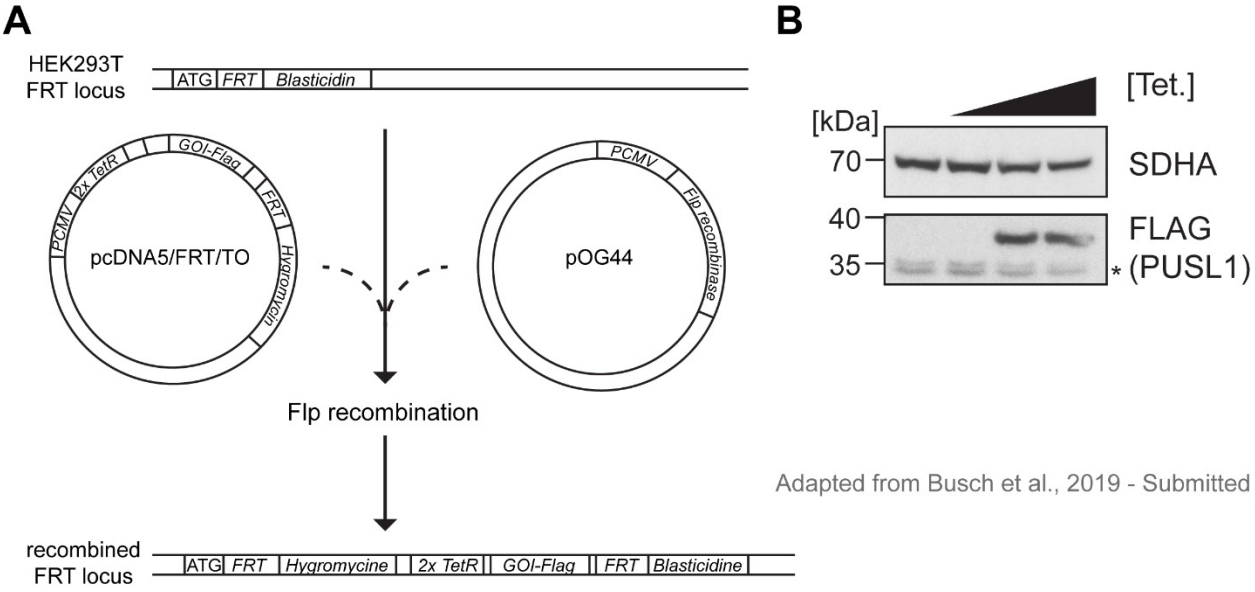

Figure 2.22 – Generation of a Flp-In TREx HEK293 cell line to inducibly express PUSL1-FLAG. (A) Schematic representation of the procedure to generate a Flp-In TREx

HEK293 expression cell line (HEK293T). The following abbreviations are used: FLP recombination site (FRT), gene-of-interest (GOI), tetracycline repressor (TetR) and cytomegalo virus promotor (PCMV). **(B)** Western blot analysis of HEK293T PUSL1-FLAG cells cultured for 24 hours in the presence of 10, 50 or 100 ng/ml tetracycline-supplemented (Tet.) culture media. Total cellular protein was extracted and analyzed by western blot against the FLAG-tag and SDHA (loading control).

The tetracycline titration experiment shown in figure 2.22 demonstrates the successful generation of a HEK293T cell line that inducibly expresses PUSL1-FLAG. The cells were expanded to isolate mitochondria and determine the submitochondrial localization of PUSL1.

Firstly, we determined if PUSL1 is a soluble, peripherally membrane-associated or integral membrane protein by extracting proteins with sodium carbonate (Fujiki et al., 1982a; Fujiki et al., 1982b). The experiment is based on varying extraction properties of sodium carbonate at different pH values, *i.e.* a higher (basic) pH yields a stronger extraction. At pH 10.5 soluble proteins like cytochrome *c* are completely extracted, but membrane-associated proteins like TIM44 or membrane-integrated proteins like VDAC remain in the membrane pellet fraction. At a pH of 10.5, PUSL1 remains, similar to TIM44, in the membrane pellet fraction (figure 2.23.A). The majority of PUSL1 is extracted using sodium carbonate at a pH of 11.5, whereas a minor pool of PUSL1 remained in the pellet fraction even at a pH of 12.5 (figure 2.23.A). This indicates that PUSL1 is a peripherally membrane-associated mitochondrial protein.

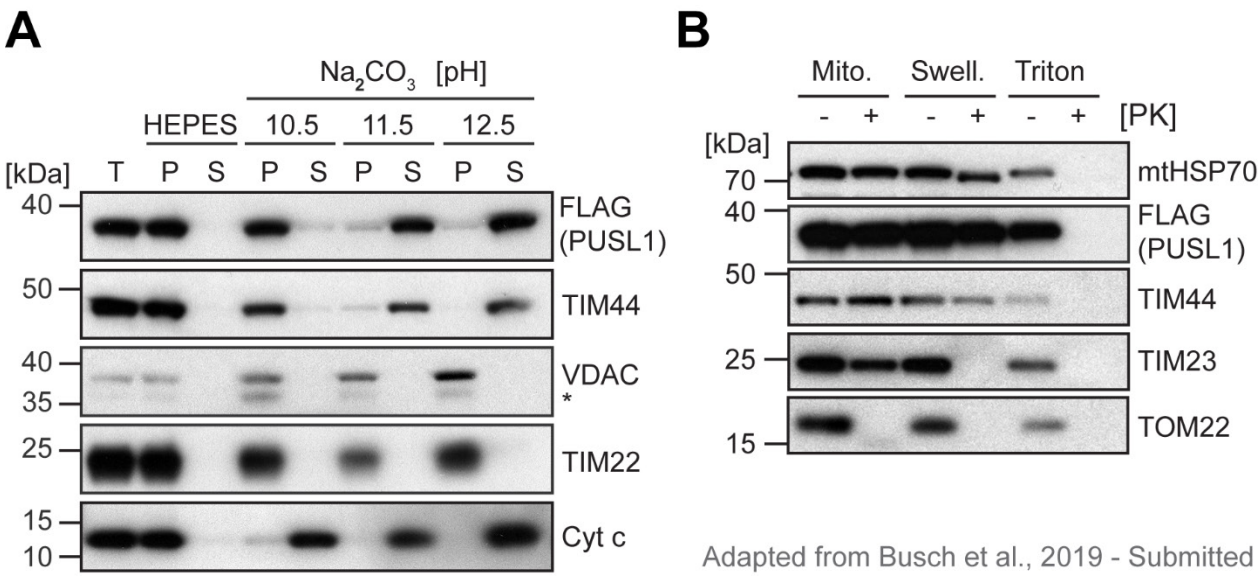

Figure 2.23 – Submitochondrial localization of PUSL1 in mitochondria from human cultured cells. (A) Sodium carbonate extraction assay of mitochondrial proteins. Mitochondria isolated from HEK293T cells expressing PUSL1-FLAG were pelleted and in resuspended in 20 mM HEPES-KOH pH 7.4 (HEPES) or 200 mM sodium carbonate (Na_2CO_3; T - Total protein fraction, S - soluble proteins, and P – membrane pellet). **(B)** Protease protection assay of isolated mitochondria (Mito. – crude mitochondria, Swell. – hypotonic buffer-swollen mitochondria, Triton – 1 % triton X-100-lyzed mitochondria) in the presence or absence of Proteinase K (PK)). Resuspended mitochondria treated for 10 min on ice with (+) or without (-) with 25 µg/ml Protease K. The protein fractions were precipitated with TCA and analyzed by SDS-PAGE and western blot against indicated proteins. Results is representative for three replicates.

A high-throughput study applying an engineered mitochondrial matrix-targeted ascorbate peroxidase indicated that PUSL1 is imported into the mitochondrial matrix (Rhee et al., 2013). Nevertheless, the submitochondrial localization of PUSL1 was investigated by means of a canonical biochemical protease protection assay. To this end, freshly isolated mitochondria from the HEK239T PUSL1-FLAG expression cell line were incubated in the presence or absence of Proteinase K to digest proteins exposing accessible domains towards the externally added protease. As shown in figure 2.23.B, PUSL1 seems to be protected by the inner membrane and imported into the mitochondrial matrix, because the protein is protected from degradation despite absence of the outer mitochondrial membrane, whereas the outer membrane protein TOM22 or the inter-membrane space-

exposed inner membrane protein TIM23 are degraded (figure 2.23.B). PUSL1 is degraded if both the outer and inner mitochondrial membrane are disrupted with a triton X-100 buffer and shows similar properties as the mitochondrial matrix protein mtHSP70 or the integral inner membrane TIM44 protein (figure 2.23.B).

In summary, the biochemical localization experiments suggest that PUSL1 is an inner membrane-associated mitochondrial matrix protein, based on the findings that it harbors a putative N-terminal mitochondrial targeting signal, is solubilized with sodium carbonate at pH 11.5 and protected from degradation if the inner membrane is intact (figure 2.23 and 2.24).

2.4.1. PUSL1 interacts with the mitoribosome

Next, we sought out to determine the composition of PUSL1 complexes. To this end, we expressed PUSL1-FLAG in HEK293T cells, isolated mitochondria and performed co-immunoprecipitation-coupled mass spectrometry (figure 2.24).

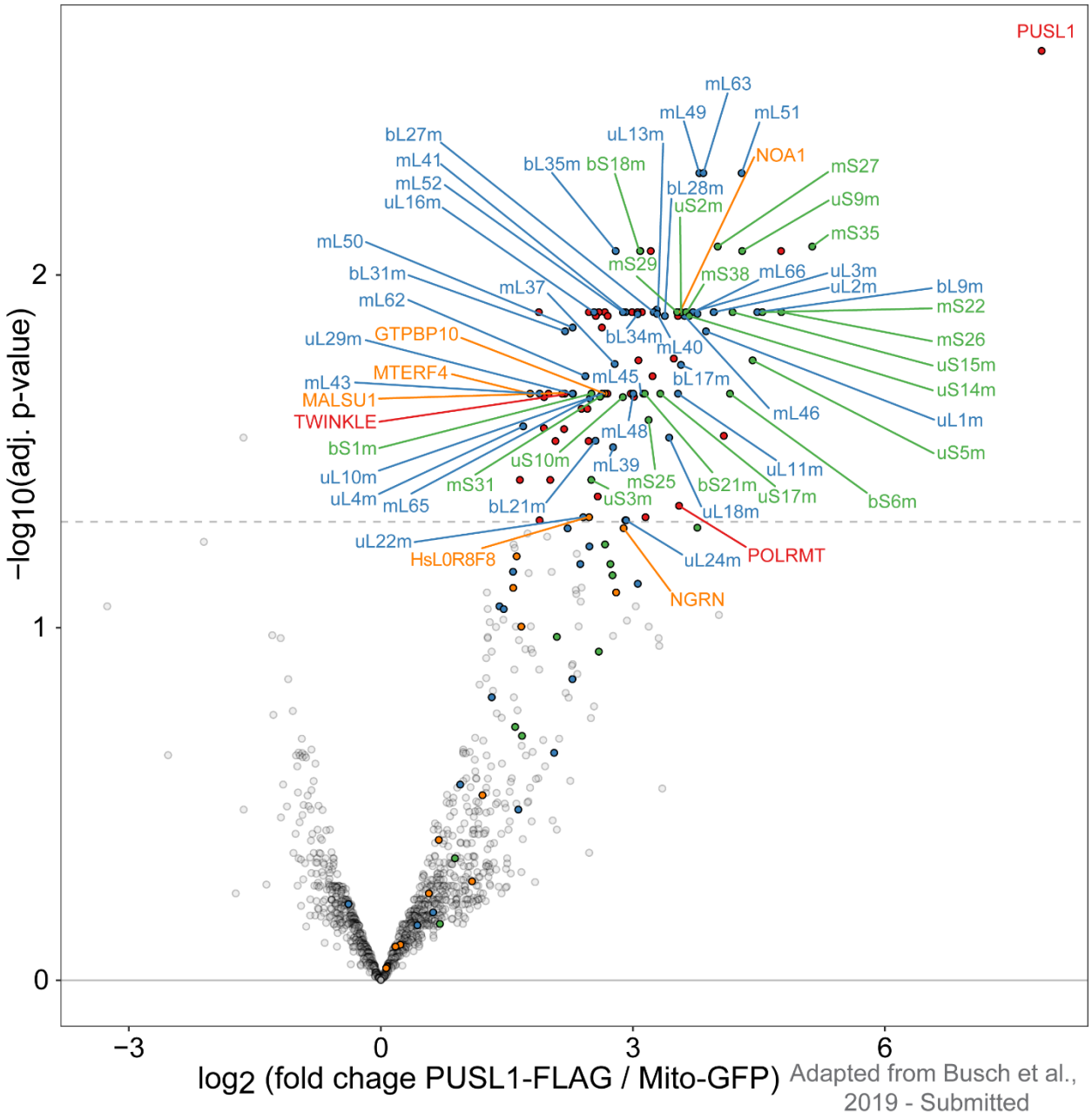

Figure 2.24 – Determination of PUSL1-FLAG associated complexes in human mitochondria. Mitochondria from HEK293T cells expressing PUSL1-FLAG were isolated and applied to FLAG co-immunoprecipitation-coupled LFQ-MS/MS. Dots represent mitoribosome 39S proteins (blue), 28S proteins (green), translation-associated factors (orange) and other significantly enriched proteins (red). The x-axis indicates the enrichment expressed as $\log_2$ (fold change of PUSL1-FLAG/Mito-GFP) and the y-axis shows the $-\log_{10}$(adjusted p-value). Proteins with an adjusted p-value of less than 0.05 (5 % false discovery rate, dashed line) were termed significant. The result represents four replicates of PUSL1-FLAG and three Mito-GFP replicates.

As indicated by figure 2.24, PUSL1 indeed interacts with the mitoribosome or a putative biogenesis intermediate, as suggested by the mL62-FLAG co-immunoprecipitation experiments from *Mterf4* knock-out MitoRibo-Tag mice (figure 2.24). Many mitoribosome proteins are co-enriched and interestingly these belong to the 28S and 39S subunits, suggesting that PUSL1 engages with a late stage mitoribosome biogenesis intermediate, under basal cell culture conditions (figure 2.24). In addition to the mitoribosome proteins, PUSL1-associated complexes also interact to some degree with the mitoribosome assembly factors GTPBP10, HsL0R8F8, MALSU1, MTERF4, and NOA1 (figure 2.24; Arroyo et al., 2016; Brown et al., 2017; Kolanczyk et al., 2011). Furthermore, some of the co-enriched proteins belong the mtDNA transcription and replication machineries represented by the mitochondrial RNA polymerase (POLRMT) and the mtDNA helicase Twinkle (figure 2.24).

It is interesting to note that the PUSL1 interactome from HEK293T mitochondria and the composition of the mitoribosome biogenesis intermediate found in *Mterf4* knock-out MitoRibo-Tag mice partially overlap, because GTPBP10, L0R8F8 and MALSU1 are significantly co-enriched in both experimental systems (figures 2.19 and 2.24).

2.4.2. PUSL1 is required for normal mitochondrial translation

As PUSL1 is an uncharacterized mitoribosome-interacting protein (MIP) it was important to investigate if it is required for mitochondrial translation. For this purpose, two commercially available siRNAs against human *PUSL1* were obtained and transfected using Lipofectamine RNAiMAX into the HEK293T cells. To verify the knock-down efficiency, mitochondria from siRNA-treated HEK293T cells were isolated and analyzed by standard western blot analysis using an antibody against the endogenous PUSL1 (figures 2.25).

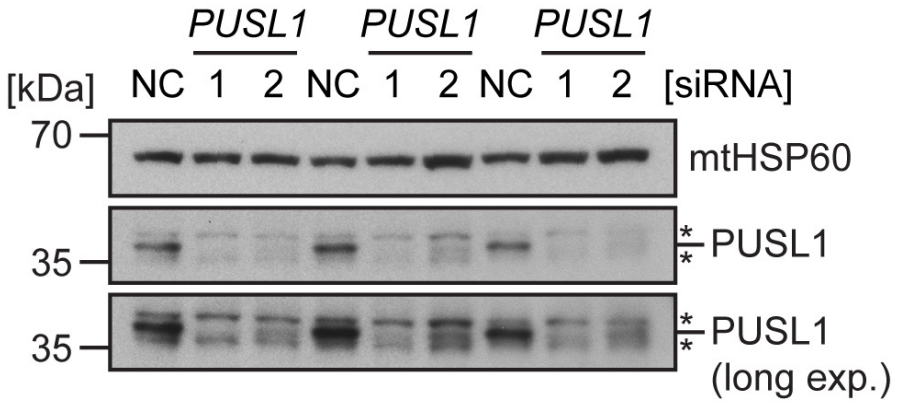

Adapted from Busch et al., 2019 - Submitted

Figure 2.25 – Western blot analysis of PUSL1 steady-state levels upon siRNA-mediated knock-down in HEK293T mitochondria. HEK293T cells were seeded and transfected after 24 h with a negative control siRNA (NC) or one of two siRNAs against *PUSL1* (1 and 2). After three days, the transfection was repeated and cells were incubated for additional two to three days prior isolation of mitochondria. The western blot shows three independent and replicate siRNA treatments. The PUSL1 western blot shows a shorter and longer exposure to highlight the PUSL1-specific and cross-reacting bands highlighted with asterisks (*). Mitochondrial HSP60 is used as loading control.

The western blot from HEK293T mitochondria shows that both applied *PUSL1*-targeting siRNAs downregulate PUSL1 in mitochondria (figure 2.25). *PUSL1* siRNA1 completely abolished PUSL1 expression, whereas 10 to 20 % of PUSL1 remain using *PUSL1* siRNA2 (figure 2.25).

In parallel, *in cellulo* [^{35}S]-methionine labeling experiments were performed with *PUSL1* siRNA-treated cells. For this purpose, cells were shortly incubated in methionine- and cysteine-depleted culture media and subsequently mixed with the radioactively labeled [^{35}S]-methionine, which is incorporated into *de novo* synthesized proteins. A cell line where an administered siRNA specifically targets a gene required for translation would lead to a less efficient or abolished incorporation of [^{35}S]-methionine in contrast to cells which are treated with a non-targeting control siRNA. To distinguish the incorporation of [^{35}S]-methionine into mtDNA-encoded proteins from translation in the cytosol, cytosolic ribosomes were inhibited with the antibiotic emetine.

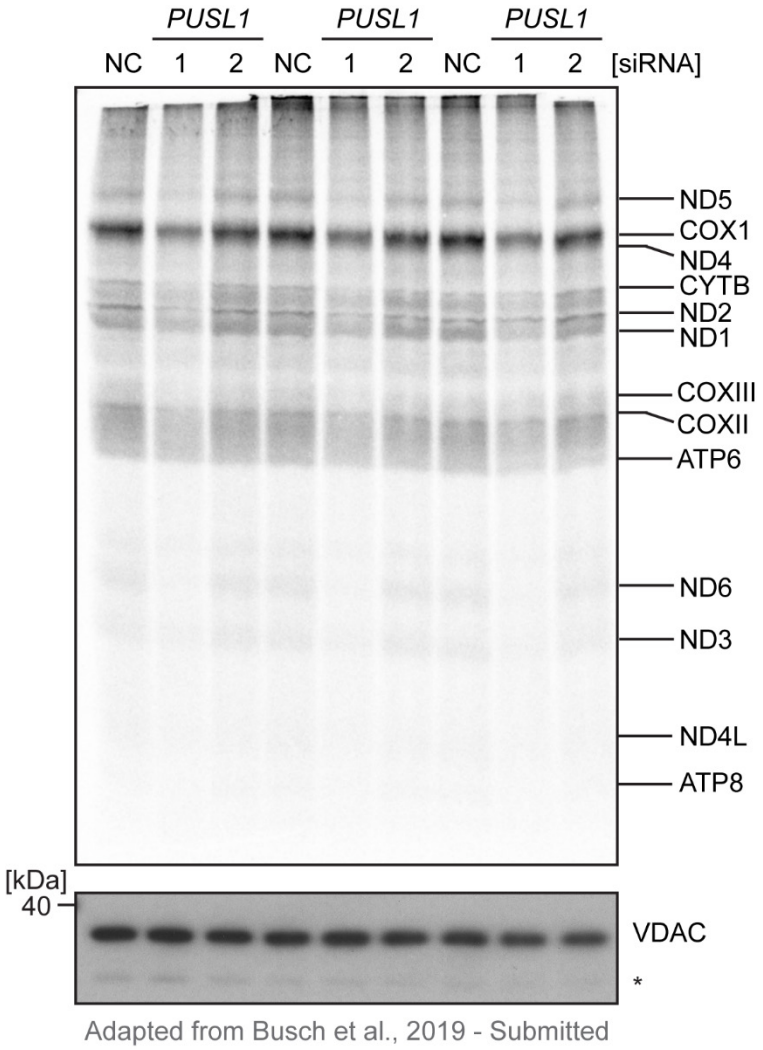

Figure 2.26 – *In cellulo* translation assay using siRNA-treated HEK293T cells analyzed on a SDS-PAGE. 25 µg total cellular protein lysate of each approach were loaded onto a 17 % SDS-PAGE gel, followed by fixation, gel drying and exposure to a phosphoimager screen. The cell lysates were loaded in parallel on a second gel to assess loading by western blot and decoration against VDAC shown in the lower panel.

As shown in in figure 2.26, transfection of *PUSL1* siRNA1, but not siRNA2, reduced the mitochondrial *de novo* translation by ~50 %. Mitochondrial DNA-encoded proteins were not be well resolved on 17 % SDS-PAGE gels, therefore the samples were separated on 12 % SDS-NuPAGE mini gels (figure 2.27).

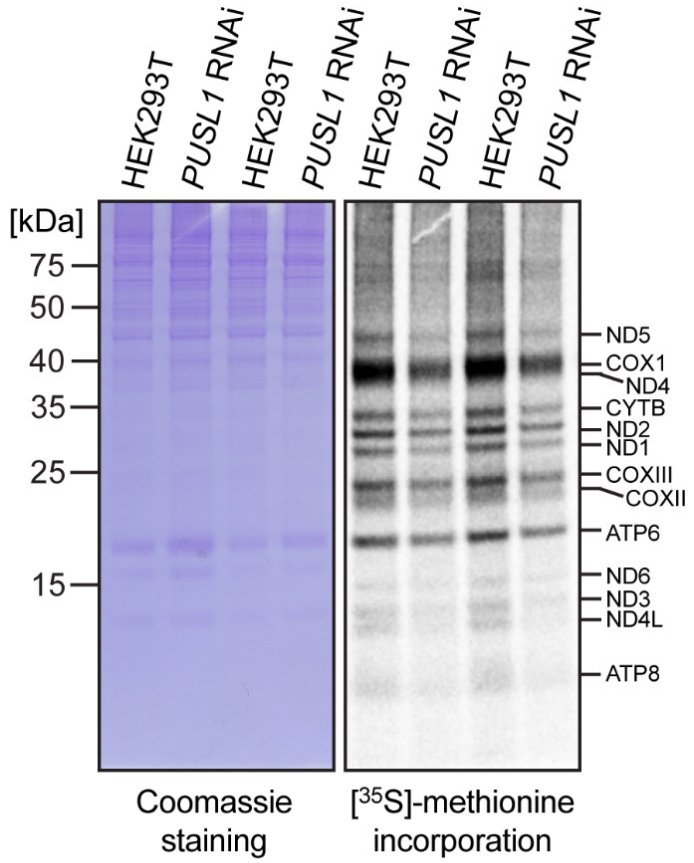

Adapted from Busch et al., 2019 - Submitted

Figure 2.27 – *In cellulo* translation assay using siRNA-treated HEK293T cells analyzed on a 12 % SDS-PAGE. 25 µg total cellular protein lysate were loaded per approach and after separation fixed, Coomassie-stained, dried and used to expose a phosphoimager screen. The result is representative for four independent replicates applying a non-targeting negative control siRNA (HEK293T) or *PUSL1*-siRNA1 (*PUSL1* siRNA.

Interestingly, the *in cellulo* translation assays indicate that *PUSL1* siRNA1, which completely abolishes PUSL1 expression, leads a 50 % reduction of mitochondrial *de novo* translation (figures 2.26 and 2.27). This is in strong contrast to *PUSL1*-siRNA2, which despite reducing PUSL1 levels by 80 – 90 %, does not affect the rate of mitochondrial translation (figures 2.25, 2.26 and 2.27). This result suggests that low levels of PUSL1 are sufficient to maintain normal mitochondrial translation, whereas a completely abolished PUSL1 expression leads to a markedly reduced mitochondrial *de novo* translation (figures 2.26 and 2.27). Initial western blot analyses did not indicate a pleiotropic destabilization of mitoribosome proteins when *PUSL1* was knocked down

(data not shown). To further investigate the molecular consequences of *PUSL1* knock-down, mitochondria were isolated from control and *PUSL1* knock-down cells and mitochondrial protein steady-state levels were determined with LFQ-MS/MS.

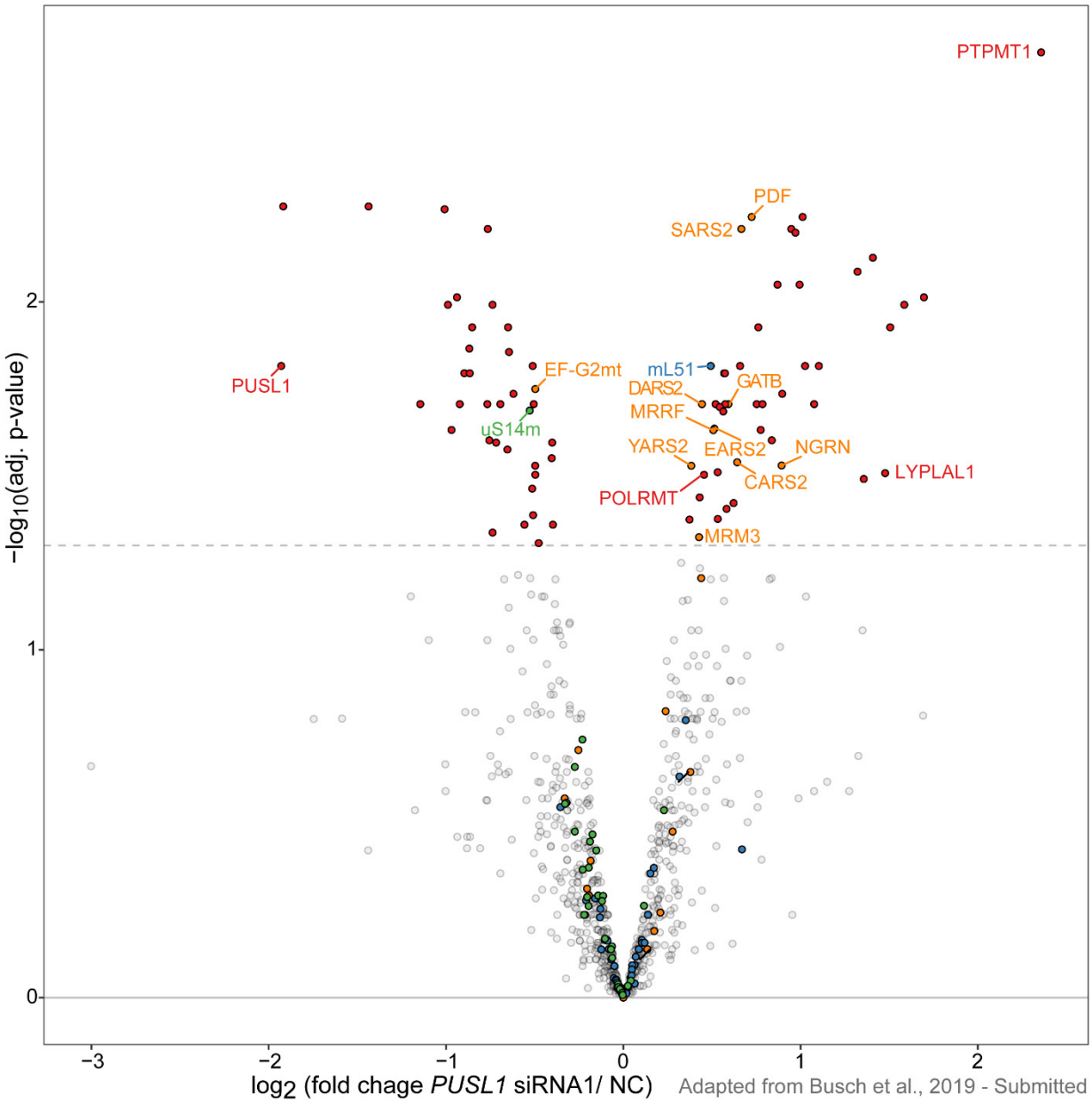

Figure 2.28 – Label-free quantitative mass spectrometry analysis of mitochondrial protein steady-state levels after siRNA1-mediated knock-down of *PUSL1*. Mitochondria were isolated from HEK293T cells previously transfected with a non-targeting negative control siRNA (NC) or a *PUSL1* siRNA1. The siRNAs were transfected two times within a week, prior harvesting and preparation of mitochondria. The result represents three independent replicate experiments.

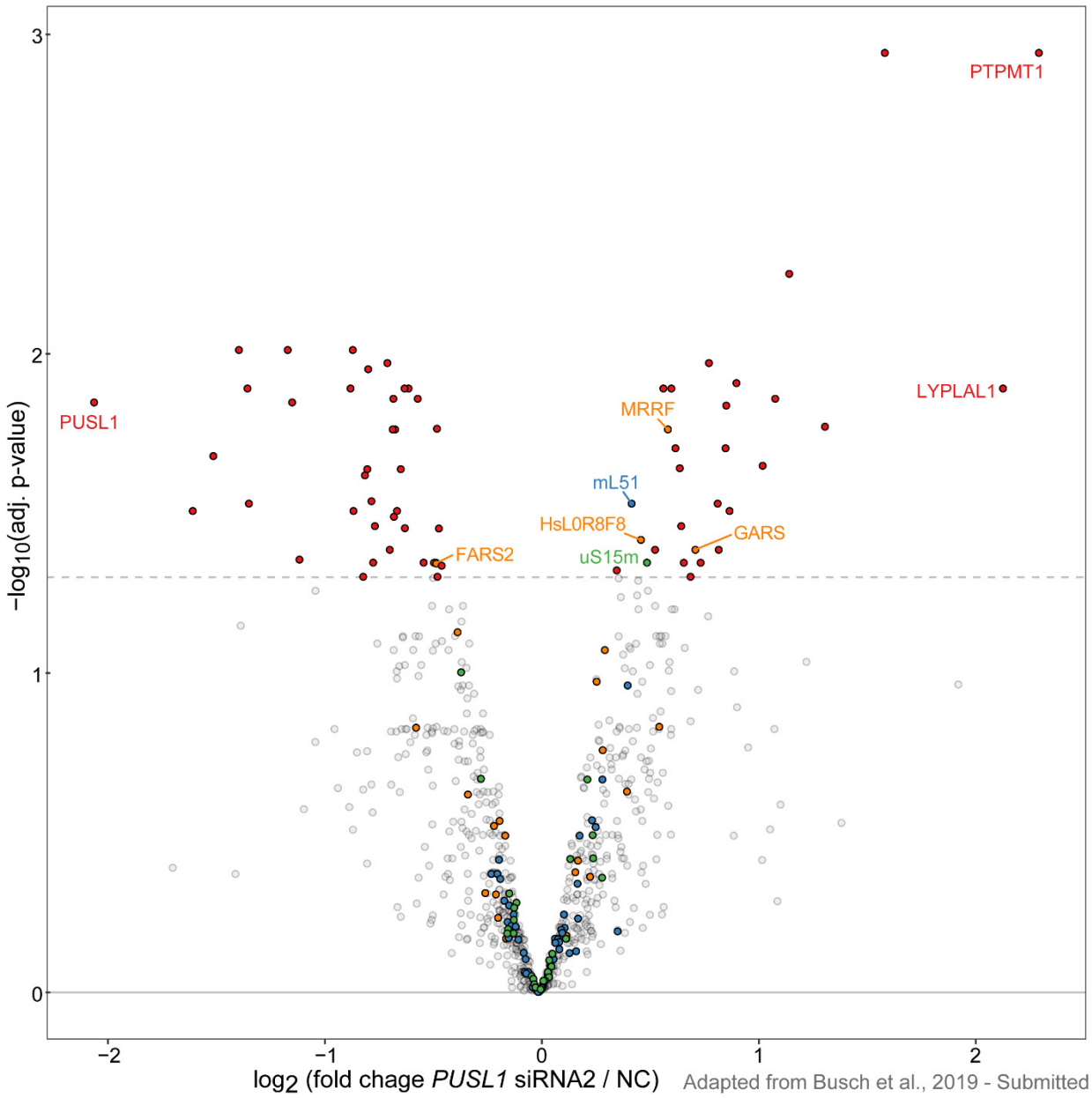

Figure 2.29 – Label-free quantitative mass spectrometry analysis of steady-state levels of mitochondrial proteins after siRNA2-mediated knock-down of *PUSL1*. Mitochondria were isolated from HEK293T cells transfected with a non-targeting negative control siRNA (NC) or *PUSL1* siRNA2. The siRNAs were transfected two times within one week, prior harvesting and preparation of mitochondria. The result represents three independent replicate experiments.

The LFQ-MS/MS-based quantification of mitochondrial proteins from HEK293T cells treated with the *PUSL1* siRNAs, confirms that both siRNAs significantly downregulate

PUSL1 (figures 2.28 and 2.29). Mitochondria isolated from cells treated with *PUSL1* siRNA1 or siRNA2 are characterized by numerous proteomic changes, whereas the most upregulated proteins are lysophospholipase-like protein 1 (LYPLAL1) and mitochondrial protein tyrosine phosphatase 1 (PTPMT1; figures 2.28 and 2.29). Unexpectedly, mitoribosome proteins were not universally destabilized upon *PUSL1* knock-down (figures 2.28 and 2.29). A slight increase in the steady-state levels of the 39S large mitoribosome subunit protein mL51 and the mitoribosome recycling factor MRRF are detected when applying *PUSL1* siRNA1 or siRNA2. The 28S subunit protein uS15m and the putative mitoribosome assembly factor HsL0R8F8 seem to be exclusively increased upon transfection of *PUSL1* siRNA2 (figure 2.29). Furthermore, HEK293T mitochondria treated with *PUSL1* siRNA1 show a specific increase of the 16S rRNA-module component NGRN and the mitochondrial Peptide deformylase (PDF), as well as reduced levels of the 28S small mitoribosome subunit protein uS14m and EF-G2mt (figure 2.29). Strikingly, both *PUSL1* siRNAs led to an upregulation of several mitochondrial tRNA synthetases, (figure 2.28 and 2.29).

These results suggest that PUSL1 downregulation leads to an increase of the mitoribosome protein mL51, the recycling factor MRRF and several proteins involved in mitochondrial tRNA metabolism. PUSL1 may coordinate mitochondrial translation by directly or indirectly affecting the levels or modifications of mitoribosome-associated tRNAs, whereas an additional role for PUSL1 in promoting mitoribosome assembly cannot be excluded.

3. Discussion and future perspectives

3.1. On the hierarchical coupling of transcription and translation

Mitochondrial transcription and translation are tightly coupled, as the synthesized polycistronic transcripts have to be cleaved and post-transcriptionally modified to provide rRNA, mRNAs and tRNAs for mitochondrial translation (Rackham et al., 2016; Rorbach & Minczuk, 2012). Despite tremendous progress of our knowledge about the enzymes involved in different reactions during RNA maturation and mitoribosome assembly, many steps and underlying mechanisms of those processes are only poorly understood. This is especially evident in the case of RNA modifications, that are performed by yet unknown enzymes, including methylations of the 12S mt-rRNA and methylations and pseudouridylations of mt-tRNAs (Suzuki et al., 2011; Van Haute et al., 2015). Proper RNA processing is required for mitochondrial function and hence mutations affecting modifying enzymes or mtDNA can cause impaired RNA maturation leading to severe human diseases (Suzuki et al., 2011; Van Haute et al., 2015).

During the course of this thesis, we analyzed *Mrpp3* and *Ptcd1* knock-out mice and obtained new mechanistic insights into RNA processing (Perks et al., 2018; Rackham et al., 2016). Molecular characterization of *Mrpp3* knock-out mice revealed two important aspects of the RNase P function in mitochondrial RNA processing *in vivo* (Rackham et al., 2016). Firstly, MRPP3 is required for 5' tRNA processing, which was found to proceed 3' end maturation (Rackham et al., 2016). Interestingly, 5' ends of the mt-*Co3* and mt-*CytB* transcripts remained unchanged in the absence of MRPP3, suggesting that another enzyme with a similar function is responsible for their cleavage (Rackham et al., 2016). Secondly, altered RNA processing impairs overall mitoribosome assembly, although some proteins can assemble on the premature 12S-16S mt-rRNA-containing transcript. Moreover, proteomics of ribosomal density gradients allowed us to determine the composition of the mitoribosome biogenesis intermediate formed in absence of functional MRPP3. In future studies, it will be interesting to quantitatively assess the putative ribosome biogenesis intermediates by proteomics in *Mrpp3* knock-out mice to identify early mitoribosome assembly factors in the absence of RNA processing (Rackham et al.,

2016). Another intriguing approach would be to determine the structure of the biogenesis intermediates formed in the absence of *Mrpp3* by cryo-EM to reveal putative assembly factors or the architectural organization of transcription-translation coupling *in vivo* (Brown et al., 2017). Additionally, CRISPR/Cas9 engineering may help to generate knock-out or mutant cell lines of *Mrpp3* to enrich putative biogenesis intermediates (Bogenhagen et al., 2014, 2018; Pearce, et al., 2017). Recently, single nucleotide polymorphisms altering catalytic efficiency of MRPP3/ RNAse P were described in humans (Hodgkinson et al., 2014). The identified missense polymorphism (rs11156878, Asn to Ser) in the human *MRPP3* gene likely affects MRPP3 processing efficiency and compromises metabolic state of the cell, which may be worth investigating (Hodgkinson et al., 2014).

Work presented in this thesis also contributed to the molecular characterization of PTCD1, which associates with the 16S mt-rRNA protein-module and recruits RPUSD4 to the 16S mt-rRNA to catalyze the pseudouridylation (Antonicka et al., 2017; Perks et al., 2018). We showed that loss of *Ptcd1* in the mouse heart disturbs mitoribosome assembly and, hence, it will be interesting to analyze the subassembled mitoribosome intermediates formed in the absence of PTCD1 by using cryo-EM or co-immunoprecipitation-coupled proteomics to build an assembly map of mitoribosomes.

3.2. On MitoRibo-Tag mice and knock-out models

In this work, we present the MitoRibo-Tag knock-in mouse model to study the composition and interactome of mitoribosomes *in vivo* in different tissues and under different physiological states, dysfunction or disease. MitoRibo-Tag knock-in mice are a novel tool to study mitoribosome protein and RNA content and to define a set of novel interacting proteins, denoted MIPs. Additionally, this model will allow future investigation of native mitoribosomes in different normal physiological states, *e.g.* exercise and fasting, as well as in mitochondrial disease, different types of common diseases, *e.g.* diabetes and neurodegeneration, and in ageing.

Earlier studies have defined the majority of the mitoribosome core components and the recent atomic structures indicate structural adaptations for membrane protein synthesis (Amunts et al., 2015; Greber, Bieri, et al., 2014; Suzuki et al., 2001a, 2001b). These studies applied models, which firstly may not resemble the *in vivo* situation, and secondly, do not allow the precise (proteomic) analysis of transient biogenesis intermediates. Protein complexes might be less stable in highly proliferative cells, which are characterized by rapid protein turnover rates and thereby not accurately representing the situation in tissues. Moreover, cell lines often harbor chromosomal rearrangements, aneuploidies or polyploidies, which can strongly influence nuclear and mitochondrial gene expression generating metabolic effects not seen in real tissues. In contrast, MitoRibo-Tag mice are suitable to analyze mitochondrial translation *in vivo* in its physiological context. This thesis provides protocols to purify mitoribosomes from various mouse tissues. The developed MitoRibo-Tag method significantly improved quantification of mitoribosome proteins by 22 % to an average quantification of 98.8 %, *i.e*. 81 of 82 proteins from heart, liver and kidney mitochondria, compared to cultured cells (Brown et al., 2017; Richter et al., 2010). The second advantage of using MitoRibo-Tag mice is that mitoribosomes are purified without extensively perturbing the biological system by means of protein overexpression. In future studies, the basic MitoRibo-Tag methodology may be further improved by incorporation of stable-isotope labeling (SILAC) to further improve the coverage and thereby quantification and identification rates to directly determine the exact stoichiometry of mitoribosome-interacting protein complexes (Krüger et al., 2008).

The latter may be especially useful for quantification of lowly abundant proteins, like bL36m, the only non-quantified mitoribosomal protein in our data set, or transiently bound MIPs (Brown et al., 2017).

The current co-immunoprecipitation-coupled LFQ-MS/MS analyses of mitoribosomes revealed strikingly tissue-specific compositional differences between the interactomes in heart, liver and kidney mitochondria. These differences may be a result of the tissue-specific energy demands and biosynthetic capacities previously indicated by large-scale proteomics studies (Calvo et al., 2016; Mootha et al., 2003; Pagliarini et al., 2008). Notably, mitochondrial disorders also display tissue heterogeneity, a phenomenon that is yet not fully understood (Hällberg & Larsson, 2014).

Mitoribosomes of liver and kidney mitochondria, in contrast to heart mitoribosomes, are co-purified with subunits of the *m*-AAA protease AFG3L2 and SPG7, which maybe be important to control or chaperone biogenesis of mitoribosomes or mtDNA-encoded subunits, like bL32m and co-enriched mtCOX2 (figures 2.14 to 2.16; Nolden et al., 2005). Moreover, the comparison of mitoribosome interactomes reveals novel and putative tissue-specific MIPs including some poorly or completely uncharacterized proteins including PREPL and ZNF22 in heart, RDH13 in liver, and SMIM4 in heart and kidney. Regarding the tissue-specific interactomes, heart mitoribosomes seem to have the most diverse interactome, with co-enriched proteins belonging to various pathways including RNA metabolism, mitoribosome assembly and respiratory chain biogenesis. Similarly, large mitoribosome-assemblies, denoted MIOREX complexes, were found in yeast and composed of RNA-binding proteins, mitoribosomes and respiratory chain assembly factors suggesting that these complexes are evolutionary conserved (Bogenhagen et al., 2014; Kehrein et al., 2015; Rackham et al., 2016; Stoldt et al., 2018). Interestingly, the newly identified MIPs are strongly binding to the mitoribosome as they persist after several rigorous washing steps. Another aspect to evaluate in the future would be to test more stringent detergents like triton X-100 or triton X-114 for lysis (Bordier, 1981; Mathias et al., 2011; Metodiev et al., 2009). These experiments will be particularly interesting to perform because triton derivatives more efficiently lyze membranes and allow to separate lipophilic membrane-associated or hydrophilic soluble complexes (Bordier, 1981). This may be especially useful to distinguish soluble or membrane-associated mitoribosome or

MIP complexes, because previous biochemical and cryo-electron tomography studies indicated that only approximately 50 % of mitoribosomes are membrane-associated (Englmeier et al., 2017; Liu & Spremulli, 2000). These experiments may also help to understand the molecular basis of inner membrane-association of mitoribosomes. It is possible that mitoribosomes dynamically interact with several membrane-associated complexes in addition to OXA1L and C12ORF62, similar to the binding of mitoribosomes to the inner membrane receptors Mba1 and Mrx15 in yeast (Haque, et al., 2010; Liu & Spremulli, 2000; Ott et al., 2006; Richter-Dennerlein et al., 2016; Möller-Hergt et al., 2018). Furthermore, chemical crosslinking might also support detection of weakly binding MIPs and to locate the interaction sites on the mitoribosome (Greber et al., 2014; Liu et al., 2017; Rappsilber, 2011). These experiments probably require an extensive downstream computational analysis, because many crosslinks will be produced between mitoribosome proteins.

To further increase the number of adequate *in vivo* models a MitoRibo-Tag mouse model expressing a FLAG-tag on the 28S small mitoribosome subunit should be developed. This could help to distinguish 28S- and 39S-binding MIPs and determine the mitoribosome-MIP binding interface ultimately giving insights into the molecular mechanism of translation. A reasonable candidate protein to tag the 28S subunit in the mouse would be mS40, protein which was recently shown to efficiently purify the small subunit (Lavdovskaia et al., 2018). It would be advisable to knock-in a different tag, *e.g.* Myc- or HA-tagged variant of mS40, as this would allow combining mouse lines to specifically purify mitoribosomes or subunits from the same sample, due to the different nature of the tags. The 28S-tag knock-in model may be especially important to define the composition of biogenesis intermediates in knock-out animals with defective 39S assembly such as *Mterf3* knock-out mice (Park et al., 2007; Wredenberg et al., 2013). Moreover, combination of the future 28S animal model with the presented MitoRibo-Tag mice, although costly and laborious, may be very useful to discriminate 28S and 39S interactomes *in vivo* and under different physiological conditions, dysfunction or disease.

The previously mentioned SILAC experiments may also allow a precise definition of post-translational modifications including phosphorylation and acetylation of mitoribosome proteins, and their impact on regulating translation (Koc & Koc, 2012; Koc et al., 2017; Miller et al., 2008). The steady-state levels of the mitoribosome proteins, uL30m, mL41 and mS26 are regulated by PPTC7-mediated dephosphorylation, indicating that mitochondrial translation can be controlled by the metabolic state of mitochondria (Guo et al., 2017; Niemi et al., 2018).

Taken together, diverse experimental setups can be envisioned to apply MitoRibo-Ta mice to investigate mitochondrial translation under different physiological conditions. These experiments could include metabolic experiments such as exercise, fasting or high fat diet treatments to analyze the mitoribosome or mitochondrial translation during altered mitochondrial biogenesis (Hansson et al., 2004; Lopez-Lluch et al., 2006; Vernochet et al., 2012; Wai et al., 2015). Another interesting metabolic intervention may be to switch MitoRibo-Tag mice to hypoxia (decreased levels of oxygen), as it was recently shown that lowered oxygen levels reduce the cellular requirement for mitochondria and that certain mt-tRNA modifications can be remodeled by altering bicarbonate concentration in cells (Jain et al., 2016; Lin et al., 2018).

An intriguing but yet not tested application for MitoRibo-Tag mice might be ribosome profiling experiments, which allow measuring mitochondrial translation at single nucleotide level by deep sequencing of mitoribosome-protected mRNA fragments (Ingolia et al., 2009). Some pioneering studies determined the translation profiles of yeast mitoribosomes revealing that cytosolic and mitochondrial protein synthesis a synchronized to efficiently form OXPHOS complexes, and human mitoribosomes finding that pathogenic mt-tRNA mutations can arrest mitoribosomes on corresponding codons (Couvillion et al., 2016; Rooijers et al., 2013). MitoRibo-Tag mice tissues or mitochondria may allow enriching mitoribosomes from complex homogenates to investigate tissue-specific features of mitochondrial translation under cellular stress, disease, dysfunction, exercise or fasting. Another possibility to simultaneously measure mitochondrial translation by ribosome profiling, and to determine the mitoribosome interactome by proteomics would be to cross MitoRibo-Tag mice with mouse models carrying pathogenic

mtDNA mutations as developed by Kauppila et al. (2016). These models could advance the mechanistic understanding how mt-mRNAs or mt-tRNA mutations contribute to defective mitochondrial translation *in vivo* and ultimately to human disease.

In general, the crossing of MitoRibo-Tag mice with knock-outs of the mitochondrial gene expression components or models of mitochondrial dysfunction will be very powerful in to decipher the mitoribosome assembly and translation coordination, which are largely unexplored. In the current study, several knock-out MitoRibo-Tag mouse lines could be generated including transgenic knock-out mutants of *Mterf3*, *Mterf4*, *Nsun4*, *Tfb1m*, *Lrpprc* and *Slirp*. These transgenic knock-out MitoRibo-Tag models will be important to identify MIPs involved in mitochondrial translation. Due to the tremendous work required to obtain adequate genotypes for breeding, well-sized animal colonies and biological replicates, our analyses focused on the *Mterf4* knock-out MitoRibo-Tag mouse strain, which is discussed below.

Nsun4 and *Tfb1m* knock-out MitoRibo-Tag mice are characterized by discrete 28S assembly defects (Metodiev et al., 2009; Metodiev et al., 2014). Conditional knock-out of *Nsun4,* similar to *Mterf4,* causes subunit separation loss of monosomes, whereas removal of *Tfb1m* severely reduces steady-state levels of the 28S subunit (Metodiev et al., 2009; Metodiev et al., 2014). Hence, both models can be envisioned to determine the composition and interactome of at least two 39S large subunit biogenesis intermediates in absence fully assembled mitoribosomes or the 28S subunit (Metodiev et al., 2009; Metodiev et al., 2014).

Lrpprc knock-out MitoRibo-Tag mice are especially interesting to be analyzed as knock-out mice have a characteristic unbalanced translation phenotype, *i.e.* mtND1, mtND2 and mtND5 are increased, whereas other mtDNA-encoded proteins are produced much less including mtND3, mtND6, mtCOX1 and mtATP6, despite increased mitoribosome abundance (Ruzzenente et al., 2012). This molecular phenotype is of particular interest because the differential effect on mtDNA-encoded proteins is not observed in cultured cells (Ruzzenente et al., 2012; Sasarman et al., 2010). Therefore, *Lrpprc* knock-out MitoRibo-Tag mice may be a unique tool to study deregulated translation by ribosome profiling, and concomitantly the effects on the mitoribosome interactome to identify

putative mammalian translation factors or regulators such as TACO1 (Richman et al., 2016; Weraarpachai et al., 2009). The combined profiling and proteomic experiments may also help to decipher the exact molecular function of polyadenylation of mitochondrial RNAs and why it strongly impacts translation (Pearce, et al., 2017; Rorbach et al., 2011; Ruzzenente et al., 2012; Siira et al., 2017).

Another interesting model to analyze would be *Slirp* knock-out MitoRibo-Tag mice. Those knock-outs have a profound decrease of mitochondrial mt-mRNAs of 50 to 70 % but only a slightly reduced protein synthesis rate in liver mitochondria (Lagouge et al., 2015). Hence, the mentioned ribosome profiling and proteomic experiments may also include *Slirp* knock-out mice, as SLIRP seems to fine-tune translation in proliferative tissues, which could unravel how mt-mRNAs are selectively engaged with mitoribosomes (Lagouge et al., 2015).

The comprehensive analyses of different tissues and various knock-out models may also shed light into the enigmatic tissue-specificity underlying mitochondrial translation-associated diseases (Calvo & Mootha, 2010; Jackson et al., 2018; Lake et al., 2017; Richman et al., 2015; Sasarman et al., 2015; Smits et al., 2011). A dozen mutations in 28S and 39S mitoribosome proteins were recently identified to cause mitochondrial disease often accompanied by cardiomyopathy (Jackson et al., 2018). It is likely that similar mutations will be identified in the future by diagnostic sequencing technologies.

Furthermore, it will be very interesting to analyze the specific requirement of mitoribosome proteins for mitochondrial translation in mammals in a more systematic manner. Accordingly, Zeng, et al. (2018) could show that some the mitoribosome proteins bL1m, bL9m, bL35m, bL36m, mL53 and mL61, are not required for mitochondrial translation in yeast. Regarding the latter, it is very interesting that some mitoribosome proteins seem to be specifically required for the synthesis of particular mtDNA-encoded proteins, like bL34m and bL35m for mtCOX1 in yeast (Box et al., 2017; Guedes-Monteiro et al., 2018). Therefore, these mitoribosome proteins might be valuable candidates to be removed from the mouse genome to investigate if their function is conserved or if novel functions were acquired during evolution.

The above mentioned knock-out MitoRibo-Tag mouse strains may be useful to decipher the assembly pathways of mitoribosomes in detail, because subassembled biogenesis

intermediates are likely more stable than in cultured cells and thereby easily analyzed by mass spectrometry or cryo-EM (Bogenhagen et al., 2018; Brown et al., 2017). Novel gene-editing technologies may also allow changing certain conserved amino acids in mitoribosome proteins to study altered mitoribosome functionality like synthesis accuracy, which was recently found to inversely alter cytosolic protein quality control systems in yeast (Suhm et al., 2018). Investigation of this phenomenon is of special interest as the molecular signals mediating communication of mitochondrial and cytosolic translation are largely enigmatic (Isaac et al., 2018; Suhm et al., 2018).

3.3. On PUSL1 - a novel mitoribosome-interacting protein

In fulfilment of this thesis, it was shown that crossing mitochondrial gene expression knock-out mouse mutants with MitoRibo-Tag mice is a powerful approach to catalog and characterize yet unknown MIPs, which are not identified under basal conditions. Here, the mitoribosome biogenesis intermediate formed in the absence of *Mterf4* in mouse heart mitochondria was co-immunoprecipitated by mL62-FLAG and its composition quantitatively determined by proteomics revealing the orphan protein PUSL1 as a novel MIP (this work; Cámara et al., 2011). PUSL1 is homologous to the TruA pseudouridine synthase of *E. coli*, which catalyzes pseudouridylation in the anti-codon stem at position 38, 39 and 40 of seventeen bacterial tRNAs, because the protein harbors TruA-like domains at the N- and C-termini (this work; Hur & Stroud, 2007).

We confirmed that PUSL1 is a mitochondrial protein, likely imported to the organelle by the N-terminal MTS within the first 38 amino acids (this work; Zaganelli et al., 2017). Additionally, submitochondrial fractionation experiments demonstrate that PUSL1 is located in the mitochondrial matrix where it peripherally associates with inner membrane. This finding was unexpected because *in silico* analysis using the transmembrane prediction algorithm TMHMM indicated very weak hydrophobic patches in PUSL1 (this work; Sonnhammer et al., 1998). Interestingly, three recent studies suggested that mitoribosomes may assemble on inner membrane-localized protein platforms composed of mitoribosome proteins, bL21m, mL43, mL50, mL57, mL58 and uL13 in yeast, and assembly factors including GTPBP7 and GTPBP10 in mammalian cells (Kim & Barrientos, 2018; Lavdovskaia et al., 2018; Zeng et al., 2018). It is possible that PUSL1 participates or transiently binds these platforms to promote mitoribosome assembly.

The newly identified interaction of mitoribosomes with PUSL1 was confirmed by reverse co-immunoprecipitation-coupled proteomics of PUSL1-associated complexes from human cultured cells. Those experiments reveal a reciprocal purification of mitoribosome proteins and several assembly factors, including GTPBP10, HsL0R8F8, MALSU1, MTERF4, and NOA1.

We demonstrated that PUSL1 is required for mitochondrial translation in cultured cells. Knock-down of *PUSL1* significantly reduced the rate of *de novo* mitochondrial translation,

showing that PUSL1 is needed to maintain mitochondrial translation. This finding is unexpected, because there is only one essential pseudouridine synthase called RluD in *E. coli* known to be required for translation and normal growth (Del Campo et al., 2004). Moreover, the RNAi-coupled *in cellulo* translation assays are intriguing because PUSL1 was not identified in recent genome-wide genetic screen of genes essential for OXPHOS (Arroyo et al., 2016). The results indicate that PUSL1 may have a regulatory role in coordinating mitochondrial translation or promoting mitoribosome assembly. In fact, the similar composition of PUSL1-associated complexes and the *Mterf4* knock-out mitoribosome biogenesis intermediate indicate that these putative processes occur concomitantly or consecutively late during assembly or translation. This hypothesis is supported by proteomic analysis of mitochondria isolated from *PUSL1* knock-down cells, which imply altered steady-state levels of the mitoribosome proteins mL51, uS14m, uS15m, the translation factors PDF, MRRF and EF-G2$_{mt}$, and the mitoribosome assembly factors NGRN and HsL0R8F8.

The exact molecular role of each ψ in ribosome-associated RNAs is not understood, it is generally thought that pseudouridines stabilize RNAs or their conformation during ribosome assembly (Ofengand, 2002). PUSL1 may pseudouridylate, similar to its bacterial homolog TruA, several mitochondrial RNAs harboring uracil bases at position 40, *e.g.* glutamine or glutamate mt-tRNAs, and as predicted by the Suzuki laboratory (Suzuki et al., 2011). Regarding this, the proteome analysis of *PUSL1* knock-down mitochondria also indicated that several mitochondrial aminoacyl tRNA synthetases, including the glutamate-tRNA synthetase, are upregulated upon loss of PUSL1, which may be a cellular response to compensate the reduced mitochondrial translation. The lack of pseudouridines in mt-rRNAs and mt-tRNAs can have deleterious consequences on mitochondrial function, as indicated by lack of the 16S mt-rRNA pseudouridylation in *Ptcd1* knock-out mice, and possibly cause human disease (Antonicka et al., 2017; Perks et al., 2018; Suzuki et al., 2011). The disease potential of altered pseudouridylation was recently discovered in patients harboring mutations in the mitochondrial pseudouridylate synthase 1 (PUS1), who lack pseudouridines at mt-tRNA base positions 27 and 28 and suffer from myopathy, lactic acidosis and sideroblastic anemia (MLASA; Bykhovskaya et al., 2004; Fernandez-Vizarra et al., 2007; Kasapkara et al., 2017). Due to the limited

available time, the precise molecular function of PUSL1 or its RNA targets could not be determined in the course of this work. However, it is tempting to speculate about the putative functions and substrates of PUSL1 in mitochondria, which should be addressed in future studies. PUSL1 might target several uridines in mt-tRNAs or even the integral mitoribosome CP-mt-tRNA, which could be identified by RNA-mass spectrometry or pseudouridine sequencing of knock-out cells (Antonicka et al., 2017; Suzuki & Suzuki, 2014). PUSL1 could also exert a RNA chaperone-like function to promote RNA folding during an active translation cycle. Furthermore, it is possible that PUSL1 safeguards a quality control step during mitoribosome biogenesis, because the protein was specifically identified as a component of the *Mterf4* knock-out intermediate and found to co-enrich with several mitoribosome assembly factors (figures 2.19 and 2.25). PUSL1 may ensure that only mitoribosome subunits with adequately folded RNAs are incorporated into mature mitoribosomes. To investigate these scenarios systematically, the catalytic aspartate could be substituted to generate an inactive *PUSL1* mutant variant in cells. Moreover, knocking-out *PUSL1* in cells or *Pusl1* in mice by homologous recombination or CRISPR/Cas9 may help to decipher the function of PUSL1 *in vitro* and *in vivo*.

In summary, this thesis established MitoRibo-Tag mice as valuable tool in future research to molecularly define mitoribosome assembly and translation coordination of OXPHOS biogenesis. The technological advantages of MitoRibo-Tag mice are to analyze mitoribosome content in differentiated tissues and the possibility to generate additional mutants by intercrossing mouse strains to enrich for biogenesis intermediates, which are likely more stably formed than in cultured cells. MitoRibo-Tag mice can be envisioned as a tool to be used by the community to study mitoribosome function and its composition or interactome across various tissues and under different physiological conditions. Using MitoRibo-Tag mice it may also be possible to investigate the spatial orchestration of mitochondrial translation, to determine the RNA composition enabling ribosome profiling studies, and to discover yet unknown proteins involved in mitochondrial gene expression and translation.

4. Material and methods

4.1. Mouse genetics and animal experiments

4.1.1. Generation of *mL62*-Flag knock-in animals and housing

The mL62-Flag knock-in (MitoRibo-Tag) targeting vector was constructed using BAC clones from the C57BL/6J RPCIB-731 BAC library by Taconic Biosciences (Cologne, Germany). The targeting vector harbored exons three to six of mL62, the FLAG-tag DNA sequence (copyright Sigma-Aldrich; introduced after the last amino acid of exon six: …MTMD-DYKDDDDK), a Puromycin resistance selection marker (PuroR) flanked by F3 recombination sites (downstream of the *mL62* 3'UTR) and a thymidine kinase (Tk) cassette. After transfection of a C57BL/6N embryonic stem cell line, homologous recombinant clones were isolated using positive PuroR and negative Tk selections. The PuroR cassette was removed by crossing heterozygous *mL62*-Flag knock-in mice with transgenic mice ubiquitously expressing the Flp recombinase. The remaining F3 recombination site remained in a non-conserved region of the genome. Heterozygous *mL62*-Flag knock-in mice were backcrossed with C57BL/6N-wild type mice for several generations. The backcrossed heterozygous *mL62*-Flag knock-in mice were intercrossed to generate homozygous *mL62*-Flag (MitoRibo-Tag) mice constitutively expressing the mL62-FLAG fusion protein controlled by the endogenous promotor.

4.1.2. Ethics statement and animal housing

The study was approved by the Landesamt für Natur, Umwelt und Verbraucherschutz Nordrhein–Westfalen (reference numbers 84-02.04.2015.A103 and 84-02.50.15.004) and performed in accordance with the recommendations and guidelines of the Federation of European Laboratory Animal Science Associations (FELASA). WT C57BL/6N and transgenic mice were housed in individually ventilated cages (45 × 29 × 12 cm) with a

12 h light/dark cycle and controlled environmental conditions of 22 ± 2°C and 50 + 10 % relative humidity. The animals were fed a normal chow diet and water *ad libitum*.

4.2. Biochemical methods

4.2.1. SDS-polyacrylamide gel electrophoresis

Protein samples obtained from isolated mitochondria or cell lysates were diluted with 4x NuPAGE© LDS sample buffer (Thermo Fisher, cat. no. NP0007) to a final concentration of 2x freshly supplemented with 100 mM dithiothreitol. Between 5 to 20 µg of mitochondrial protein or 50 to 75 µg total cell protein were loaded and separated on NuPAGE 4 – 12 % or 10 % Bis-Tris Midi gels (Thermo Fisher, cat. no. WG1202BOX and WG1402BOX) using NuPAGE 1x MOPS (cat. no. NP0001) or 1x MES (cat. no. NP0002) running buffer for appropriate separation.

4.2.2. Western blot

Proteins separated by SDS-PAGE were blotted onto Poly(vinylidene fluoride)-membrane using 1x wet western blot buffer (38.63 mM Glycine, 47.87 mM Tris and 10 % Methanol) at 4°C for 2 h and 400 mA or overnight at 80 mA. Membranes were blocked with blocking buffer (Rockland, Cat. No. MB-070) or 5 % milk-Tris buffer saline (Merck, cat. no. 108382) TBS, 50 mM Tris-HCl pH 7.4 and 150 mM NaCl)) by incubation for 1 h at RT. The blocked membranes were incubated overnight with primary antibodies at indicated dilutions (see chapter 4.5.). Following overnight incubation, membranes were washed three times with 1x TBS-Tween20 (TBST; TBS with 0.1 % Tween20) and incubated with HRP-conjugated secondary antibodies (anti-rabbit IgG $F(ab')_2$, GE Healthcare, cat. no. NA9340V), anti-mouse IgG (GE Healthcare, cat. no. NXA931) or anti-goat IgG (Thermo Fisher, cat. no. A16005)) for 1.5 to 2 h at RT. Membranes were washed two times with TBST and TBS

prior development using Amersham ECL Western Blotting Detection reagent (GE Healthcare, Amersham, cat. no. RPN2106) and exposure to a X-ray film.

4.2.3. Isolation of mitochondria from mouse tissues

Mice were quickly killed by cervical dislocation and heart, liver and kidneys were dissected and subsequently washed two times with ice cold phosphate-buffered saline (PBS, Thermo Fisher, cat. no. 14190-094). Heart tissues were additionally washed once with mitochondrial isolation buffer (MIB, 310 mM sucrose, 10 mM Tris-HCl and 0.05 % fatty acid-free BSA (w/v, Sigma-Aldrich, cat. not. A8806) to remove residual blood. Following washing, tissues were cut and gently homogenized within five to 15 ml of MIB with a Potter S (Sartorius). The volume of heart and kidney homogenates was brought to 15 ml and of liver samples to 50 ml with MIB to allow fractionation of cell debris by centrifugation for 10 min/1000 g/4°C. The obtained mitochondria-containing supernatants from heart were centrifuged for 15 min/4500 g/4°C and those from kidney and liver for 10 min/10000 g/4°C to isolate crude mitochondria. The crude mitochondrial pellets were resuspended in MIB supplemented with 1x Complete EDTA-free protease inhibitor cocktail (PIC, Roche, cat. no. 05056489001), aliquoted and snap frozen for further use. The protein concentration was determined by means of the Bradford assay, using BSA as standard, or the Qubit™ Protein Assay Kit (Thermo Fisher, cat. no. Q33211).

4.2.4. Mitoribosome co-immunoprecipitation from mouse mitochondria

One mg of crude mitochondria was pelleted by a quick centrifugation at 5 min/9200 g/ 4°C. The supernatant was removed and the pellet resuspended with 200 µl purification-lysis buffer (10 mM Tris-HCl pH 7.5, 100 mM Potassium chloride (KCl, Merck, cat. no. 1.04936.1000), 20 mM Magnesium dichloride ($MgCl_2$, Merck, cat. no. M2670), 1x PIC, 1 % digitonin (Calbiochem, cat. no. 300410, 2 gram detergent per gram

protein)). The mitochondrial protein lysates were incubated for 20 min on ice to solubilize proteins, followed by a clarifying centrifugation at 9200 g for 45 min at 4°C. The resulting supernatants containing the soluble proteins were diluted 1:10 with dilution buffer (10 mM Tris-HCl pH 7.5, 100 mM KCl, 20 mM $MgCl_2$) to decrease the detergent concentration. The diluted lysates were subsequently incubated for 2 h at 4°C with 100 µl Anti-FLAG M2 beads (Sigma-Aldrich, cat. no. A2220), which were equilibrated twice with 15 volumes TBS and wash buffer (= dilution buffer supplemented with 0.1 % digitonin)), rotating at 10 rpm to allow protein binding. Afterwards, beads with bound proteins were washed three times with 15 volumes of wash buffer and two times with dilution buffer. The remaining bound proteins were eluted with 300 µl elution buffer (50 mM Tris-HCl pH 7.5, 1 mM Tris(2-carboxyethyl)phosphine (TCEP, Thermo Fisher, cat. no. T2556), 5 mM 2-Chloracetamid (Merck, cat. no. 8024120100) freshly supplemented with1 ng/µl Trypsin Gold (Promega, cat. no. V5280, resuspended in 50 mM acetic acid)) rotating for 30 min at RT (for protein analysis by mass spectrometry) or 60 min at 4°C (for RNA analysis by northern blot) rotating at 5 rpm. The protein eluates were transferred to ice and subsequently prepared for mass spectrometry or mixed 3:1 with TRIzol LS reagent (Thermo Fisher, cat. no. 10296028) to isolate RNA.

4.2.5. Sucrose density gradient analysis of mitochondrial ribosomes from mouse mitochondria

To analyze the assembly of mitoribosomes sucrose density gradient fractionation of was performed according to Matthews et al., 1982 and Rackham et al., 2016. One mg of crude mitochondria isolated from mouse tissues were pelleted by centrifugation for 5 min/9200 g/4°C. Mitochondria were resuspended with 100 µl lysis buffer (260 mM sucrose, 10 mM Tris-HCl pH 7.5, 100 mM KCl, 20 mM $MgCl_2$, 2 % digitonin , 40 U/ml RNAse inhibitor (New England Biolabs, cat. no. M0307L) and 1x PIC) to concentration of 10 mg/ml and incubated for 20 min on ice. After lysis, mitochondrial protein lysates were clarified by centrifugation for 45 min/9200 g/4°C. Ten to 30 % sucrose density gradients were casted as described by Metodiev et al., 2009. Essentially, 6 ml of 10 % sucrose solution

(prepared in 10 mM Tris-HCl pH 7.5, 100 mM KCl and 20 mM $MgCl_2$) were pipetted into a 14 x 89 mm-Ultra-Clear Open-Top Thinwall tube (Beckman, cat. no. 344059). Next, 6 ml of the 30 % sucrose solution (also prepared in 10 mM Tris-HCl pH 7.5, 100 mM KCl, 20 mM $MgCl_2$) were carefully and very slowly pipetted below the 10 % sucrose solution with a 90° blunt end needle (Cadence). The correct pipetting visualized by formation of an interphase between the sucrose solutions. The gradient tubes were sealed with a perforated short-replacement cap (Laborgeräte Beranek, cat. not. 105-414-6) to remove excess of 10 % sucrose solution, without disturbing the interphase, and gradients were casted with the following program 1 min, 54 sec/81,5°/16 rpm using a Gradient Master (BioComp Instruments, Inc.). The cleared mitochondrial lysate was loaded on top of the 10 % - 30 % sucrose density gradient, whereas ten percent of the lysate were saved as input control. The gradients were subsequently centrifuged for 15 h/71092 g/4°C in a SW 41 Ti Swinging-Bucket rotor (Beckman, cat . no. 331362). Fractions were collected from the top (first fraction 840 µl, including 90 µl lysate and 750 µl gradient fraction, fractions two to 15: 750 µl and fraction 16: residual volume), whereas one third of each fraction was precipitated with 0.02 % sodium deoxycholate and 12 % trichloroacetic acid (final concentrations) for SDS-PAGE and western blot analysis. Mitoribosome proteins were detected using the following primary antibodies, rabbit anti-mL37 (MRPL37, 1:1000, Sigma-Aldrich, cat. no. HPA025826), rabbit anti-bS16m (MRPS16, 1:500, Sigma-Aldrich, cat. no. HPA054538)), goat anti-DDDDK tag (1:1000, Abcam, cat. no. ab1257) and HRP-conjugated secondary antibodies diluted 1:8000 (anti-rabbit IgG $F(ab')_2$ (GE Healthcare, cat. no. NA9340V) or anti-rabbit IgG (Thermo Fisher, cat. no. G21234), anti-mouse IgG (GE Healthcare, cat. no. NXA931) and anti-goat IgG (Thermo Fisher, cat. no. A16005)). Chemiluminescent detection was carried out with Amersham ECL Western Blotting Detection reagent (GE Healthcare, cat. no. RPN2106).

4.2.6. Preparation of sucrose density gradient fractions prior mass spectrometry

The remaining two thirds of each sucrose density gradient fraction were subjected to chloroform/methanol precipitation to remove sucrose according to Wessel & Flügge (1984) with some modifications. Two thirds of the gradient fraction were mixed with 1000 µl methanol (Carl Roth GmbH & Co. KG, cat. no. P717.1). Subsequently, 400 µl chloroform (Merck, cat. no. 1.02445) and 200 µl water were added and samples were vortexed. Centrifugation for 5 min/20817 g/4°C yielded and phase separation. The resulting aqueous phase, containing sucrose, was discarded. The remaining interphase and lower phase, harboring proteins, were mixed with 1500 µl fresh methanol and centrifuged again for 5 min/20817 g/4°C to pellet precipitated proteins. The resulting supernatant was discarded and the protein pellets were dried for five to ten minutes at RT and stored for further use.

4.2.7. Preparation of mitochondria or cell lysates for mass spectrometry

Hundred to 150 µg freshly prepared or thawn mitochondria or cell pellets were centrifuged for 5 min/9200 g/4°C to remove remaining buffer, and resuspended with 20 to 30 µl of guanidinium hydrochloride lysis buffer (6 M guanidinium chloride (Sigma-Aldrich, cat. no. G3272) 10 mM TCEP, 40 mM chloroacetamide and 100 mM Tris-HCl) as previously described by Kulak et al., 2014 with some modifications. The protein lysates were denatured at 95°C for 10 min and vigorous shaking at 1400 rpm using a Thermomixer comfort (Eppendorf) and sonicated at high amplitude for ten min, 30 sec/30 sec break, using a Bioruptor® Plus sonication device (Diagenode, cat. no. B01020001) to break remaining cell debris. If cellular particles remained, the denaturation and sonication steps were repeated. The protein lysates were diluted 1:10 with 20 mM Tris pH 8.3 to determine the protein concentration with a NanoDrop2000 (Thermofisher). Two hundred fifty µg mitochondrial or cellular protein lysate were digested overnight at 37°C with at least

1.25 µg Trypsin Gold (Promega), corresponding to a 1:200 protein:Trypsin, to achieve complete tryptic digest. To clean peptide-containing digests and to remove salts, digests were applied to home-made StageTips (Empore Octadecyl C18, 3M; Rappsilber et al., 2003) on the next day. The digest was stopped by adding formic acid (FA, Fisher Scientific, cat. no. 10229884) to the samples to a final concentration of 1 %. The C18-membrane was activated by 200 µl methanol followed by centrifugation with a StageTip centrifuge (Sonation, cat. no. STC-V2). Next, the StageTips were washed with 200 µl 60 % acetonitrile/0.1 % FA (Thermo Scientific, cat. no. 85174) and equilibrated with 200 µl of 0.1 % FA by centrifugation. The protein digest was loaded on the StageTip and washed two times with 200 µl 0.1 % FA. The clean peptides were eluted with 80 µl of 60 % acetonitrile / 0.1% FA buffer by centrifugation for 4 min/1500 g at RT. Finally, eluted peptides were dried with a vacuum concentrator plus (Eppendorf) and resuspended with 0.1 % formic acid prior mass spectrometry.

4.2.8. Liquid-chromatography mass spectrometry (LC-MS/MS)

Peptides obtained from co-immunoprecipitations were separated on a 25 cm, 75 µm internal diameter PicoFrit analytical column (New Objective) packed with 1.9 µm ReproSil-Pur 120 C18-AQ media (Dr. Maisch) using an EASY-nLC 1000 (Thermo Fisher Scientific). The column was maintained at 50°C. Buffer A and B were 0.1 % formic acid in water and 0.1 % formic acid in acetonitrile. Peptides were separated on a segmented gradient from 3 % to 25 % buffer B for 45 min and from 25 % to 40 % buffer B for five min at 300 nl/min. Eluting peptides were analyzed on an Orbitrap Fusion mass spectrometer (Thermo Fisher Scientific). Peptide precursor m/z measurements were carried out at 60000 resolution in the 300 to 1500 m/z range. The most intense precursors with charge state from two to seven only were selected for HCD fragmentation using 27 % normalized collision energy. The m/z values of the peptide fragments were measured in the orbitrap at a resolution of 30000 using a minimum AGC target of 1e5 and 100 ms maximum injection time. Upon fragmentation, precursors were put on a dynamic exclusion list for 45 sec. The cycle time was set to three sec.

Peptides derived from the input for the Co-IPs were separated on the analytical column described above, using an EASY-nLC 1200. Buffer A and B were 0.1 % formic acid in water and 0.1 % formic acid in 80 % acetonitrile. Peptides were separated on a segmented gradient from 3 % to 6 % buffer B for ten min, from 6 % buffer B to 25 % buffer B for 100 min, from 25% buffer B to 31% buffer B for 10 min, and from 31 % to 60 % buffer B for 10 min at 200 nl/min. Eluting peptides were analyzed on a Q Exactive (Thermo Fisher Scientific). Peptide precursor m/z measurements were carried out at 60000 resolution in the 300 to 1800 m/z range. The ten most intense precursors with charge state from two to seven only were selected for HCD fragmentation using 27 % normalized collision energy. The m/z values of the peptide fragments were measured at a resolution of 30000 using a minimum AGC target of 1e5 and 80 ms maximum injection time. Upon fragmentation, precursors were put on a dynamic exclusion list for 45 sec.

4.2.9. Protein identification and quantification (MS data analysis)

The raw data were analyzed with MaxQuant version 1.5.2.8 using the integrated Andromeda search engine. Peptide fragmentation spectra were searched against the canonical and isoform sequences of the mouse (Uniprot proteome ID: UP000000589, November 15, 2018) or the human (Uniprot proteome ID: UP000005640, from November 17, 2018) proteome (Cox & Mann, 2008; Cox et al., 2011). Methionine oxidation and protein N-terminal acetylation were set as variable modifications; cysteine carbamidomethylation was set as fixed modification. The digestion parameters were set to “specific” and “Trypsin/P,” The minimum number of peptides and razor peptides for protein identification was one and the minimum number of unique peptides was zero. Protein identification was performed at a peptide spectrum matches and protein false discovery rate of 0.01. The “second peptide” option was on. Successful identifications were transferred between the different raw files using the “Match between runs” option. Label-free quantification (LFQ) was performed using an LFQ minimum ratio count of two (Cox et al., 2014). LFQ intensities were filtered for at least three valid values in at least one group and imputed from a normal distribution with a width of 0.3 and down shift of

1.8. Differential abundance analysis was performed using limma (Ritchie et al., 2015). Protein copy numbers per 1 g of total mitochondrial protein mass were calculated from the intensity values of the razor peptides in peptides.txt according to the total protein approach (Wiśniewski & Rakus, 2014). The anova analysis was performed in R using the aov function (R development core team, 2008). The results of the anova analysis were adjusted for multiple testing using the Benjamini & Hochberg procedure (Benjamini & Hochberg, 1995). Only proteins with an adjusted p-value of less than 0.05 (5 % FDR) were termed significant.

4.2.10. Isolation of mitochondria from cultured cells for co-immunoprecipitation and mass spectrometry

Mitochondria from cultured cells were isolated according to Lee & Bogenhagen, 2016 to remove substantial nuclear contaminants from mitochondria with some modifications. For the Lee and Bogenhagen-isolation, the stock solution buffer 2.5x mannitol-sucrose-HEPES buffer (MSH, 525 mM mannitol, 175 mM sucrose, 50 mM HEPES pH 8) was prepared with DEPC-treated water and supplemented with 1x PIC, but prepared without EDTA. Initially, the cell culture media was decanted and cells were carefully washed with 20 ml PBS. Then cells were collected with 5 ml PBS and pelleted by centrifugation for 5 min/800 g/4°C. Cells from two to three square dishes were pooled and resuspended in 3 ml MSH-mitochondrial isolation buffer (1x MSH freshly supplemented with 0.2 mg fatty acid-free BSA per ml and 1x PIC). The washed cells were treated subsequently with 36 µl 10 % digitonin (in H_2O) to permeabilize the cell membranes, which was assessed by mixing 3 µl of cell suspension with 3 µl of Trypan blue visualized using a light microscope. If cells were not completely permeabilized, 2 to 4 µl digitonin were additionally and stepwise added until approximately 90 % of cells were permeable visualized by trypan blue staining. Once complete cell permeabilization was achieved, the digitonin concentration was reduced by adding 7 ml MSH-MIB to the cell suspension. The permeable cells were centrifuged for 5 min/1200 g/4°C to remove the digitonin-containing buffer, whereas the cell pellet was resuspended in 3 ml fresh MSH-MIB and homogenized with ten careful strokes through a 25 gauge-needle. The homogenate was diluted by

addition of 5 ml fresh MSH-MIB and were centrifuged for 5 min/900 g/4°C to pellet nuclei. The resulting supernatant was carefully removed with a pipet to avoid nuclear contamination and centrifuged again for 15 min/16000 g/4°C to obtain a crude mitochondrial pellet. This crude mitochondrial pellet was resuspended in 3 ml 1 M potassium chloride-MIB to remove majority of remaining nuclear contaminants and was centrifuged again. The KCl-treated mitochondrial pellet was subsequently resuspended with 1 ml nuclease buffer (1x MSH, 1 mM ADP, 5 mM glutamic acid, 5 mM Di-sodium malate, 0.25 mg/ml fatty acid-free BSA, 60 mM KCl, 10 mM $MgCl_2$, and 1 mM K_2HPO_4) freshly supplemented with 0.25 µl HS-Nuclease (benzoase, Mobitec, cat. no. GE-NUC10700-01) and 1x PIC)) followed by incubation for 20 min at 37°C to digest residual nucleic acids. After nuclease treatment (step 12 of medium/large scale preparation according to original Lee and Bogenhagen protocol), the procedure was modified as mitochondria were subsequently pelleted by centrifugation for 15 min/16000 g/4°C. The crude mitochondrial pellet was washed two times with 1 ml MSH-MIB to remove the nuclease buffer, aliquoted, snap frozen and stored at -80°C for further experiments.

4.2.11. Isolation of mitochondria from cultured for submitochondrial localization assays

Eighty to 90 % confluent cells from two to three square dishes were scrapped off, centrifuged for 5 min/800 g/4°C and washed two times with cold PBS. The cell pellet was initially resuspended with two ml cell mitochondrial isolation buffer (CMIB, 20 mM HEPES pH 7.6, 220 mM mannitol, 20 mM sucrose, 1 mM EDTA (Merck, cat. no. 108418), 2 mg/ml fatty acid-free BSA and 1x PIC). Afterwards, six ml isolation buffer were added to samples followed by 15 min incubation on ice to facilitate cell swelling. Swollen cells were gently homogenized with 20x strokes at 500 rpm using a Schuett homgenplus (Schuett Biotec, cat. no. 3.201-011). The cell homogenates were centrifuged for 5 min/800 g/4°C to remove cell debris. The resulting supernatant, containing mitochondria, was centrifuged for 10 min/10000 g/4°C to obtain a crude mitochondrial pellet, which was washed two times with one ml CMIB without BSA prior protein quantification with the Qubit™ Protein Assay Kit (Thermo Fisher).

4.2.12. Sodium carbonate extraction of proteins

To assess solubility of mitochondrial proteins 200 µg of crude mitochondria were resuspended in 100 µl mitochondrial isolation buffer and sonicated for 5 min (30 sec sonication/30 sec break) in a cold water bath. One aliquot of mitochondria from was resuspended and kept on ice as total protein control. The sonicated mitochondria were pelleted and subsequently resuspended in 200 µl of 20 mM HEPES-KOH pH 7.4 supplemented with 1x PIC. Following the initial resuspension, additionally 200 µl of HEPES buffer or 200 µl of 200 mM sodium carbonate (Sigma-Aldrich, cat. no. S7795) buffer, at pH 10.5, 11. 5 or 12.5, were added to the samples, gently mixed and incubated for 30 min incubation on ice to extract soluble and membrane-associated or membrane-bound proteins. The samples were centrifuged for 30 min/45000 rpm/4°C for to separate soluble and membrane (-associated) proteins. The obtained supernatants were precipitated in the presence of 0.02 % sodium deoxycholate with 12 % trichloroacetic acid (final concentrations). Precipitated supernatant and pellet fractions were solubilized with 30 µl 2x SDS sample buffer (100 mM Tris-HCl, 8 mM EDTA-NaOH, 20 % glycerol (v/v), 4 % SDS (v/v; Merck, cat. no. 112533), 200 mM DTT, 0.2 % Bromophenol blue)), whereas 5 µl of each sample were loaded onto a 10 % Bis-Tris gel for SDS-PAGE and western blot analysis.

4.2.13. Protease protection assay

To investigate the submitochondrial localization of proteins, two hundred µg of freshly prepared mitochondria were pelleted, and resuspended in 200 µl isolation buffer to maintain mitochondrial membrane integrity, hypotonic swelling buffer (10 mM HEPES-KOH, pH 7.4) to swell the outer mitochondrial membrane, or Triton X-100-supplemented isolation buffer (isolation buffer supplemented with 1 % Triton X-100) to open outer and inner mitochondrial membranes. Mitochondrial proteins protected from intact membranes are protected from proteolytic degradation, whereas opening the mitochondrial membranes would expose the proteins and allow their degradation. Here, the above

mentioned samples were split into two, whereas Proteinase K (Roche, cat. no. 03450384103) was added to one aliquot of each approach to a final concentration of 25 µg/ml. Afterwards, the samples were incubated on ice for 10 min and subsequently inhibited with 2 µl of 0.1 M Phenylmethylsulfonyl fluoride (PMSF, Sigma-Aldrich, cat. no. P7626). Proteins were precipitated with 0.02 % sodium deoxycholate and 12 % trichloroacetic acid and resuspended with a final volume of 30 µl 2x SDS sample buffer. Five µl of each sample were loaded onto a 10 % Bis-Tris gel and analyzed by western blot.

4.2.14. Co-immunoprecipitation of mitoribosome-interacting proteins from mitochondria of cultured cells

To analyze the interaction of putative MIPs with the mitoribosome, co-immunoprecipitations of candidate proteins were performed with mitochondria isolated from control or HEK293T cells expressing a FLAG-tagged protein according to Lee & Bogenhagen (2016). Here, 750 µg of mitochondria were pelleted and lyzed with 150 µl purification-lysis buffer supplemented with 3 % digitonin and 1x PIC (corresponding to six gram detergent per gram protein). Protein complexes were purified, eluted and analyzed by mass spectrometry as described in the chapters 4.2.4., 4.2.8., and 4.2.9.

4.2.15. *In cellulo* translation assay

To assess possible effects of the candidate protein levels on mitochondrial translation, *de novo* synthesized (mitochondrial) translation products were labeled with L-[^{35}S]-methionine. siRNA-treated HEK293T cells were carefully washed with 3 ml PBS and incubated for 30 min in labeling media (DMEM, high glucose, no glutamine, no methionine, no cysteine, 1x GlutaMax (Thermo Fisher, cat. no. 3505003), sodium pyruvate (Thermo Fisher, cat. no. 11360039), 50 µg/ml uridine (Sigma-Aldrich, cat. no. U3003) and freshly supplemented with 10 % dialyzed fetal bovine serum (Thermo Fisher,

cat. no. A3382001). Meanwhile, emetine (Sigma-Aldrich, cat. no. E2375) was solubilized in PBS, sterile filtered and added to a final concentration of 100 µg/ml to inhibit cytosolic translation followed by 5 min-equilibration at 37°C. Subsequently, 1000 µCi L-[^{35}S]-methionine (Hartmann Analytic, cat. no. SCM-01) were added to each dish, gently mixed and incubated for 1 h at 37°C / 5 % CO_2 to label *de novo* synthesized mtDNA-encoded proteins. Following incorporation or radiolabeled amino acids, cells were washed three times with 5 ml PBS, transferred into 1.5 ml Eppendorf tubes, resuspended with 50 to 150 µl 2x RIPA buffer (300 mM sodium chloride, 2 % triton X-100, 1 % sodium deoxycholate, 0.2 % SDS, 100 mM Tris, pH 8 supplemented with 1x PIC)) and snap frozen. Cell lysates were thawn on ice and sonicated two to three times for 30 sec at 90 % amplitude with a Sonoplus mini20 (Bandelin, cat. no. 3665) equipped with a MS 1.5 Sonotrode (Bandelin, cat. no. 3639). Insoluble cell debris was removed by centrifugation for 5 min/2000 rpm/4°C. The resulting supernatants were saved and quantified using Qubit™ Protein Assay Kit (Thermo Fisher, cat. no. Q33211). Protein lysates were mixed with 4x SDS sample buffer (200 mM Tris-HCl, 8 mM EDTA-NaOH, 40 % glycerol (v/v), 8 % SDS (v/v), 400 mM DTT, 0.4 % bromophenol blue) to a final protein concentration of 5 µg/µl, whereas cell lysate corresponding to 20 or 25 µg protein of each approach were loaded onto NuPAGE 12% Bis-Tris protein gels ran with 1x MES buffer. SDS-PAGE was stopped when the Coomassie running front reached the gel bottom. Gels were subsequently incubated for 30 min in protein fixation buffer (20 % ethanol and 10 % acetic acid) supplemented with PhastGel Blue R (Sigma-Aldrich, cat. no. B4921) to stain separated proteins to compare loaded protein amounts. Next, gels were destained with fixation buffer and incubated for 30 min in Amersham Amplify (GE Healthcare, cat. no. NAMP100) to increase sensitivity of the radioactive signal. The gels were vacuum-dried for 1.5 h at 75°C onto Whatman paper and exposed for 24 to 72 h to a phosphoimager screen followed by detection of the radioactive signal with a Typhoon FLA7000 (GE Healthcare).

4.3. Molecular biology methods

4.3.1. Isolation of genomic DNA from murine tissue

400 µl tissue lysis buffer (0.5 % SDS, 100 mM NaCl, 20 mM Tris pH 8, 2.5 mM EDTA pH 8), supplemented with 80 µg Proteinase K, were added to each mouse ear or tail clip. The samples were lyzed for 5 to 24 h at 56°C to degrade (tissues) proteins. Afterwards, firstly 40 µl 8 M potassium acetate and secondly 500 µl chloroform were added to each sample to separate molecules into a lower organic and upper inorganic aqueous phase containing nucleic acids. The aqueous phase was carefully taken up and mixed with 1 ml of 95 % ethanol to precipitate DNA by incubation for 30 min at -80°C. The precipitated DNA was pelleted by centrifugation for 15 min/13000 rpm/4°C, whereas the resulting supernatant was discarded. The DNA pellets were washed once with 500 µl of 70 % ethanol for by 15 min drying at 60°C using a vacuum concentrator plus (Eppendorf). Finally, the DNA was dissolved with 125 µl water and stored at 4°C for further use.

4.3.2. Genotyping polymerase-chain reaction

The genotypes of WT and transgenic mice were determined with PCRs using the primers (table 1) and the PCR programs listed (table 2) below:

Table 1 – Primer used for mouse genotyping

Primer name	Sequence
mL62-Flag knock-in forward primer	5'-AGCAACAGAGGATTGTGAGTCCC-3'
mL62-Flag knock-in reverse primer	5'-TGGGAATGGAGCTCAATGG-3'
Ckmm Cre forward primer	5'-CACGACCAAGTGACAGCAAT-3'
Ckmm Cre reverse primer	5'-AGAGACGGAAATCCATCGCT-3'
Mterf4 loxP forward primer	5'-CTCCCGGGTGGCGTGTG-3'
Mterf4 loxP reverse primer	5'-TTTGGGGGAAGGAATCTGTCG-3'

Nsun4 loxP forward primer	5'-CTACACTCATCAGGGACTCTGC-3'
Nsun4 loxP reverse primer	5'-AAATGGCTGACTTTCTAGCAGTC-3'
Tfb1m loxP forward primer	5'-ATG TTT ACA GGC TTA GTT GAA-3'
Tfb1m loxP reverse primer	5'-TAGTAGAGAATACTGCCACAG-3'
Lrpprc loxP forward primer	5'-GGAGAACAGGCCGCATCACAA-3'
Lrpprc loxP reverse primer	5'-TGCCTTCCACCTCAGCTTACCACT-3'
Slirp WT forward primer	5'-TGTATCTGGCAGGACACTGG-3'
Slirp WT reverse primer	5'-ATACTAGGCAAGCGCTCCAC-3'
Slirp knock-out forward primer	5'-GAGGAGATGAGCGTACTGGC -3'
Slirp knock-out reverse primer	5'-CCCTCCCTGTGGGAGAGG-3'

Table 2 – PCR programs used for mouse genotyping

***mL62*-Flag genotyping PCR program (WT allele: 246 bp, knock-in allele: 393 bp)**			
Step	**Cycles**	**Temperature**	**Duration**
Denaturation	1x	95°C	3 min
Denaturation (continued)	35x	95°C	30 sec
Annealing		55°C	30 sec
Elongation		72°C	45 sec
Elongation (continued)	1x	72°C	5 min
Stop	1x	8°C	5 min
***Ckmm* Cre genotyping PCR program (WT allele: no product, Cre allele: 371 bp)**			
Step	**Cycles**	**Temperature**	**Duration**
Denaturation	1x	95°C	3 min
Denaturation (continued)	30x	95°C	30 sec
Annealing		53°C	30 sec
Elongation		72°C	45 sec
Elongation (continued)	1x	72°C	5 min
Stop	1x	8°C	5 min

***Mterf4* loxP genotyping PCR program (WT allele: 233 bp, loxP allele: 330 bp)**			
Step	**Cycles**	**Temperature**	**Duration**
Denaturation	1x	95°C	5 min
Denaturation (continued)	35x	95°C	30 sec
Annealing		60°C	30 sec
Elongation		72°C	1 min
Elongation (continued)	1x	72°C	5 min
Stop	1x	8°C	5 min
***Nsun4* loxP genotyping PCR program (WT allele: 300 bp, loxP allele: 500 bp)**			
Step	**Cycles**	**Temperature**	**Duration**
Denaturation	1x	95°C	2 min
Denaturation (continued)	30x	95°C	15 sec
Annealing		60°C	15 sec
Elongation		72°C	30 sec
Elongation (continued)	1x	72°C	5 min
Stop	1x	8°C	5 min
***Tfb1m* loxP genotyping PCR program (WT allele: 300 bp, loxP allele: 500 bp)**			
Step	**Cycles**	**Temperature**	**Duration**
Denaturation	1x	95°C	2 min
Denaturation (continued)	35x	95°C	30 sec
Annealing		50°C	30 sec
Elongation		72°C	30 sec
Elongation (continued)	1x	72°C	5 min
Stop	1x	8°C	5 min

***Lrpprc* loxP genotyping PCR program (WT allele: 420 bp, loxP allele: 520 bp)**			
Step	**Cycles**	**Temperature**	**Duration**
Denaturation	1x	95°C	3 min
Denaturation (continued)	35x	95°C	30 sec
Annealing		60°C	30 sec
Elongation		72°C	35 sec
Elongation (continued)	1x	72°C	5 min
Stop	1x	8°C	5 min
***Slirp* WT allele genotyping PCR program (WT allele: 383 bp)**			
Step	**Cycles**	**Temperature**	**Duration**
Denaturation	1x	95°C	5 min
Denaturation (continued)	38x	95°C	30 sec
Annealing		60°C	30 sec
Elongation		72°C	30 sec
Elongation (continued)	1x	72°C	5 min
Stop	1x	8°C	5 min
***Slirp* knock-out allele genotyping PCR program (WT allele: ~700 bp)**			
Step	**Cycles**	**Temperature**	**Duration**
Denaturation	1x	95°C	5 min
Denaturation (continued)	38x	95°C	30 sec
Annealing		62°C	30 sec
Elongation		72°C	45 sec
Elongation (continued)	1x	72°C	5 min
Stop	1x	8°C	5 min

4.3.3. RNA isolation

RNA was isolated using the Trizol or Trizol LS reagent (Thermo Fisher, cat. no. 15596026 and cat. no. 10296028) or the ToTALLY RNA Total RNA Isolation Kit (Thermo Fisher, cat. no. AM1910) according to manufacturer's instructions with some modifications detailed below. Essentially, liquid eluates containing RNA, co-purified with mitoribosomes during co-immunoprecipitation experiments, were mixed with 750 µl Trizol LS. Next, 200 µl RNAse-free Chloroform were added to each sample followed by vigorous mixing for 15 seconds at RT and short incubation on ice. The homogenates were centrifuged for 15 min/12000 g/4°C to separate nucleic acids and proteins, whereas the RNA remained in the upper colorless aqueous phase. The aqueous phase was carefully removed and transferred to a new Eppendorf tube harboring 500 µl RNAse-free Isopropanol and 10 µg glycogen to precipitate all RNAs including the smaller tRNAs overnight at -20°C. In the next morning, precipitated RNAs were pelleted by centrifugation for 10 min/12000 g/4°C. The pelleted whitish RNA attached loosely to the tube bottom, hence the supernatant was carefully removed. The RNA pellet was washed carefully with 750 µl RNAse-free 75 % ethanol by gentle mixing, without disrupting the pellet, followed by an additional centrifugation for 5 min/7500 g/4°C. The supernatant was completely removed and the RNA was air dried on ice, turning the RNA transparent. Finally, the RNA was mixed with 20 to 50 µl RNAse-free water, solubilized by heating at 57.5°C for 10 min and stored at -80°C for further use.

4.3.4. Northern blot

RNA concentrations were determined with the Qubit™ RNA broad range assay kit (Thermo Fisher, cat. no. Q10210) and one µg of RNA and total-eluate RNA obtained from co-immunoprecipitations, were solubilized in NorthernMax™-Gly Sample loading dye (Thermo Fisher, Ambion, cat. no. AM8551) and loaded onto 18 % formaldehyde-containing 1.2 % LE Agarose (Ambion) gels. Following separation, gels were soaked in 0.05 M NaOH to nick RNA and RNA was blotted overnight onto Hybond™-N+ membrane

(GE Healthcare, cat. no. 45-000-927) according to standard procedures. In the morning, RNAs were cross-linked to the membrane and blocked for 1 h at 42°C with PerfectHyb™ Plus Hybridization buffer (Sigma-Aldrich, cat. no. H7033). Next, tRNA probes against mouse mt-tRNA tryptophan, phenylalanine, valine, serine (see primer sequences in table 3) were prepared with 50 µCi α-^{32}P-CTP (Hartmann Analytic, cat. no. SRP-209) using the Prime-It II Random Primer labeling kit (Agilent, cat. no. #300385). The membranes were incubated with the radioactive probes overnight at 42°C. On the next day, membranes were washed with 2x SSC 0.1 % SDS at 23°C, 2x SSC 0.1 % SDS at 42°C and lastly 0.2x SSC 0.1 % SDS at 42°C and exposed to a phosphoimager screen. tRNA probes were removed (stripped off) by incubation in 0.2x SSC 0.1 % SDS at 65°C and the membrane was blocked again with PerfectHyb Plus Hybridization buffer. Accordingly, probes for mouse 12S and 16S mt-rRNAs were prepared, exposed and stripped off by incubation 0.2x SSC 0.1 % SDS at 75°C.

Table 3 – Primer used for northern blot

Primer species	Sequence
12S mt-rRNA	5'- TACACATGCAAACCTCCATAGACCGGTGTAAAATCCCTTAAACATTT ACTTAAAATTTAAGGAGAGGGTATCAAGCACATTAAAATAGCTTAAG ACACCTTGCCTAGCCACACCCCCACGGGACTCAGCAGTGATAAATA TTAAGCAATAAACGAAAGTTTGACTAAGTTATACCTCTTAGGGTTGG TAAATTTCGTGCCAGCCACCGCGGTCATACGATTAACCCAAACTAA TTATCTTCGGCGTAAAACGTGTCAACTATAAATAAATAAATAGAATTA AAATCCAACTTATATGTGAAAATTCATTGTTAGGACCTAAACTCAATA ACGAAAGTAATTCTAGTCATTTATAATACACGACAGCTAAGACCCAA ACTGGGATTAGATACCCCACTATGCTTAGCCATAAACCTAAATAATT AAATTTAACAAAACTATTTGCCAGAGAACTACTAGCCATAGCTTAAA ACTCAAAGGACTTGGCGGTACTTTATATCCATCTAGAGGAGCCTGT TCTATAATCGATAAACCCCGCTCTACCTCACCATCTCTTGCTAA-3'
16S mt-rRNA	5'- ATGCAACACTGTTAGTATGAGTAACAAGAATTCCAATTCTCCAGGCA TACGCGTATAACAACTCGGATAACCATTGTTAGTTAATCAGACTATA GGCAATAATCACACTATAAATAATCCACCTATAACTTCTCTGTTAAC CCAACACCGGAATGCCTAAAGGAAAGATCCAAAAAGATAAAAGGAA CTCGGCAAACAAGAACCCCGCCTGTTTACCAAAAACATCACCTCTA GCATTACAAGTATTAGAGGCACTGCCTGCCCAGTGACTAAAGTTTA ACGGCCGCGGTATCCTGACCGTGCAAAGGTAGCATAATCACTTGTT CCTTAATTAGGGACTAGCATGAACGGCTAAACGAGGGTCCAACTGT CTCTTATCTTTAATCAGTGAAATTGACCTTTCAGTGAAGAGGCTGAA ATATAATAATAAGACGAGAAGACCCTATGGAG-3'
mt-tRNA Phenylalanine (Phe)	5'-CATTTTCAGTGCTTTGCTTTGTTATTA-3'
mt-tRNA Serine (Ser, AGY codon)	5'-GCATGAATTAGCAGTTCTTGCAATC-3'

mt-tRNA Tryptophan (Trp)	5'-GTGTGTTTTCTTAGGGCTTTGAAGGC-3'
mt-tRNA Valine (Val)	5'-GTGTAGGCCAGATGCTTTAAT-3'

4.3.5. Maintenance of cultured mammalian cells

Cells were quickly thawn at 37°C and immediately transferred to dish or flask with pre-warmed DMEM+GlutaMAX culture media (Thermo Fisher, cat. no. 31966-021) supplemented with 10 % fetal bovine serum (Thermo Fisher, cat. no.10270-106), 1x non-essential amino acids (Thermo Fisher, Gibco, cat. no. 11140050), 100 U/ml Penicillin, 100 µg/ml Streptomycin (Thermo Fisher, Gibco, cat. no. 15140122) and maintained at 37°C and 5 % CO_2. One day after thawing, culture media was refreshed to remove residual DMSO. Cells were split by gentle washing with PBS, incubated with 500 µl to 2 ml Trypsin-EDTA (Thermo Fisher, cat. no. 25300054) for detaching, and seeded diluted 1:10, 1:20 or a certain cell number required for subsequent experiment, every second to fourth day and at least maintained for one week prior experiments.

4.3.6. RNA interference using siRNAs

HEK293T cells were cultured for at least seven days before being seeded 24 h before first transfection in DMEM+GlutaMAX culture media supplemented additionally with 50 µg/ml Uridine (Sigma-Aldrich, cat. no. U3003) but without antibiotics. For *in cellulo* translation experiments 300.000 control and 400.000 cells for knock-downs were seeded in a total volume of 8 ml, into 10 cm-dishes, whereas 1.5 mio control and 3 mio cells were seeded onto 500 cm^2 square dishes in a total of 55 ml culture media for preparation of mitochondria (Thermo Fisher, cat. no. 10489282). On the next day, 6.325 µg (for 2.2x 10 cm-dishes) or 39,6 µg siRNA (for 2.2x square dishes) of silencer select© siRNA (Thermo Fisher, negative control: cat. no. 4390844, Pusl1 siRNAs: cat. no. s43084, Pusl1 siRNA2 cat. no. s225579) were diluted in 2193.765 µl or 5460.4 µl OptiMEM (Thermo Fisher, cat. no. 31985070). The Lipofectamine RNAiMAX transfection reagent (Thermo Fisher, cat. no. 13778150) was diluted in OptiMEM as follows: for 2.2x 10 cm-dishes 33 µl

Lipofectamine in 2167 µl, corresponding to 15 µl Lipofectamine per dish, or for 2.2x square dishes 198 µl Lipofectamine, corresponding to 90 µl per dish respectively. Next, the diluted siRNA mix was added in a 1:1 ratio to the Lipofectamine mix followed by incubation for 5 to 15 min at RT to allow liposome formation harboring siRNAs. Subsequently, 2 ml or 5 ml of transfection mix were pipetted slowly and dropwise onto the respective dishes and incubated for two to three days at 37°C and 5 % CO_2. On the third day, the siRNA transfection was repeated and cells were incubated for two to three additional days prior further experimental analysis or cell harvesting.

4.3.7. Generation of Flp-In T-REx expression cell lines and protein expression

Flp-In T-REx HEK293 expression cell lines (HEK293T) were generated according manufactures instructions with some modifications (Thermo Fisher, cat. no. K6500-01) as detailed below. Essentially, HEK293T host cells were split and 300.000 cells were seeded into a 6-well dish with a final volume of 1 ml DMEM+GlutaMAX culture media, supplemented with 10 % Tet-approved FBS (Clontech, cat. no. 631106) and non-essential amino acids but without antibiotics. On the next day, the pcDNA5/FRT/TO vector harboring *PUSL1* (Ensembl ID: ENST00000379031.9 and NCBI gene ID: 126789, with a 5' BamHI restriction site and a 3' XhoI restriction site) and the pOG44 vector, harboring the FLP recombinase, were co-transfected with Lipofectamine2000 transfection reagent (Thermo Fisher, cat. no. 11668027) to generate HEK293T expression cell lines. Initially, 150 µl OptiMEM were mixed with nine µl Lipofectamine2000, whereas in another tube 100 µl OptiMEM were mixed with 0.3 µg pcDNA/FRT/TO-gene-of-interest vector and 2.7 µg pOG44 filled up to a final volume of 150 µl. The diluted DNA was carefully added to the Lipofectamine mix, gently mixed and incubated for 5 to 15 min at RT. Next, 100 µl of transfection mix were added dropwise to each well, corresponding to 1 µg total DNA per well with 0.1 µg pcDNA5/FRT/TO-gene of interest and 0.9 µg pOG44. On the next day, the culture media was changed to antibiotic-free culture media. On the second day, each well was split with 500 µl trypsin-

EDTA and diluted 3.5 ml culture media (1:8 dilution) containing with 15 µg/ml blasticidin S (Thermo Fisher, cat. no. R21001) and 100 µg/ml hygromycin B (Thermo Fisher, cat. no. 10687010), as well as 100 U/ml Penicillin / 100 µg/ml streptomycin, to select for resistant transfected clones. At this point, three new 6-well dishes were prepared, each with one part of the 1:8-diluted cell suspension, whereas the residual cell suspension was pelleted and frozen as a backup as elucidated below, for screening purposes. The media was carefully refreshed every fourth to fifth day to supply cells with fresh nutrients. Approximately two to three weeks post transfection, positive colonies appeared and single colonies were picked, expanded and stored in freezing media (90 % Tet-approved FBS and 10 % DMSO). Protein expression was induced adding tetracycline (Sigma-Aldrich, cat. no. T7760) to a final concentration of 50 ng/ml to culture media 24 h prior experimental analysis according to manufacturer's instructions.

4.3.8. Immunocytochemistry and confocal microscopy of HeLa cells

Confocal microscopy was applied to investigate the cellular localization of proteins. Hence, 30000 HeLa cells were seeded onto coverslips in 12 well-dish plates. On the next day, cells were transiently transfected with one µg of vector DNA, harboring the gene-of-interest, and 0.5 µl Lipofectamine2000 per well according to manufacturer's instructions. Following additional 24 h, cells were fixed with 4 % paraformaldehyde (EM sciences, cat. no. 15710) in PBS for 10 min at RT. After three washes with PBS, cells were permeabilized with 0.1 % triton X-100 in PBS for five minutes at RT. Unspecific sites were blocked with 3 % BSA (Sigma-Aldrich, cat. no. A3858) in PBS. Primary and secondary antibodies were diluted 3 % BSA. The following primary antibodies were used and incubated at 4°C overnight, mouse anti-Flag (1:1000, Cell Signaling, cat. no. 8146) and rabbit anti-TOM20 (1:1000, Santa Cruz Biotechnology, cat. no. 11415). After three washes with 3 % BSA, to remove excess of primary antibody, the following secondary antibodies were diluted 1:500 and incubated for 2 h at RT: donkey anti-mouse conjugated to Alexa Fluor 488 nm (Jackson Immuno, cat. no. 715-546-151) and donkey anti-rabbit conjugated to Cy3 (Jackson Immuno, cat. no. 711-165-152). Coverslips were washed

with PBS and nuclei were counterstained with 50 µl 1:1000-diluted DAPI (in PBS) and incubated two to five min. After three additional PBS washes, cover slips were mounted with Aqua-Poly/Mount (Polysciences, cat. no. 18606) and samples were dried, protected from light, overnight at RT. On the next day, mounted cover slips were carefully cleaned with 70 % ethanol. A laser-scanning confocal microscope (Leica, TCS SP5-X and TCS SP8-X) equipped with a white light laser, a 405-diode UV laser, a 100x objective lens (HCX Plan-Apochromat CS 100x oil, 1.46 NA), and hybrid detectors was used to acquire fluorescence images. The following parameters were used for acquisition: image size of 1,024 x 1,024 pixels, bi-directional X, scan speed 200 Hertz, and z-step size 0.2 µm.

4.4. Antibodies used in this study

Table 4 – Antibodies used for western blot in this study

Antigen	Dilution	Company, cat. no.	RRID
bS16 / MRPS16	1:500	Proteintech Group, 16735-1-AP	AB_2180166
Cyt c	1:2000	Abcam, ab13575	AB_300470
DDDDK tag (FLAG-tag)	1:2500	Abcam, ab1257	AB_299216
DYKDDDDK Tag (9A3) mouse antibody	1:1000	Cell Signaling, 8146S	AB_10950495
mL37 / MRPL37	1:1000	Sigma-Aldrich, HPA025826	AB_1854106
mtHSP60	1:1000	Santa Cruz, sc-1052	AB_631683
mtHSP70	1:1000	Abcam, ab47455	AB_881520
OXPHOS cocktail human	1:250	Abcam, ab110411	
OXPHOS cocktail mouse	1:250	Abcam, ab110413	AB_2629281
PUSL1	1:500	Sigma-Aldrich, HPA032057	AB_10601251
SDHA	1:4000	Invitrogen, 459200	AB_1501830

TIM22	1:1000	Proteintech Group, 14927-1-AP	AB_11183050
TIM23	1:1000	Abcam, ab116329	AB_10903878
TIM44	1:2000	Abcam, ab194829	
TOM20	1:1000	Santa Cruz Biotechnology, sc-11415	AB_2207533
TOM22	1:1000	Abcam, ab57523	AB_945897
VDAC	1:4000	Abcam, ab14734	AB_443084
anti-rabbit IgG F(ab')$_2$-HRP	1:8000	GE Healthcare, cat. no. NA9340	AB_772191
Sheep Anti-Mouse IgG, Whole Ab ECL Antibody, HRP conjugated	1:8000	GE Healthcare, NXA931	AB_772209
Donkey anti-Goat IgG (H+L) Cross-Adsorbed Secondary Antibody, HRP conjugated	1:8000	Thermo Fisher, A16005	AB_2534679
Alexa Fluor 488 donkey anti-mouse antibody	1:500	Jackson Immuno, 715-546-151	AB_2340850
Cy3-AffiniPure Donkey Anti-Rabbit IgG (H+L) antibody	1:500	Jackson Immuno, 711-165-152	AB_2307443

4.5. Animal and cell culture models used in this study

Table 5 – Animal and cell cultures models used in this study

Model	Organism/ strain	Genotype	Reference
C57BL/6N control / wild-type mice	*Mus musculus* C57BL/6N	$WT^{+/+}$	RRID: MGI:5795896
Heterozygous MitoRibo-Tag mice (*mL62-Flag* knock-in)	*Mus musculus* C57BL/6N	*mL62-Flag*$^{+/T}$	This study
MitoRibo-Tag mice (*mL62-Flag* knock-in)	*Mus musculus* C57BL/6N	*mL62-Flag*$^{T/T}$	This study
MitoRibo-Tag *Mterf3* control mice	*Mus musculus* C57BL/6N	*mL62-Flag*$^{T/T}$ *Mterf3* loxP$^{P/P}$ *Ckmm Cre*$^{+/+}$	Park et al., 2009 and this study
MitoRibo-Tag *Mterf3* knock-out mice	*Mus musculus* C57BL/6N	*mL62-Flag*$^{T/T}$ *Mterf3* loxP$^{P/P}$ *Ckmm Cre*$^{+/Cre}$	Park et al., 2009 and this study
MitoRibo-Tag *Mterf4* control mice	*Mus musculus* C57BL/6N	*mL62-Flag*$^{T/T}$ *Mterf4* loxP$^{P/P}$ *Ckmm Cre*$^{+/+}$	Cámara et al., 2011 and this study
MitoRibo-Tag *Mterf4* knock-out mice	*Mus musculus* C57BL/6N	*mL62-Flag*$^{T/T}$ *Mterf4 loxP*$^{P/P}$ *Ckmm Cre*$^{+/Cre}$	Cámara et al., 2011 and this study
MitoRibo-Tag *Nsun4* control mice	*Mus musculus* C57BL/6N	*mL62-Flag*$^{T/T}$ *Nsun4 loxP*$^{P/P}$ *Ckmm Cre*$^{+/+}$	Metodiev et al., 2014 and this study
MitoRibo-Tag *Nsun4* knock-out mice	*Mus musculus* C57BL/6N	*mL62-Flag*$^{T/T}$ *Nsun4* loxP$^{P/P}$ *Ckmm Cre*$^{+/Cre}$	Metodiev et al., 2014 and this study
MitoRibo-Tag *Lrpprc* control mice	*Mus musculus* C57BL/6N	*mL62-Flag*$^{T/T}$ *Lrpprc* loxP$^{P/P}$ *Ckmm Cre*$^{+/+}$	Ruzzenente et al., 2012 and this study
MitoRibo-Tag *Lrpprc* knock-out mice	*Mus musculus* C57BL/6N	*mL62-Flag*$^{T/T}$ *Lrpprc* loxP$^{P/P}$ *Ckmm Cre*$^{+/Cre}$	Ruzzenente et al., 2012 and this study
MitoRibo-Tag *Slirp* control mice	*Mus musculus* C57BL/6N	*mL62-Flag*$^{T/T}$ *Slirp* +/+	Lagouge et al., 2015 and this study
MitoRibo-Tag *Slirp* knock-out mice	*Mus musculus* C57BL/6N	*mL62-Flag*$^{T/T}$ *Slirp* -/-	Lagouge et al., 2015 and this study
Flp-In T-REx 293 cell Line	*Homo sapiens*		RRID: CVCL_U427
Flp-In T-REx 293 PUSL1-FLAG expression cell line	*Homo sapiens*	*PUSL1-FLAG*	This study

5. References

Akabane, S., Ueda, T., Nierhaus, K. H., & Takeuchi, N. (2014). Ribosome Rescue and Translation Termination at Non-Standard Stop Codons by ICT1 in Mammalian Mitochondria. *PLoS Genetics*, *10*(9), e1004616. https://doi.org/10.1371/journal.pgen.1004616

Allen, J. F. (2015). Why chloroplasts and mitochondria retain their own genomes and genetic systems: Colocation for redox regulation of gene expression. *Proceedings of the National Academy of Sciences of the United States of America*, *112*(33), 10231–10238. https://doi.org/10.1073/pnas.1500012112

Allen, J. F., & Martin, W. F. (2016). Why have organelles retained genomes? *Cell Systems*, *2*(2), 70–72. https://doi.org/10.1016/j.cels.2016.02.007

Amunts, A., Brown, A., Toots, J., Scheres, S. H. W., & Ramakrishnan, V. (2015). The structure of the human mitochondrial ribosome. *Science*, *348*(6230), 95–98. https://doi.org/10.1126/science.aaa1193

Anderson, S., Bankier, A. T., Barrell, B. G., de Bruijn, M. H. L., Coulson, A. R., Drouin, J., … Young, I. G. (1981). Sequence and organization of the human mitochondrial genome. *Nature*, *290*(5806), 457–465. https://doi.org/10.1038/290457a0

Antonicka, H., Choquet, K., Lin, Z., Gingras, A., Kleinman, C. L., & Shoubridge, E. A. (2017). A pseudouridine synthase module is essential for mitochondrial protein synthesis and cell viability. *EMBO Reports*, *18*(1), 28–38. https://doi.org/10.15252/embr.201643391

Antonicka, H., & Shoubridge, E. A. (2015). Mitochondrial RNA Granules Are Centers for Posttranscriptional RNA Processing and Ribosome Biogenesis. *Cell Reports*, *10*(6), 920–932. https://doi.org/10.1016/j.celrep.2015.01.030

Arroyo, J. D., Jourdain, A. A., Calvo, S. E., Ballarano, C. A., Doench, J. G., Root, D. E., & Mootha, V. K. (2016). A Genome-wide CRISPR Death Screen Identifies Genes Essential for Oxidative Phosphorylation. *Cell Metabolism*, *24*(6), 875–885. https://doi.org/10.1016/j.cmet.2016.08.017

Baer, R. J., & Dubin, D. T. (1981). Methylated regions of hamster mitochondrial ribosomal RNA: structural and functional correlates. *Nucleic Acids Research*, *9*(2), 323–337. Retrieved from http://www.ncbi.nlm.nih.gov/pubmed/6782552

Ban, N., Beckmann, R., Cate, J. H. D., Dinman, J. D., Dragon, F., Ellis, S. R., … Yusupov, M. (2014). A new system for naming ribosomal proteins. *Current Opinion in Structural Biology*, *24*(1), 165–169. https://doi.org/10.1016/j.sbi.2014.01.002

Ban, N., Nissen, P., Hansen, J., Moore, P. B., & Steitz, T. a. (2000). The complete atomic structure of the large ribosomal subunit at 2. *4 A Resolution. Science*, *289*(August), 905±920.

Bateman, A., Martin, M. J., O'Donovan, C., Magrane, M., Alpi, E., Antunes, R., … Zhang, J. (2017). UniProt: The universal protein knowledgebase. *Nucleic Acids Research*, *45*(D1), D158–D169. https://doi.org/10.1093/nar/gkw1099

Baughman, J. M., Nilsson, R., Gohil, V. M., Arlow, D. H., Gauhar, Z., & Mootha, V. K. (2009). A computational screen for regulators of oxidative phosphorylation implicates SLIRP in mitochondrial RNA homeostasis. *PLoS Genetics*, *5*(8).

https://doi.org/10.1371/journal.pgen.1000590
Benjamini, Y., & Hochberg, Y. (1995). Controlling the False Discovery Rate: A Practical and Powerful Approach to Multiple testing. *Journal of the Royal Statistical Society. Series B*, *57*(1), 289–300. https://doi.org/10.2307/2346101
Bibb, M. J., Van Etten, R. A., Wright, C. T., Walberg, M. W., & Clayton, D. A. (1981). Sequence and gene organization of mouse mitochondrial DNA. *Cell*, *26*(2 PART 2), 167–180. https://doi.org/10.1016/0092-8674(81)90300-7
Bogenhagen, D. F., Martin, D. W., & Koller, A. (2014). Initial steps in RNA processing and ribosome assembly occur at mitochondrial DNA nucleoids. *Cell Metabolism*, *19*(4), 618–629. https://doi.org/10.1016/j.cmet.2014.03.013
Bogenhagen, D. F., Ostermeyer-Fay, A. G., Haley, J. D., & Garcia-Diaz, M. (2018). Kinetics and Mechanism of Mammalian Mitochondrial Ribosome Assembly. *Cell Reports*, *22*(7), 1935–1944. https://doi.org/10.1016/j.celrep.2018.01.066
Bordier, C. (1981). Phase separation of integral membrane protein in Triton X-114 solution. *Journal of Biological Chemistry*, *256*(4), 1604–1607.
Borna, N. N., Kishita, Y., Kohda, M., Lim, S. C., Shimura, M., & Wu, Y. (2019). Mitochondrial ribosomal protein PTCD3 mutations cause oxidative phosphorylation defects with Leigh syndrome. *Neurogenetics*. https://doi.org/https://doi.org/10.1007/s10048-018-0561-9
Box, J. M., Kaur, J., & Stuart, R. A. (2017). MrpL35, a mitospecific component of mitoribosomes, plays a key role in cytochrome *c* oxidase assembly. *Molecular Biology of the Cell*, *28*(24), 3489–3499. https://doi.org/10.1091/mbc.e17-04-0239
Braymer, J. J., & Lill, R. (2017). Iron–sulfur cluster biogenesis and trafficking in mitochondria. *Journal of Biological Chemistry*, *292*(31), 12754–12763. https://doi.org/10.1074/jbc.R117.787101
Brown, A., Amunts, A., Bai, X. C., Sugimoto, Y., Edwards, P. C., Murshudov, G., … Ramakrishnan, V. (2014). Structure of the large ribosomal subunit from human mitochondria. *Science*, *346*(6210), 718–722. https://doi.org/10.1126/science.1258026
Brown, A., Rathore, S., Kimanius, D., Aibara, S., Bai, X. C., Rorbach, J., … Ramakrishnan, V. (2017a). Structures of the human mitochondrial ribosome in native states of assembly. *Nature Structural and Molecular Biology*, *24*(10), 866–869. https://doi.org/10.1038/nsmb.3464
Brown, A., Rathore, S., Kimanius, D., Aibara, S., Bai, X. C., Rorbach, J., … Ramakrishnan, V. (2017b). Structures of the human mitochondrial ribosome in native states of assembly SUPPLEMENTARY. *Nature Structural and Molecular Biology*, *24*(10), 866–869. https://doi.org/10.1038/nsmb.3464
Bykhovskaya, Y., Casas, K., Mengesha, E., Inbal, A., & Fischel-Ghodsian, N. (2004). Missense Mutation in Pseudouridine Synthase 1 (PUS1) Causes Mitochondrial Myopathy and Sideroblastic Anemia (MLASA). *The American Journal of Human Genetics*, *74*(6), 1303–1308. https://doi.org/10.1086/421530
Calvo, S. E., Clauser, K. R., & Mootha, V. K. (2016). MitoCarta2.0: An updated inventory of mammalian mitochondrial proteins. *Nucleic Acids Research*, *44*(D1), D1251–D1257. https://doi.org/10.1093/nar/gkv1003
Calvo, S. E., & Mootha, V. K. (2010). The Mitochondrial Proteome and Human Disease. *Annual Review of Genomics and Human Genetics*, *11*(1), 25–44.

https://doi.org/10.1146/annurev-genom-082509-141720
Cámara, Y., Asin-Cayuela, J., Park, C. B., Metodiev, M. D., Shi, Y., Ruzzenente, B., … Larsson, N. G. (2011). MTERF4 regulates translation by targeting the methyltransferase NSUN4 to the mammalian mitochondrial ribosome. *Cell Metabolism*, *13*(5), 527–539. https://doi.org/10.1016/j.cmet.2011.04.002
Carroll, C. J., Isohanni, P., Pöyhönen, R., Euro, L., Richter, U., Brilhante, V., … Suomalainen, A. (2013). Whole-exome sequencing identifies a mutation in the mitochondrial ribosome protein MRPL44 to underlie mitochondrial infantile cardiomyopathy. *Journal of Medical Genetics*, *50*(3), 151–159. https://doi.org/10.1136/jmedgenet-2012-101375
Claros, M. G., & Vincens, P. (1996). Computational Method to Predict Mitochondrially Imported Proteins and their Targeting Sequences. *European Journal of Biochemistry*, *241*(3), 779–786. https://doi.org/10.1111/j.1432-1033.1996.00779.x
Couvillion, M. T., Soto, I. C., Shipkovenska, G., & Churchman, L. S. (2016). Synchronized mitochondrial and cytosolic translation programs. *Nature*, *533*(7604), 499–503. https://doi.org/10.1038/nature18015
Cox, J., Hein, M. Y., Luber, C. A., Paron, I., Nagaraj, N., & Mann, M. (2014). Accurate Proteome-wide Label-free Quantification by Delayed Normalization and Maximal Peptide Ratio Extraction, Termed MaxLFQ. *Molecular & Cellular Proteomics*, *13*(9), 2513–2526. https://doi.org/10.1074/mcp.M113.031591
Cox, J., & Mann, M. (2008). MaxQuant enables high peptide identification rates, individualized p.p.b.-range mass accuracies and proteome-wide protein quantification. *Nature Biotechnology*, *26*(12), 1367–1372. https://doi.org/10.1038/nbt.1511
Cox, J., Neuhauser, N., Michalski, A., Scheltema, R. A., Olsen, J. V., & Mann, M. (2011). Andromeda: A peptide search engine integrated into the MaxQuant environment. *Journal of Proteome Research*, *10*(4), 1794–1805. https://doi.org/10.1021/pr101065j
Davis, J. H., & Williamson, J. R. (2017). Structure and dynamics of bacterial ribosome biogenesis. *Philosophical Transactions of the Royal Society of London. Series B, Biological Sciences*, *372*(1716). https://doi.org/10.1098/rstb.2016.0181
Del Campo, M., Ofengand, J., & Malhotra, A. (2004). Crystal structure of the catalytic domain of RluD, the only rRNA pseudouridine synthase required for normal growth of Escherichia coli. *Rna*, *10*(2), 231–239. https://doi.org/10.1261/rna.5187404
Dennerlein, S., Rozanska, A., Wydro, M., Chrzanowska-Lightowlers, Z. M. A., & Lightowlers, R. N. (2010). Human ERAL1 is a mitochondrial RNA chaperone involved in the assembly of the 28S small mitochondrial ribosomal subunit. *Biochemical Journal*, *430*(3), 551–558. https://doi.org/10.1042/BJ20100757
Desai, N., Brown, A., Amunts, A., & Ramakrishnan, V. (2017). The structure of the yeast mitochondrial ribosome. *Science (New York, N.Y.)*, *355*(6324), 528–531. https://doi.org/10.1126/science.aal2415
Distelmaier, F., Haack, T. B., Catarino, C. B., Gallenmüller, C., Rodenburg, R. J., Strom, T. M., … Klopstock, T. (2015). MRPL44 mutations cause a slowly progressive multisystem disease with childhood-onset hypertrophic cardiomyopathy. *Neurogenetics*, *16*(4), 319–323. https://doi.org/10.1007/s10048-015-0444-2
Dubin, D. T. (1974). Methylated nucleotide content of mitochondrial ribosomal RNA from

hamster cells. *Journal of Molecular Biology*, *84*(2), 257–273. https://doi.org/10.1016/0022-2836(74)90584-1

Dubin, D. T., & Taylor, R. H. (1978). Modification of mitochondrial ribosomal RNA from hamster cells: the presence of GmG and late-methylated UmGmU in the large subunit (17S) RNA. *Journal of Molecular Biology*, *121*(4), 523–540. https://doi.org/10.1006/jmbi.1996.0737

Englmeier, R., Pfeffer, S., & Förster, F. (2017). Structure of the Human Mitochondrial Ribosome Studied in Situ by Cryoelectron Tomography. *Structure*, *25*(10), 1574–1581.e2. https://doi.org/10.1016/j.str.2017.07.011

Fernandez-Vizarra, E., Berardinelli, A., Valente, L., Tiranti, V., & Zeviani, M. (2007). Nonsense mutation in pseudouridylate synthase 1 (PUS1) in two brothers affected by myopathy, lactic acidosis and sideroblastic anaemia (MLASA). *Journal of Medical Genetics*, *44*(3), 173–180. https://doi.org/10.1136/jmg.2006.045252

Fujiki, Y., Fowler, S., Shio, H., Hubbard, A. L., & Lazarow, P. B. (1982). Polypeptide and Phospholipid Composition of the Membrane of Rat Liver Peroxisomes: Comparison with Endoplasmic Reticulum and Mitochondrial Membranes Preparation of Membranes by Means of Sodium Carbonate Treatment Characterization of Peroxisomal Membranes. *The Journal of Cell Biology*, *93*(7), 103–110. https://doi.org/10.1083/jcb.93.1.103

Fujiki, Y., Hubbard, A. L., Fowler, S., & Lazarow, P. B. (1982). Isolation of Intracellular Membranes by Means of Sodium Carbonate Treatment : Application to Endoplasmic Reticulum. *Journal of Cell Biology*, *93*(3), 97–102.

Fung, S., Nishimura, T., Sasarman, F., & Shoubridge, E. A. (2013). The conserved interaction of C7orf30 with MRPL14 promotes biogenesis of the mitochondrial large ribosomal subunit and mitochondrial translation. *Molecular Biology of the Cell*, *24*(3), 184–193. https://doi.org/10.1091/mbc.E12-09-0651

Fusté, J. M., Wanrooij, S., Jemt, E., Granycome, C. E., Cluett, T. J., Shi, Y., … Falkenberg, M. (2010). Mitochondrial RNA polymerase is needed for activation of the origin of light-strand DNA replication. *Molecular Cell*, *37*(1), 67–78. https://doi.org/10.1016/j.molcel.2009.12.021

Galmiche, L., Serre, V., Beinat, M., Assouline, Z., Lebre, A. S., Chretien, D., … Rötig, A. (2011). Exome sequencing identifies MRPL3 mutation in mitochondrial cardiomyopathy. *Human Mutation*, *32*(11), 1225–1231. https://doi.org/10.1002/humu.21562

Gardeitchik, T., Mohamed, M., Ruzzenente, B., Karall, D., Guerrero-Castillo, S., Dalloyaux, D., … Morava, E. (2018). Bi-allelic Mutations in the Mitochondrial Ribosomal Protein MRPS2 Cause Sensorineural Hearing Loss, Hypoglycemia, and Multiple OXPHOS Complex Deficiencies. *American Journal of Human Genetics*, *102*(4), 685–695. https://doi.org/10.1016/j.ajhg.2018.02.012

Gaur, R., Grasso, D., Datta, P. P., Krishna, P. D. V., Das, G., Spencer, A., … Varshney, U. (2008). A Single Mammalian Mitochondrial Translation Initiation Factor Functionally Replaces Two Bacterial Factors. *Molecular Cell*, *29*(2), 180–190. https://doi.org/10.1016/j.molcel.2007.11.021

Gray, M. W. (2017). Lynn Margulis and the endosymbiont hypothesis: 50 years later. *Molecular Biology of the Cell*, *28*(10), 1285–1287. https://doi.org/10.1091/mbc.E16-07-0509

Gray, M. W., Burger, G., & Lang, B. F. (2008). Mitochondrial Evolution. *Science*, *1476*(March), 1–16. https://doi.org/10.1126/science.283.5407.1476

Greber, B. J., & Ban, N. (2016). Structure and Function of the Mitochondrial Ribosome. *Annual Review of Biochemistry*, *85*(1), 103–132. https://doi.org/10.1146/annurev-biochem-060815-014343

Greber, B. J., Bieri, P., & Leibundgut, M. (2015). The complete structure of the 55 S mammalian mitochondrial ribosome. *Science*, (April), 1–11.

Greber, B. J., Bieri, P., Leibundgut, M., Leitner, A., Aebersold, R., Boehringer, D., & Ban, N. (2014). The complete structure of the 55S mammalian mitochondrial ribosome. *Nature*, *348*(6232), 303–308. https://doi.org/10.1016/0022-2852(62)90219-9

Greber, B. J., Boehringer, D., Leibundgut, M., Bieri, P., Leitner, A., Schmitz, N., … Ban, N. (2014). The complete structure of the large subunit of the mammalian mitochondrial ribosome. *Nature*, *515*(7526), 283–286. https://doi.org/10.1038/nature13895

Greber, B. J., Boehringer, D., Leitner, A., Bieri, P., Voigts-Hoffmann, F., Erzberger, J. P., … Ban, N. (2014). Architecture of the large subunit of the mammalian mitochondrial ribosome. *Nature*, *505*(7484), 515–519. https://doi.org/10.1038/nature12890

Grohmann, K., Amairic, F., Crews, S., & Attardi, G. (1978). Failure to detect "cap" structures in mitochondrial DNA-coded poly(A)-containing RNA from HeLa cells. *Nucleic Acids Research*, *5*(3), 637–651. Retrieved from http://www.ncbi.nlm.nih.gov/pubmed/643614

Gruschke, S., Kehrein, K., Römpler, K., Gröne, K., Israel, L., Imhof, A., … Ott, M. (2011). Cbp3-Cbp6 interacts with the yeast mitochondrial ribosomal tunnel exit and promotes cytochrome b synthesis and assembly. *Journal of Cell Biology*, *193*(6), 1101–1114. https://doi.org/10.1083/jcb.201103132

Guarani, V., Paulo, J., Zhai, B., Huttlin, E. L., Gygi, S. P., & Harper, J. W. (2014). TIMMDC1/C3orf1 Functions as a Membrane-Embedded Mitochondrial Complex I Assembly Factor through Association with the MCIA Complex. *Molecular and Cellular Biology*, *34*(5), 847–861. https://doi.org/10.1128/MCB.01551-13

Guedes-Monteiro, R. F., Ferreira-Junior, J. R., Bleicher, L., Nóbrega, F. G., Barrientos, A., & Barros, M. H. (2018). Mitochondrial ribosome bL34 mutants present diminished translation of cytochrome c oxidase subunits. *Cell Biology International*, *42*(6), 630–642. https://doi.org/10.1002/cbin.10913

Guo, X., Niemi, N. M., Hutchins, P. D., Condon, S. G. F., Jochem, A., Ulbrich, A., … Pagliarini, D. J. (2017). Ptc7p Dephosphorylates Select Mitochondrial Proteins to Enhance Metabolic Function. *Cell Reports*, *18*(2), 307–313. https://doi.org/10.1016/j.celrep.2016.12.049

Gustafsson, C. M., Falkenberg, M., & Larsson, N.-G. (2016). Maintenance and Expression of Mammalian Mitochondrial DNA. *Annual Review of Biochemistry*, *85*(1), 133–160. https://doi.org/10.1146/annurev-biochem-060815-014402

Haack, T. B., Kopajtich, R., Freisinger, P., Wieland, T., Rorbach, J., Nicholls, T. J., … Prokisch, H. (2013). ELAC2 mutations cause a mitochondrial RNA processing defect associated with hypertrophic cardiomyopathy. *American Journal of Human Genetics*, *93*(2), 211–223. https://doi.org/10.1016/j.ajhg.2013.06.006

Hällberg, B. M., & Larsson, N. G. (2014). Making proteins in the powerhouse. *Cell Metabolism*, *20*(2), 226–240. https://doi.org/10.1016/j.cmet.2014.07.001

Hansson, A., Hance, N., Dufour, E., Rantanen, A., Hultenby, K., Clayton, D. A., … Larsson, N.-Go. (2004). A switch in metabolism precedes increased mitochondrial biogenesis in respiratory chain-deficient mouse hearts. *Proceedings of the National Academy of Sciences*, *101*(9), 3136–3141. https://doi.org/10.1073/pnas.0308710100

Haque, M. E., Elmore, K. B., Tripathy, A., Koc, H., Koc, E. C., & Spremulli, L. L. (2010). Properties of the C-terminal tail of human mitochondrial inner membrane protein Oxa1L and its interactions with mammalian mitochondrial ribosomes. *Journal of Biological Chemistry*, *285*(36), 28353–28362. https://doi.org/10.1074/jbc.M110.148262

Haque, M. E., Spremulli, L. L., & Fecko, C. J. (2010). Identification of protein-protein and protein-ribosome interacting regions of the C-terminal tail of human mitochondrial inner membrane protein Oxa1L. *Journal of Biological Chemistry*, *285*(45), 34991–34998. https://doi.org/10.1074/jbc.M110.163808

He, J., Cooper, H. M., Reyes, A., Di Re, M., Kazak, L., Wood, S. R., … Holt, I. J. (2012). Human C4orf14 interacts with the mitochondrial nucleoid and is involved in the biogenesis of the small mitochondrial ribosomal subunit. *Nucleic Acids Research*, *40*(13), 6097–6108. https://doi.org/10.1093/nar/gks257

Heublein, M., Burguillos, M. A., Vogtle, F. N., Teixeira, P. F., Imhof, A., Meisinger, C., & Ott, M. (2014). The novel component Kgd4 recruits the E3 subunit to the mitochondrial -ketoglutarate dehydrogenase. *Molecular Biology of the Cell*, *25*(21), 3342–3349. https://doi.org/10.1091/mbc.E14-07-1178

Hillen, H. S., Temiakov, D., & Cramer, P. (2018). Structural basis of mitochondrial transcription. *Nature Structural and Molecular Biology*, *25*(9), 754–765. https://doi.org/10.1038/s41594-018-0122-9

Hodgkinson, A., Idaghdour, Y., Gbeha, E., Grenier, J.-C., Hip-Ki, E., Bruat, V., … Awadalla, P. (2014). High-Resolution Genomic Analysis of Human Mitochondrial RNA Sequence Variation. *Science*, *344*(6182), 413–415. https://doi.org/10.1126/science.1251110

Holt, I. J., Harding, A. E., & Morgan-Hughes, J. A. (1988). Deletions of muscle mitochondrial DNA in patients with mitochondrial myopathies. *Nature*, *331*(6158), 717–719. https://doi.org/10.1038/331717a0

Holzmann, J., Frank, P., Löffler, E., Bennett, K. L., Gerner, C., & Rossmanith, W. (2008). RNase P without RNA: Identification and Functional Reconstitution of the Human Mitochondrial tRNA Processing Enzyme. *Cell*, *135*(3), 462–474. https://doi.org/10.1016/j.cell.2008.09.013

Hur, S., & Stroud, R. M. (2007). How U38, 39, and 40 of Many tRNAs Become the Targets for Pseudouridylation by TruA. *Molecular Cell*, *26*(2), 189–203. https://doi.org/10.1016/j.molcel.2007.02.027

Ingolia, N. T., Ghaemmaghami, S., Newman, J. R. S., & Weissman, J. S. (2009). Genome-wide analysis in vivo of translation with nucleotide resolution using ribosome profiling. supplementary material. *Science (New York, N.Y.)*, *324*(5924), 218–223. https://doi.org/10.1126/science.1168978

Isaac, R. S., McShane, E., & Churchman, L. S. (2018). The Multiple Levels of

Mitonuclear Coregulation. *Annual Review of Genetics*, *52*(1), annurev-genet-120417-031709. https://doi.org/10.1177/0885328210391495

Jackson, C. B., Huemer, M., Bolognini, R., Martin, F., Szinnai, G., Donner, B. C., … Schaller, A. (2018). A variant in MRPS14 (uS14m) causes perinatal hypertrophic cardiomyopathy with neonatal lactic acidosis, growth retardation, dysmorphic features and neurological involvement. *Human Molecular Genetics*, *00*(00), 1–11. https://doi.org/10.1093/hmg/ddy374

Jain, I. H., Zazzeron, L., Goli, R., Alexa, K., Schatzman-Bone, S., Dhillon, H., … Mootha, V. K. (2016). Hypoxia as a therapy for mitochondrial disease. *Science*, *352*(6281), 54–61. https://doi.org/10.1126/science.aad9642

Jin, C., Myers, A. M., & Tzagoloff, A. (1997). Cloning and characterization of MRP10, a yeast gene coding for a mitochondrial ribosomal protein. *Current Genetics*, *31*(3), 228–234. Retrieved from http://www.ncbi.nlm.nih.gov/pubmed/9065385

Jourdain, A. A., Koppen, M., Rodley, C. D., Maundrell, K., Gueguen, N., Reynier, P., … Martinou, J. C. (2015). A Mitochondria-Specific Isoform of FASTK Is Present In Mitochondrial RNA Granules and Regulates Gene Expression and Function. *Cell Reports*, *10*(7), 1110–1121. https://doi.org/10.1016/j.celrep.2015.01.063

Jourdain, A. A., Koppen, M., Wydro, M., Rodley, C. D., Lightowlers, R. N., Chrzanowska-Lightowlers, Z. M., & Martinou, J. C. (2013). GRSF1 regulates RNA processing in mitochondrial RNA granules. *Cell Metabolism*, *17*(3), 399–410. https://doi.org/10.1016/j.cmet.2013.02.005

Jourdain, A. A., Popow, J., De La Fuente, M. A., Martinou, J. C., Anderson, P., & Simarro, M. (2017). The FASTK family of proteins: Emerging regulators of mitochondrial RNA biology. *Nucleic Acids Research*, *45*(19), 10941–10947. https://doi.org/10.1093/nar/gkx772

Kasapkara, Ç. S., Tümer, L., Zanetti, N., Ezgü, F., Lamantea, E., & Zeviani, M. (2017). A Myopathy, Lactic Acidosis, Sideroblastic Anemia (Mlasa) Case Due to A Novel Pus1 Mutation. *Turkish Journal of Hematology*, (Table 1), 1–2. https://doi.org/10.4274/tjh.2017.0231

Kauppila, J. H. K., Baines, H. L., Bratic, A., Simard, M. L., Freyer, C., Mourier, A., … Stewart, J. B. (2016). A Phenotype-Driven Approach to Generate Mouse Models with Pathogenic mtDNA Mutations Causing Mitochondrial Disease. *Cell Reports*, *16*(11), 2980–2990. https://doi.org/10.1016/j.celrep.2016.08.037

Kehrein, K., Schilling, R., Möller-Hergt, B. V., Wurm, C. A., Jakobs, S., Lamkemeyer, T., … Ott, M. (2015). Organization of Mitochondrial Gene Expression in Two Distinct Ribosome-Containing Assemblies. *Cell Reports*, *10*(6), 843–853. https://doi.org/10.1016/j.celrep.2015.01.012

Keilhauer, E. C., Hein, M. Y., & Mann, M. (2015). Accurate Protein Complex Retrieval by Affinity Enrichment Mass Spectrometry (AE-MS) Rather than Affinity Purification Mass Spectrometry (AP-MS). *Molecular & Cellular Proteomics*, *14*(1), 120–135. https://doi.org/10.1074/mcp.M114.041012

Khatami, S., Rokni-Zadeh, H., Mohsen-Pour, N., Biglari, A., Changi-Ashtiani, M., Shahrooei, M., & Shahani, T. (2018). Whole exome sequencing identifies both nuclear and mitochondrial variations in an Iranian family with non-syndromic hearing loss. *Mitochondrion*. https://doi.org/10.1016/J.MITO.2018.08.006

Kim, H.-J., & Barrientos, A. (2018). MTG1 couples mitoribosome large subunit assembly

with intersubunit bridge formation. *Nucleic Acids Research*, (August), 1–19. https://doi.org/10.1093/nar/gky672

Koc, E. C., & Koc, H. (2012). Regulation of mammalian mitochondrial translation by post-translational modifications. *Biochimica et Biophysica Acta (BBA) - Gene Regulatory Mechanisms*, *1819*(9–10), 1055–1066. https://doi.org/10.1016/j.bbagrm.2012.03.003

Koc, E. C., Miller-Lee, J. L., & Koc, H. (2017). Fyn kinase regulates translation in mammalian mitochondria. *Biochimica et Biophysica Acta - General Subjects*, *1861*(3), 1–5. https://doi.org/10.1016/j.bbagen.2016.12.004

Kohda, M., Tokuzawa, Y., Kishita, Y., Nyuzuki, H., Moriyama, Y., Mizuno, Y., … Okazaki, Y. (2016). A Comprehensive Genomic Analysis Reveals the Genetic Landscape of Mitochondrial Respiratory Chain Complex Deficiencies. *PLoS Genetics*, *12*(1), 1–31. https://doi.org/10.1371/journal.pgen.1005679

Kolanczyk, M., Pech, M., Zemojtel, T., Yamamoto, H., Mikula, I., Calvaruso, M.-A., … Mundlos, S. (2011). NOA1 is an essential GTPase required for mitochondrial protein synthesis. *Molecular Biology of the Cell*, *22*(1), 1–11. https://doi.org/10.1091/mbc.E10-07-0643

Kressler, D., Hurt, E., & Baßler, J. (2010). Driving ribosome assembly. *Biochimica et Biophysica Acta - Molecular Cell Research*, *1803*(6), 673–683. https://doi.org/10.1016/j.bbamcr.2009.10.009

Krüger, M., Moser, M., Ussar, S., Thievessen, I., Luber, C. A., Forner, F., … Mann, M. (2008). SILAC Mouse for Quantitative Proteomics Uncovers Kindlin-3 as an Essential Factor for Red Blood Cell Function. *Cell*, *134*(2), 353–364. https://doi.org/10.1016/j.cell.2008.05.033

Kruse, B., Narasimhan, N., & Attardi, G. (1989). Termination of transcription in human mitochondria: identification and purification of a DNA binding protein factor that promotes termination. *Cell*, *58*(2), 391–397. https://doi.org/10.1016/0092-8674(89)90853-2

Kühl, I., Kukat, C., Ruzzenente, B., Milenkovic, D., Mourier, A., Miranda, M., … Larsson, N. G. (2014). POLRMT does not transcribe nuclear genes. *Nature*, *514*(7521), E7–E11. https://doi.org/10.1038/nature13690

Kühl, I., Miranda, M., Atanassov, I., Kuznetsova, I., Hinze, Y., Mourier, A., … Larsson, N. G. (2017). Transcriptomic and proteomic landscape of mitochondrial dysfunction reveals secondary coenzyme Q deficiency in mammals. *ELife*, *6*, 1–33. https://doi.org/10.7554/eLife.30952

Kühl, I., Miranda, M., Posse, V., Milenkovic, D., Mourier, A., Siira, S. J., … Larsson, N. G. (2016). POLRMT regulates the switch between replication primer formation and gene expression of mammalian mtDNA. *Science Advances*, *2*(8), 1–15. https://doi.org/10.1126/sciadv.1600963

Kukat, C., Wurm, C. A., Spahr, H., Falkenberg, M., Larsson, N.-G., & Jakobs, S. (2011). Super-resolution microscopy reveals that mammalian mitochondrial nucleoids have a uniform size and frequently contain a single copy of mtDNA. *Proceedings of the National Academy of Sciences*, *108*(33), 13534–13539. https://doi.org/10.1073/pnas.1109263108

Kulak, N. A., Pichler, G., Paron, I., Nagaraj, N., & Mann, M. (2014). Minimal, encapsulated proteomic-sample processing applied to copy-number estimation in

eukaryotic cells. *Nat Methods*, *11*(3), 319–324. https://doi.org/10.1038/nmeth.2834
Kummer, E., Leibundgut, M., Rackham, O., Lee, R. G., Boehringer, D., Filipovska, A., & Ban, N. (2018). Unique features of mammalian mitochondrial translation initiation revealed by cryo-EM. *Nature*, *560*(7717), 263–267. https://doi.org/10.1038/s41586-018-0373-y
Kuzmenko, A., Derbikova, K., Salvatori, R., Tankov, S., Atkinson, G. C., Tenson, T., … Hauryliuk, V. (2016). Aim-less translation: Loss of Saccharomyces cerevisiae mitochondrial translation initiation factor mIF3/Aim23 leads to unbalanced protein synthesis. *Scientific Reports*, *6*(June 2015), 1–9. https://doi.org/10.1038/srep18749
Lagouge, M., Mourier, A., Lee, H. J., Spåhr, H., Wai, T., Kukat, C., … Larsson, N. G. (2015). SLIRP Regulates the Rate of Mitochondrial Protein Synthesis and Protects LRPPRC from Degradation. *PLoS Genetics*, *11*(8), 1–19. https://doi.org/10.1371/journal.pgen.1005423
Lake, N. J., Webb, B. D., Stroud, D. A., Richman, T. R., Ruzzenente, B., Compton, A. G., … Thorburn, D. R. (2017). Biallelic Mutations in MRPS34 Lead to Instability of the Small Mitoribosomal Subunit and Leigh Syndrome. *American Journal of Human Genetics*, *101*(2), 239–254. https://doi.org/10.1016/j.ajhg.2017.07.005
Larsson, N.-G. (2010). Somatic Mitochondrial DNA Mutations in Mammalian Aging. *Annual Review of Biochemistry*, *79*(1), 683–706. https://doi.org/10.1146/annurev-biochem-060408-093701
Larsson, N. G., Wang, J., Wilhelmsson, H., Oldfors, A., Rustin, P., Lewandoski, M., … Clayton, D. A. (1998). Mitochondrial transcription factor A is necessary for mtDNA maintenance and embryogenesis in mice. *Nature Genetics*, *18*(3), 231–236. https://doi.org/10.1038/ng0398-231
Lavdovskaia, E., Kolander, E., Steube, E., Mai, M. M.-Q., Urlaub, H., & Richter-Dennerlein, R. (2018). The human Obg protein GTPBP10 is involved in mitoribosomal biogenesis. *Nucleic Acids Research*, (August), 1–12. https://doi.org/10.1093/nar/gky701
Lee, K., & Bogenhagen, D. F. (2016). Scalable Isolation of Mammalian Mitochondria for Nucleic Acid and Nucleoid Analysis. *Methods in Molecular Biology*, *1351*, 67–79. https://doi.org/10.1007/978-1-4939-3040-1
Lee, K. W., & Bogenhagen, D. F. (2014). Assignment of 2'-O-methyltransferases to modification sites on the mammalian mitochondrial large subunit 16 S ribosomal RNA (rRNA). *Journal of Biological Chemistry*, *289*(36), 24936–24942. https://doi.org/10.1074/jbc.C114.581868
Lee, K. W., Okot-Kotber, C., La Comb, J. F., & Bogenhagen, D. F. (2013). Mitochondrial ribosomal RNA (rRNA) methyltransferase family members are positioned to modify nascent rRNA in foci near the mitochondrial DNA nucleoid. *Journal of Biological Chemistry*, *288*(43), 31386–31399. https://doi.org/10.1074/jbc.M113.515692
Lee, R. G., Rudler, D. L., Rackham, O., & Filipovska, A. (2018). Is mitochondrial gene expression coordinated or stochastic? *Biochemical Society Transactions*, (August), BST20180174. https://doi.org/10.1042/BST20180174
Li, F., Liu, X., Zhou, W., Yang, X., & Shen, Y. (2015). Auto-inhibitory mechanism of the human mitochondrial RNase P protein complex. *Scientific Reports*, *5*, 1–7. https://doi.org/10.1038/srep09878
Lill, R., & Mühlenhoff, U. (2008). Maturation of Iron-Sulfur Proteins in Eukaryotes:

Mechanisms, Connected Processes, and Diseases. *Annual Review of Biochemistry*, *77*(1), 669–700. https://doi.org/10.1146/annurev.biochem.76.052705.162653

Lin, H., Miyauchi, K., Harada, T., Okita, R., Takeshita, E., Komaki, H., … Suzuki, T. (2018). CO2-sensitive tRNA modification associated with human mitochondrial disease. *Nature Communications*, *9*(1). https://doi.org/10.1038/s41467-018-04250-4

Liu, F., Lössl, P., Rabbitts, B. M., Balaban, R. S., & Heck, A. J. R. (2017). The interactome of intact mitochondria by cross-linking mass spectrometry provides evidence for co-existing respiratory supercomplexes. *Molecular & Cellular Proteomics*, mcp.RA117.000470. https://doi.org/10.1074/mcp.RA117.000470

Liu, M., & Spremulli, L. (2000). Interaction of mammalian mitochondrial ribosomes with the inner membrane. *Journal of Biological Chemistry*, *275*(38), 29400–29406. https://doi.org/10.1074/jbc.M002173200

Loh, P. C., Morimoto, T., Matsuo, Y., Oshima, T., & Ogasawara, N. (2007). The GTP-binding protein YqeH participates in biogenesis of the 30S ribosome subunit in Bacillus subtilis. *Genes & Genetic Systems*, *82*(4), 281–289. https://doi.org/10.1266/ggs.82.281

Longen, S., Woellhaf, M. W., Petrungaro, C., Riemer, J., & Herrmann, J. M. (2014). The Disulfide Relay of the Intermembrane Space Oxidizes the Ribosomal Subunit Mrp10 on Its Transit into the Mitochondrial Matrix. *Developmental Cell*, *28*(1), 30–42. https://doi.org/10.1016/j.devcel.2013.11.007

Lopez-Lluch, G., Hunt, N., Jones, B., Zhu, M., Jamieson, H., Hilmer, S., … de Cabo, R. (2006). Calorie restriction induces mitochondrial biogenesis and bioenergetic efficiency. *Proceedings of the National Academy of Sciences*, *103*(6), 1768–1773. https://doi.org/10.1073/pnas.0510452103

Lorenzi, I., Oeljeklaus, S., Aich, A., Ronsör, C., Callegari, S., Dudek, J., … Rehling, P. (2018). The mitochondrial TMEM177 associates with COX20 during COX2 biogenesis. *Biochimica et Biophysica Acta - Molecular Cell Research*, *1865*(2), 323–333. https://doi.org/10.1016/j.bbamcr.2017.11.010

Maiti, P., Kim, H.-J., Tu, Y.-T., & Barrientos, A. (2018). Human GTPBP10 is required for mitoribosome maturation. *Nucleic Acids Research*, 1–15. https://doi.org/10.1093/nar/gky938

Martin, W. F., Tielens, A. G. M., Mentel, M., Garg, S. G., & Gould, S. B. (2017). The Physiology of Phagocytosis in the Context of Mitochondrial Origin. *Microbiology and Molecular Biology Reviews*, *81*(3), e00008-17. https://doi.org/10.1128/MMBR.00008-17

Martin, W., & Müller, M. (1998). The hydrogen hypothesis for the first eukaryote. *Nature*, *392*(6671), 37–41. https://doi.org/10.1038/32096

Mathias, R. A., Chen, Y. S., Kapp, E. A., Greening, D. W., Mathivanan, S., & Simpson, R. J. (2011). Triton X-114 phase separation in the isolation and purification of mouse liver microsomal membrane proteins. *Methods*, *54*(4), 396–406. https://doi.org/10.1016/j.ymeth.2011.01.006

Matthews, D. E., Hessler, R. A., Denslow, N. D., Edwards, J. S., & O'Brien, T. W. (1982a). Protein composition of the bovine mitochondrial ribosome. *Journal of Biological Chemistry*, *257*(15), 8788–8794.

Matthews, D. E., Hessler, R. A., Denslow, N. D., Edwards, J. S., & O'Brien, T. W. (1982b). Protein composition of the bovine mitochondrial ribosome. *J Biol Chem*, *257*(15), 8788–8794. Retrieved from http://www.ncbi.nlm.nih.gov/pubmed/7047527

McShane, E., Sin, C., Zauber, H., Wells, J. N., Donnelly, N., Wang, X., … Selbach, M. (2016). Kinetic Analysis of Protein Stability Reveals Age-Dependent Degradation. *Cell*, *167*(3), 803–815.e21. https://doi.org/10.1016/j.cell.2016.09.015

Menezes, M. J., Guo, Y., Zhang, J., Riley, L. G., Sandra, T., Davis, R. L., … Alexander, S. I. (2015). Mutation in mitochondrial ribosomal protein S7 (MRPS7) causes congenital sensorineural deafness, progressive hepatic and renal failure, and lactic acidemia. *Hum Mol Genet*, *7*, 1–32.

Metodiev, M. D., Lesko, N., Park, C. B., Cámara, Y., Shi, Y., Wibom, R., … Larsson, N. G. (2009). Methylation of 12S rRNA Is Necessary for In Vivo Stability of the Small Subunit of the Mammalian Mitochondrial Ribosome. *Cell Metabolism*, *9*(4), 386–397. https://doi.org/10.1016/j.cmet.2009.03.001

Metodiev, M. D., Spåhr, H., Loguercio Polosa, P., Meharg, C., Becker, C., Altmueller, J., … Ruzzenente, B. (2014). NSUN4 Is a Dual Function Mitochondrial Protein Required for Both Methylation of 12S rRNA and Coordination of Mitoribosomal Assembly. *PLoS Genetics*, *10*(2), 1–11. https://doi.org/10.1371/journal.pgen.1004110

Mick, D. U., Dennerlein, S., Wiese, H., Reinhold, R., Pacheu-Grau, D., Lorenzi, I., … Rehling, P. (2012). MITRAC links mitochondrial protein translocation to respiratory-chain assembly and translational regulation. *Cell*, *151*(7), 1528–1541. https://doi.org/10.1016/j.cell.2012.11.053

Miller, C., Saada, A., Shaul, N., Shabtai, N., Ben-Shalom, E., Shaag, A., … Elpeleg, O. (2004). Defective mitochondrial translation caused by a ribosomal protein (MRPS16) mutation. *Annals of Neurology*, *56*(5), 734–738. https://doi.org/10.1002/ana.20282

Miller, J. L., Koc, H., & Koc, E. C. (2008). Identification of phosphorylation sites in mammalian mitochondrial ribosomal protein DAP3. *Protein Science*, 251–260. https://doi.org/10.1110/ps.073185608.somes

Mitchell, A. L., Attwood, T. K., Babbitt, P. C., Blum, M., Bork, P., Bridge, A., … Finn, R. D. (2018). InterPro in 2019: improving coverage, classification and access to protein sequence annotations. *Nucleic Acids Research*, 1–10. https://doi.org/10.1093/nar/gky1100

Mitchell, P. (1961). Coupling of phosphorylation to electron and hydrogen transfer by a chemi-osmotic type of mechanism. *Nature*, *191*, 144–148. https://doi.org/10.1038/192452a0

Mootha, V. K., Bunkenborg, J., Olsen, J. V, Hjerrild, M., Wisniewski, J. R., Stahl, E., … Mann, M. (2003). Integrated analysis of protein composition, tissue diversity, and gene regulation in mouse mitochondria. *Cell*, *115*(5), 629–640. https://doi.org/S0092867403009267 [pii]

Mootha, V. K., Lepage, P., Miller, K., Bunkenborg, J., Reich, M., Hjerrild, M., … Lander, E. S. (2003). Identification of a gene causing human cytochrome c oxidase deficiency by integrative genomics. *Proceedings of the National Academy of Sciences*, *100*(2), 605–610. https://doi.org/10.1073/pnas.242716699

Nagaike, T., Suzuki, T., Katoh, T., & Ueda, T. (2005). Human mitochondrial mRNAs are

stabilized with polyadenylation regulated by mitochondria-specific poly(A) polymerase and polynucleotide phosphorylase. *The Journal of Biological Chemistry*, *280*(20), 19721–19727. https://doi.org/10.1074/jbc.M500804200

Nagao, A., Suzuki, T., Katoh, T., Sakaguchi, Y., & Suzuki, T. (2009). Biogenesis of glutaminyl-mt tRNAGln in human mitochondria. *Proceedings of the National Academy of Sciences*, *106*(38), 16209–16214. https://doi.org/10.1073/pnas.0907602106

NASS, M. M., & NASS, S. (1963). Intramitochondrial Fibers With Dna Characteristics. I. Fixation and. *The Journal of Cell Biology*, *19*(3), 593–611. https://doi.org/10.1083/jcb.19.3.593

Neupert, W. (2016). Mitochondrial Gene Expression: A Playground of Evolutionary Tinkering. *Annual Review of Biochemistry*, *85*(1), 65–76. https://doi.org/10.1146/annurev-biochem-011116-110824

Niemi, N. M., Wilson, G. M., Overmyer, K. A., Vogtle, F.-N., Lohman, D. C., Schueler, K. L., … Pagliarini, D. J. (2018). Pptc7 is an essential phosphatase for promoting mammalian mitochondrial metabolism and biogenesis. *BioRxiv*, 426247. https://doi.org/10.1101/426247

Nolden, M., Ehses, S., Koppen, M., Bernacchia, A., Rugarli, E. I., & Langer, T. (2005). The m-AAA protease defective in hereditary spastic paraplegia controls ribosome assembly in mitochondria. *Cell*, *123*(2), 277–289. https://doi.org/10.1016/j.cell.2005.08.003

O'Brien, T., & Kalf, G. F. (1967a). Ribosomes from Rat Liver Mitochondria I. ISOLATION PROCEDURE AND CONTAMINATIONS STUDIES. *Journal of Biological Chemistry*, *242*(9), 2172–2179.

O'Brien, T. W., & Kalf, G. F. (1967b). Ribosomes from Rat Liver Mitochondria: II. PARTIAL CHARACTERIZATION. *The Journal of Biological Chemistry*, *242*(9), 2180–2185.

O'Sullivan, M., Rutland, P., Lucas, D., Ashton, E., Hendricks, S., Rahman, S., & Bitner-Glindzicz, M. (2015). Mitochondrial m.1584A 12S m62A rRNA methylation in families with m.1555A>G associated hearing loss. *Human Molecular Genetics*, *24*(4), 1036–1044. https://doi.org/10.1093/hmg/ddu518

Ofengand, J. (2002). Ribosomal RNA pseudouridines and pseudouridine synthases. *FEBS Letters*, *517*(1–3), 287. https://doi.org/10.1016/S0014-5793(02)02567-X

Ofengand, J., & Bakin, A. (1997). Mapping to nucleotide resolution of pseudouridine residues in large subunit ribosomal RNAs from representative eukaryotes, prokaryotes, archaebacteria, mitochondria and chloroplasts. *Journal of Molecular Biology*, *266*(2), 246–268. https://doi.org/10.1006/jmbi.1996.0737

Ojala, D., Montoya, J., & Attardi, G. (1981). TRNA punctuation model of RNA processing in human mitochondria. *Nature*, *290*(5806), 470–474. https://doi.org/10.1038/290470a0

Ott, M., Amunts, A., & Brown, A. (2016). Organization and Regulation of Mitochondrial Protein Synthesis. *Annual Review of Biochemistry*, *85*(1), 77–101. https://doi.org/10.1146/annurev-biochem-060815-014334

Ott, M., Prestele, M., Bauerschmitt, H., Funes, S., Bonnefoy, N., & Herrmann, J. M. (2006). Mba1, a membrane-associated ribosome receptor in mitochondria. *EMBO Journal*, *25*(8), 1603–1610. https://doi.org/10.1038/sj.emboj.7601070

Pagliarini, D. J., Calvo, S. E., Chang, B., Sheth, S. A., Vafai, S. B., Ong, S. E., … Mootha, V. K. (2008). A Mitochondrial Protein Compendium Elucidates Complex I Disease Biology. *Cell*, *134*(1), 112–123. https://doi.org/10.1016/j.cell.2008.06.016

Park, C. B., Asin-Cayuela, J., Cámara, Y., Shi, Y., Pellegrini, M., Gaspari, M., … Larsson, N. G. (2007). MTERF3 Is a Negative Regulator of Mammalian mtDNA Transcription. *Cell*, *130*(2), 273–285. https://doi.org/10.1016/j.cell.2007.05.046

Paul, M. F., Alushin, G. M., Barros, M. H., Rak, M., & Tzagoloff, A. (2012). The putative GTPase encoded by MTG3 functions in a novel pathway for regulating assembly of the small subunit of yeast mitochondrial ribosomes. *Journal of Biological Chemistry*, *287*(29), 24346–24355. https://doi.org/10.1074/jbc.M112.363309

Pearce, S. F., Rebelo-Guiomar, P., D'Souza, A. R., Powell, C. A., Van Haute, L., & Minczuk, M. (2017). Regulation of Mammalian Mitochondrial Gene Expression: Recent Advances. *Trends in Biochemical Sciences*, *42*(8), 625–639. https://doi.org/10.1016/j.tibs.2017.02.003

Pearce, S. F., Rorbach, J., Van Haute, L., D'Souza, A. R., Rebelo-Guiomar, P., Powell, C. A., … Minczuk, M. (2017). Maturation of selected human mitochondrial tRNAs requires deadenylation. *ELife*, *6*, 1–22. https://doi.org/10.7554/eLife.27596

Perez-Martinez, X., Broadley, S. A., & Fox, T. D. (2003). Mss51p promotes mitochondrial Cox1p synthesis and interacts with newly synthesized Cox1p. *EMBO Journal*, *22*(21), 5951–5961. https://doi.org/10.1093/emboj/cdg566

Perks, K. L., Ferreira, N., Richman, T. R., Ermer, J. A., Kuznetsova, I., Shearwood, A.-M. J., … Filipovska, A. (2017). Adult-onset obesity is triggered by impaired mitochondrial gene expression. *Science Advances*, *3*(8), e1700677. https://doi.org/10.1126/sciadv.1700677

Perks, K. L., Rossetti, G., Kuznetsova, I., Hughes, L. A., Ermer, J. A., Ferreira, N., … Filipovska, A. (2018). PTCD1 Is Required for 16S rRNA Maturation Complex Stability and Mitochondrial Ribosome Assembly. *Cell Reports*, *23*(1), 127–142. https://doi.org/10.1016/j.celrep.2018.03.033

Petrov, A. S., Gulen, B., Norris, A. M., Kovacs, N. A., Bernier, C. R., Lanier, K. A., … Williams, L. D. (2015). History of the ribosome and the origin of translation. *Proceedings of the National Academy of Sciences*, *112*(50), 15396–15401. https://doi.org/10.1073/pnas.1509761112

Petrov, A. S., Wood, E. C., Bernier, C. R., Norris, A. M., Brown, A., & Amunts, A. (2018). Structural Patching Fosters Divergence of Mitochondrial Ribosomes, 1–24. https://doi.org/10.1093/molbev/msy221/5229934

Posse, V., & Gustafsson, C. M. (2017). Human Mitochondrial Transcription Factor B2 Is Required for Promoter Melting during Initiation of Transcription. *The Journal of Biological Chemistry*, *292*(7), 2637–2645. https://doi.org/10.1074/jbc.M116.751008

Posse, V., Hoberg, E., Dierckx, A., Shahzad, S., Koolmeister, C., Larsson, N.-G., … Gustafsson, C. M. (2014). The amino terminal extension of mammalian mitochondrial RNA polymerase ensures promoter specific transcription initiation. *Nucleic Acids Research*, *42*(6), 3638–3647. https://doi.org/10.1093/nar/gkt1397

Posse, V., Shahzad, S., Falkenberg, M., Hällberg, B. M., & Gustafsson, C. M. (2015). TEFM is a potent stimulator of mitochondrial transcription elongation in vitro. *Nucleic Acids Research*, *43*(5), 2615–2624. https://doi.org/10.1093/nar/gkv105

Prezant, T. R., Agapian, J. V., Bohlman, M. C., Bu, X., Öztas, S., Qiu, W. Q., … Fischel-

Ghodsian, N. (1993). Mitochondrial ribosomal RNA mutation associated with both antibiotic-induced and non-syndromic deafness. *Nature Genetics*, *4*(3), 289–294. https://doi.org/10.1038/ng0793-289

Pulman, J., Ruzzenente, B., Bianchi, L., Rio, M., Boddaert, N., Munnich, A., … Metodiev, M. D. (2018). Mutations in the *MRPS28* gene encoding the small mitoribosomal subunit protein bS1m in a patient with intrauterine growth retardation, craniofacial dysmorphism and multisystemic involvement. *Human Molecular Genetics*. https://doi.org/10.1093/hmg/ddy441

R development core team. (2008). R: A language and environment for statistical computing. *R Foundation for Statistical Computing*. https://doi.org/http://www.R-project.org/

Rackham, O., Busch, J. D., Matic, S., Siira, S. J., Kuznetsova, I., Atanassov, I., … Filipovska, A. (2016). Hierarchical RNA Processing Is Required for Mitochondrial Ribosome Assembly. *Cell Reports*, *16*(7), 1874–1890. https://doi.org/10.1016/j.celrep.2016.07.031

Rackham, O., Davies, S. M. K., Shearwood, A. M. J., Hamilton, K. L., Whelan, J., & Filipovska, A. (2009). Pentatricopeptide repeat domain protein 1 lowers the levels of mitochondrial leucine tRNAs in cells. *Nucleic Acids Research*, *37*(17), 5859–5867. https://doi.org/10.1093/nar/gkp627

Rak, M., & Tzagoloff, A. (2009). F1-dependent translation of mitochondrially encoded Atp6p and Atp8p subunits of yeast ATP synthase. *Proc Natl Acad Sci U S A*, *106*(44), 18509–18514. https://doi.org/10.1073/pnas.0910351106

Ramakrishnan, V. (2002). Ribosome structure and the mechanism of translation. *Cell*, *108*(4), 557–572. https://doi.org/10.1016/S0092-8674(02)00619-0

Rappsilber, J. (2011). The beginning of a beautiful friendship: Cross-linking/mass spectrometry and modelling of proteins and multi-protein complexes. *Journal of Structural Biology*, *173*(3), 530–540. https://doi.org/10.1016/j.jsb.2010.10.014

Rappsilber, J., Ishihama, Y., & Mann, M. (2003). Stop and Go Extraction Tips for Matrix-Assisted Laser Desorption / Ionization , Nanoelectrospray , and LC / MS Sample Pretreatment in Proteomics. *Analytical Chemistry*, *75*(3), 663–670. https://doi.org/10.1021/ac026117i CCC:

Reichert, A. S., Thurlow, D. L., & Mörl, M. (2001). A Eubacterial Origin for the Human tRNA Nucleotidyltransferase? *Biological Chemistry*, *382*(10), 1431–1438. https://doi.org/10.1515/BC.2001.176

Reinhard, L., Sridhara, S., & Hällberg, B. M. (2015). Structure of the nuclease subunit of human mitochondrial RNase P. *Nucleic Acids Research*, *43*(11), 5664–5672. https://doi.org/10.1093/nar/gkv481

Reinhard, L., Sridhara, S., & Hällberg, B. M. (2017). The MRPP1/MRPP2 complex is a tRNA-maturation platform in human mitochondria. *Nucleic Acids Research*, *45*(21), 12469–12480. https://doi.org/10.1093/nar/gkx902

Rhee, H., Zou, P., Udeshi, N. D., Martell, J. D., Mootha, V. K., Carr, S. A., & Ting, A. Y. (2013). Proteomic mapping of mitochondria in living cells via spatially restricted enzymatic tagging. *Science*, *339*(March), 1328. https://doi.org/10.1126/science.1230593

Richman, T. R., Ermer, J. A., Davies, S. M. K., Perks, K. L., Viola, H. M., Shearwood, A. M. J., … Filipovska, A. (2015). Mutation in MRPS34 Compromises Protein

Synthesis and Causes Mitochondrial Dysfunction. *PLoS Genetics*, *11*(3). https://doi.org/10.1371/journal.pgen.1005089

Richman, T. R., Spahr, H., Ermer, J. A., Davies, S. M. K., Viola, H. M., Bates, K. A., … Filipovska, A. (2016). Loss of the RNA-binding protein TACO1 causes late-onset mitochondrial dysfunction in mice. *Nature Communications*, *7*(May), 1–14. https://doi.org/10.1038/ncomms11884

Richter-Dennerlein, R., Dennerlein, S., & Rehling, P. (2015). Integrating mitochondrial translation into the cellular context. *Nature Reviews Molecular Cell Biology*, *16*(10), 586–592. https://doi.org/10.1038/nrm4051

Richter-Dennerlein, R., Oeljeklaus, S., Lorenzi, I., Ronsör, C., Bareth, B., Schendzielorz, A. B., … Dennerlein, S. (2016). Mitochondrial Protein Synthesis Adapts to Influx of Nuclear-Encoded Protein. *Cell*, *167*(2), 471–483.e10. https://doi.org/10.1016/j.cell.2016.09.003

Richter, R., Rorbach, J., Pajak, A., Smith, P. M., Wessels, H. J., Huynen, M. A., … Chrzanowska-Lightowlers, Z. M. (2010). A functional peptidyl-tRNA hydrolase, ICT1, has been recruited into the human mitochondrial ribosome. *EMBO Journal*, *29*(6), 1116–1125. https://doi.org/10.1038/emboj.2010.14

Ritchie, M. E., Phipson, B., Wu, D., Hu, Y., Law, C. W., Shi, W., & Smyth, G. K. (2015). Limma powers differential expression analyses for RNA-sequencing and microarray studies. *Nucleic Acids Research*, *43*(7), e47. https://doi.org/10.1093/nar/gkv007

Rooijers, K., Loayza-Puch, F., Nijtmans, L. G., & Agami, R. (2013). Ribosome profiling reveals features of normal and disease-associated mitochondrial translation. *Nature Communications*, *4*, 1–8. https://doi.org/10.1038/ncomms3886

Rorbach, J., Boesch, P., Gammage, P. A., Nicholls, T. J. J., Pearce, S. F., Patel, D., … Minczuk, M. (2014). MRM2 and MRM3 are involved in biogenesis of the large subunit of the mitochondrial ribosome. *Molecular Biology of the Cell*, *25*(17), 2542–2555. https://doi.org/10.1091/mbc.E14-01-0014

Rorbach, J., Gammage, P. A., & Minczuk, M. (2012). C7orf30 is necessary for biogenesis of the large subunit of the mitochondrial ribosome. *Nucleic Acids Research*, *40*(9), 4097–4109. https://doi.org/10.1093/nar/gkr1282

Rorbach, J., & Minczuk, M. (2012). The post-transcriptional life of mammalian mitochondrial RNA. *Biochemical Journal*, *444*(3), 357–373. https://doi.org/10.1042/BJ20112208

Rorbach, J., Nicholls, T. J. J., & Minczuk, M. (2011). PDE12 removes mitochondrial RNA poly(A) tails and controls translation in human mitochondria. *Nucleic Acids Research*, *39*(17), 7750–7763. https://doi.org/10.1093/nar/gkr470

Rorbach, J., Richter, R., Wessels, H. J., Wydro, M., Pekalski, M., Farhoud, M., … Chrzanowska-Lightowlers, Z. M. A. (2008). The human mitochondrial ribosome recycling factor is essential for cell viability. *Nucleic Acids Research*, *36*(18), 5787–5799. https://doi.org/10.1093/nar/gkn576

Rossmanith, W., Tullo, A., Potuschak, T., Karwan, R., & Sbis, E. (1995). Human mitochondrial tRNA processing. *Journal of Biological …*. https://doi.org/10.1074/jbc.270.21.12885

Rozanska, A., Richter-Dennerlein, R., Rorbach, J., Gao, F., Lewis, R. J., Chrzanowska-Lightowlers, Z. M., & Lightowlers, R. N. (2017). The human RNA-binding protein RBFA promotes the maturation of the mitochondrial ribosome. *Biochemical Journal*,

474(13), 2145–2158. https://doi.org/10.1042/BCJ20170256
Rugarli, E. I., & Langer, T. (2012). Mitochondrial quality control: A matter of life and death for neurons. *EMBO Journal*, *31*(6), 1336–1349. https://doi.org/10.1038/emboj.2012.38
Ruzzenente, B., Metodiev, M. D., Wredenberg, A., Bratic, A., Park, C. B., Camara, Y., … Larsson, N. G. (2012). LRPPRC is necessary for polyadenylation and coordination of translation of mitochondrial mRNAs. *EMBO J*, *31*(2), 443–456. https://doi.org/10.1038/emboj.2011.392
Saada, A., Shaag, A., Arnon, S., Dolfin, T., Miller, C., Fuchs-Telem, D., … Elpeleg, O. (2007). Antenatal mitochondrial disease caused by mitochondrial ribosomal protein (MRPS22) mutation. *Journal of Medical Genetics*, *44*(12), 784–786. https://doi.org/10.1136/jmg.2007.053116
Sagan, L. (1967). On the Origin of Mitosing Cells. *Journal of Theoretical Biology*, (14), 225–274. https://doi.org/10.1016/0022-5193(67)90079-3
Sasarman, F., Brunel-Guitton, C., Antonicka, H., Wai, T., Shoubridge, E. A., & Consortium, L. (2010). LRPPRC and SLIRP Interact in a Ribonucleoprotein Complex That Regulates Posttranscriptional Gene Expression in Mitochondria. *Molecular Biology of the Cell*, *21*(1), 1315–1323. https://doi.org/10.1091/mbc.E10
Sasarman, F., Nishimura, T., Antonicka, H., Weraarpachai, W., Shoubridge, E. A., Allen, B., … Shoubridge, E. A. (2015). Tissue-specific responses to the LRPPRC founder mutation in French Canadian Leigh Syndrome. *Human Molecular Genetics*, *24*(2), 480–491. https://doi.org/10.1093/hmg/ddu468
Sasarman, F., Thiffault, I., Weraarpachai, W., Salomon, S., Maftei, C., Gauthier, J., … Shoubridge, E. A. (2015). The 3′ addition of CCA to mitochondrial tRNASer(AGY) is specifically impaired in patients with mutations in the tRNA nucleotidyl transferase TRNT1. *Human Molecular Genetics*, *24*(10), 2841–2847. https://doi.org/10.1093/hmg/ddv044
Serre, V., Rozanska, A., Beinat, M., Chretien, D., Boddaert, N., Munnich, A., … Chrzanowska-Lightowlers, Z. M. (2013). Mutations in mitochondrial ribosomal protein MRPL12 leads to growth retardation, neurological deterioration and mitochondrial translation deficiency. *Biochimica et Biophysica Acta - Molecular Basis of Disease*, *1832*(8), 1304–1312. https://doi.org/10.1016/j.bbadis.2013.04.014
Sharma, M. R., Koc, E. C., Datta, P. P., Booth, T. M., Spremulli, L. L., & Agrawal, R. K. (2003). Structure of the mammalian mitochondrial ribosome reveals an expanded functional role for its component proteins. *Cell*, *115*(1), 97–108. https://doi.org/10.1016/S0092-8674(03)00762-1
Shutt, T. E., & Gray, M. W. (2006). Homologs of Mitochondrial Transcription Factor B, Sparsely Distributed Within the Eukaryotic Radiation, Are Likely Derived from the Dimethyladenosine Methyltransferase of the Mitochondrial Endosymbiont. *Molecular Biology and Evolution*, *23*(6), 1169–1179. https://doi.org/10.1093/molbev/msk001
Sievers, F., Wilm, A., Dineen, D., Gibson, T. J., Karplus, K., Li, W., … Higgins, D. G. (2011). Fast, scalable generation of high-quality protein multiple sequence alignments using Clustal Omega. *Molecular Systems Biology*, *7*(539). https://doi.org/10.1038/msb.2011.75

Signes, A., & Fernandez-Vizarra, E. (2018). Assembly of mammalian oxidative phosphorylation complexes I–V and supercomplexes. *Essays In Biochemistry*, *62*(3), 255–270. https://doi.org/10.1042/EBC20170098

Siira, S. J., Rossetti, G., Richman, T. R., Perks, K., Ermer, J. A., Kuznetsova, I., … Filipovska, A. (2018). Concerted regulation of mitochondrial and nuclear non-coding RNAs by a dual-targeted RNase Z. *EMBO Reports*, *19*(10), e46198. https://doi.org/10.15252/embr.201846198

Siira, S. J., Spåhr, H., Shearwood, A. M. J., Ruzzenente, B., Larsson, N. G., Rackham, O., & Filipovska, A. (2017). LRPPRC-mediated folding of the mitochondrial transcriptome. *Nature Communications*, *8*(1), 1–10. https://doi.org/10.1038/s41467-017-01221-z

Smits, P., Antonicka, H., Van Hasselt, P. M., Weraarpachai, W., Haller, W., Schreurs, M., … Van Den Heuvel, L. P. (2011). Mutation in subdomain G' of mitochondrial elongation factor G1 is associated with combined OXPHOS deficiency in fibroblasts but not in muscle. *European Journal of Human Genetics*, *19*(3), 275–279. https://doi.org/10.1038/ejhg.2010.208

Smits, P., Saada, A., Wortmann, S. B., Heister, A. J., Brink, M., Pfundt, R., … Van Den Heuvel, L. P. (2011). Mutation in mitochondrial ribosomal protein MRPS22 leads to Cornelia de Lange-like phenotype, brain abnormalities and hypertrophic cardiomyopathy. *European Journal of Human Genetics*, *19*(4), 394–399. https://doi.org/10.1038/ejhg.2010.214

Sonnhammer, E. L. L., Von Heijne, G., & Krogh, A. (1998). A hidden Markov model for predicting transmembrane helices in protein sequences. *Proc. Sixth Int. Conf. on Intelligent Systems for Molecular Biology*, 175–182. Retrieved from papers://4b986d00-906f-493f-a74b-71e29d82b719/Paper/p6291

Spahr, H., Habermann, B., Gustafsson, C. M., Larsson, N.-G., & Hallberg, B. M. (2012). Structure of the human MTERF4-NSUN4 protein complex that regulates mitochondrial ribosome biogenesis. *Proceedings of the National Academy of Sciences*, *109*(38), 15253–15258. https://doi.org/10.1073/pnas.1210688109

Spinelli, J. B., & Haigis, M. C. (2018). The multifaceted contributions of mitochondria to cellular metabolism. *Nature Cell Biology*, *20*(7), 745–754. https://doi.org/10.1038/s41556-018-0124-1

Spremulli, L., & Kraus, B. L. (1987). Effect of Cations and Heterologous Dissociation Factors on Subunit Interactions. *Biochemical and Biophysical Research Communications*, *147*(3), 1077–1081.

Stoldt, S., Wenzel, D., Kehrein, K., Riedel, D., Ott, M., & Jakobs, S. (2018). Spatial orchestration of mitochondrial translation and OXPHOS complex assembly. *Nature Cell Biology*, *20*(5), 528–534. https://doi.org/10.1038/s41556-018-0090-7

Suhm, T., Kaimal, J. M., Dawitz, H., Peselj, C., Masser, A. E., Hanzén, S., … Ott, M. (2018). Mitochondrial Translation Efficiency Controls Cytoplasmic Protein Homeostasis. *Cell Metabolism*, *27*(6), 1309–1322.e6. https://doi.org/10.1016/j.cmet.2018.04.011

Suzuki, T., Nagao, A., & Suzuki, T. (2011). Human Mitochondrial tRNAs: Biogenesis, Function, Structural Aspects, and Diseases. *Annual Review of Genetics*, *45*(1), 299–329. https://doi.org/10.1146/annurev-genet-110410-132531

Suzuki, T., & Suzuki, T. (2014). A complete landscape of post-transcriptional

modifications in mammalian mitochondrial tRNAs. *Nucleic Acids Research*, *42*(11), 7346–7357. https://doi.org/10.1093/nar/gku390

Suzuki, T., Terasaki, M., Takemoto-Hori, C., Hanada, T., Ueda, T., Wada, A., & Watanabe, K. (2001a). Proteomic Analysis of the Mammalian Mitochondrial Ribosome: IDENTIFICATION OF PROTEIN COMPONENTS IN THE 28S SMALL SUBUNIT. *Journal of Biological Chemistry*, *276*(35), 33181–33195. https://doi.org/10.1074/jbc.M103236200

Suzuki, T., Terasaki, M., Takemoto-Hori, C., Hanada, T., Ueda, T., Wada, A., & Watanabe, K. (2001b). Structural compensation for the deficit of rRNA with proteins in the mammalian mitochondrial ribosome. Systematic analysis of protein components of the large ribosomal subunit from mammalian mitochondria. *Journal of Biological Chemistry*, *276*(24), 21724–21736. https://doi.org/10.1074/jbc.M100432200

Temperley, R., Richter, R., Dennerlein, S., & Lightowlers, R. N. (2010). Hungry Codons Promote Frameshifting in Human Mitochondrial Ribosomes. *Science*, *327*(January), 2010.

Thompson, K., Mai, N., Oláhová, M., Scialó, F., Formosa, L. E., Stroud, D. A., … Taylor, R. W. (2018). *OXA1L* mutations cause mitochondrial encephalopathy and a combined oxidative phosphorylation defect. *EMBO Molecular Medicine*, e9060. https://doi.org/10.15252/emmm.201809060

Tomecki, R., Dmochowska, A., Gewartowski, K., Dziembowski, A., & Stepien, P. P. (2004). Identification of a novel human nuclear-encoded mitochondrial poly(A) polymerase. *Nucleic Acids Research*, *32*(20), 6001–6014. https://doi.org/10.1093/nar/gkh923

Trifunovic, A., Wredenberg, A., Falkenberg, M., Spelbrink, J. N., Rovio, A. T., Bruder, C. E., … Larsson, N.-G. (2004). Premature ageing in mice expressing defective mitochondrial DNA polymerase. *Nature*, *429*(6990), 417–423. https://doi.org/10.1038/nature02517

Tu, Y. T., & Barrientos, A. (2015). The Human Mitochondrial DEAD-Box Protein DDX28 Resides in RNA Granules and Functions in Mitoribosome Assembly. *Cell Reports*, *10*(6), 854–864. https://doi.org/10.1016/j.celrep.2015.01.033

Tucker, E. J., Hershman, S. G., Köhrer, C., Belcher-Timme, C. A., Patel, J., Goldberger, O. A., … Mootha, V. K. (2011). Mutations in MTFMT underlie a human disorder of formylation causing impaired mitochondrial translation. *Cell Metabolism*, *14*(3), 428–434. https://doi.org/10.1016/j.cmet.2011.07.010

Turncock, S. J. S. H. and G. (1971). Stabilization of 70S Ribosomes by Spermidine. *Nature*, *229*.

Uchiumi, T., Ohgaki, K., Yagi, M., Aoki, Y., Sakai, A., Matsumoto, S., & Kang, D. (2010). ERAL1 is associated with mitochondrial ribosome and elimination of ERAL1 leads to mitochondrial dysfunction and growth retardation. *Nucleic Acids Research*, *38*(16), 5554–5568. https://doi.org/10.1093/nar/gkq305

Van Haute, L., Pearce, S. F., Powell, C. A., D'Souza, A. R., Nicholls, T. J., & Minczuk, M. (2015). Mitochondrial transcript maturation and its disorders. *Journal of Inherited Metabolic Disease*, *38*(4), 655–680. https://doi.org/10.1007/s10545-015-9859-z

Van Vranken, J. G., Jeong, M.-Y., Wei, P., Chen, Y.-C., Gygi, S. P., Winge, D. R., & Rutter, J. (2016). The mitochondrial acyl carrier protein (ACP) coordinates

mitochondrial fatty acid synthesis with iron sulfur cluster biogenesis. *ELife*, *5*. https://doi.org/10.7554/eLife.17828

Vargas Möller-Hergt, B., Carlström, A., Stephan, K., Imhof, A., & Ott, M. (2018). The ribosome receptors Mrx15 and Mba1 jointly organize co-translational insertion and protein biogenesis in mitochondria. *Molecular Biology of the Cell*, mbcE18040227. https://doi.org/10.1091/mbc.E18-04-0227

Vernochet, C., Mourier, A., Bezy, O., MacOtela, Y., Boucher, J., Rardin, M. J., … Kahn, C. R. (2012). Adipose-specific deletion of TFAM increases mitochondrial oxidation and protects mice against obesity and insulin resistance. *Cell Metabolism*, *16*(6), 765–776. https://doi.org/10.1016/j.cmet.2012.10.016

Vilardo, E., Nachbagauer, C., Buzet, A., Taschner, A., Holzmann, J., & Rossmanith, W. (2012a). A subcomplex of human mitochondrial RNase P is a bifunctional methyltransferase-extensive moonlighting in mitochondrial tRNA biogenesis. *Nucleic Acids Research*, *40*(22), 11583–11593. https://doi.org/10.1093/nar/gks910

Vilardo, E., Nachbagauer, C., Buzet, A., Taschner, A., Holzmann, J., & Rossmanith, W. (2012b). Corrigendum - A subcomplex of human mitochondrial RNase P is a bifunctional methyltransferase-extensive moonlighting in mitochondrial tRNA biogenesis. *Nucleic Acids Research*, *40*(22), 11583–11593. https://doi.org/10.1093/nar/gks910

Vögtle, F. N., Wortelkamp, S., Zahedi, R. P., Becker, D., Leidhold, C., Gevaert, K., … Meisinger, C. (2009). Global Analysis of the Mitochondrial N-Proteome Identifies a Processing Peptidase Critical for Protein Stability. *Cell*, *139*(2), 428–439. https://doi.org/10.1016/j.cell.2009.07.045

Wai, T., García-Prieto, J., Baker, M. J., Merkwirth, C., Benit, P., Rustin, P., … Langer, T. (2015). Imbalanced OPA1 processing and mitochondrial fragmentation cause heart failure in mice. *Science*, *350*(6265). https://doi.org/10.1126/science.aad0116

Wallace, D. C., Singh, G., Lott, M. T., Hodge, J. A., Schurr, T. G., Lezza, A. M., … Nikoskelainen, E. K. (1988). Mitochondrial DNA mutation associated with Leber's hereditary optic neuropathy. *Science*, *242*(4884), 1427–1430. https://doi.org/10.1126/SCIENCE.3201231

Wanschers, B. F. J., Szklarczyk, R., Pajak, A., Van Den Brand, M. A. M., Gloerich, J., Rodenburg, R. J. T., … Huynen, M. A. (2012). C7orf30 specifically associates with the large subunit of the mitochondrial ribosome and is involved in translation. *Nucleic Acids Research*, *40*(9), 4040–4051. https://doi.org/10.1093/nar/gkr1271

Wende, S., Bonin, S., Gotze, O., Betat, H., & Morl, M. (2015). The identity of the discriminator base has an impact on CCA addition. *Nucleic Acids Research*, *43*(11), 5617–5629. https://doi.org/10.1093/nar/gkv471

Weraarpachai, W., Antonicka, H., Sasarman, F., Seeger, J., Schrank, B., Kolesar, J. E., … Shoubridge, E. A. (2009). Mutation in TACO1, encoding a translational activator of COX I, results in cytochrome c oxidase deficiency and late-onset Leigh syndrome. *Nature Genetics*, *41*(7), 833–837. https://doi.org/10.1038/ng.390

Wessel, D., & Flügge, U. I. (1984). A method for the quantitative recovery of protein in dilute solution in the presence of detergents and lipids. *Analytical Biochemistry*, *138*(1), 141–143. https://doi.org/10.1016/0003-2697(84)90782-6

Westermann, B. (2010). Mitochondrial fusion and fission in cell life and death. *Nature Reviews Molecular Cell Biology*, *11*(12), 872–884. https://doi.org/10.1038/nrm3013

Wiedemann, N., & Pfanner, N. (2017). Mitochondrial Machineries for Protein Import and Assembly. *Annual Review of Biochemistry*, *86*(1), 685–714. https://doi.org/10.1146/annurev-biochem-060815-014352

Wiśniewski, J. R., & Rakus, D. (2014). Multi-enzyme digestion FASP and the 'Total Protein Approach'-based absolute quantification of the Escherichia coli proteome. *Journal of Proteomics*, *109*, 322–331. https://doi.org/10.1016/j.jprot.2014.07.012

Wredenberg, A., Lagouge, M., Bratic, A., Metodiev, M. D., Spåhr, H., Mourier, A., … Larsson, N. G. (2013). MTERF3 Regulates Mitochondrial Ribosome Biogenesis in Invertebrates and Mammals. *PLoS Genetics*, *9*(1). https://doi.org/10.1371/journal.pgen.1003178

Xu, F., Ackerley, C., Maj, M. C., Addis, J. B. L., Levandovskiy, V., Lee, J., … Robinson, B. H. (2008). Disruption of a mitochondrial RNA-binding protein gene results in decreased cytochrome b expression and a marked reduction in ubiquinol-cytochrome c reductase activity in mouse heart mitochondria. *The Biochemical Journal*, *416*(1), 15–26. https://doi.org/10.1042/BJ20080847

Yang-hao Ou, A. W. C. J. F. W. C. T. L. M. C. C. L. (2018). Aminoglycoside-associated nonsyndromic deafness and speech disorder in mitochondrial A1555g mutation in a family: A case report. *Medicine*, *97*(42), e12878. https://doi.org/10.1097/md.0000000000012878

Zaganelli, S., Rebelo-Guiomar, P., Maundrell, K., Rozanska, A., Pierredon, S., Powell, C. A., … Martinou, J. C. (2017). The pseudouridine synthase RPUSD4 is an essential component of mitochondrial RNA granules. *Journal of Biological Chemistry*, *292*(11), 4519–4532. https://doi.org/10.1074/jbc.M116.771105

Zeng, R., Smith, E., & Barrientos, A. (2018). Yeast Mitoribosome Large Subunit Assembly Proceeds by Hierarchical Incorporation of Protein Clusters and Modules on the Inner Membrane. *Cell Metabolism*, *27*(3), 645–656.e7. https://doi.org/10.1016/j.cmet.2018.01.012

Zheng, W., Khrapko, K., Coller, H. A., Thilly, W. G., & Copeland, W. C. (2006). Origins of human mitochondrial point mutations as DNA polymerase γ-mediated errors. *Mutation Research/Fundamental and Molecular Mechanisms of Mutagenesis*, *599*(1–2), 11–20. https://doi.org/10.1016/J.MRFMMM.2005.12.012

Zhu, J., Vinothkumar, K. R., & Hirst, J. (2016). Structure of mammalian respiratory complex I. *Nature*, *536*(7616), 354–358. https://doi.org/10.1038/nature19095

Zhu, Y., Zhao, J., Feng, B., Su, Y., Kang, D., Yuan, H., … Dai, P. (2015). Mutations in the mitochondrial 12S rRNA gene in elderly Chinese people. *Acta Oto-Laryngologica*, *135*(1), 26–34. https://doi.org/10.3109/00016489.2014.949849

6. Acknowledgements

Foremost, I want to thank Prof. Nils-Göran Larsson for the opportunity to pursue my PhD thesis in his laboratory. Thank you for your commitment to science, availability for discussion, guidance, and for the many occasions to participate in retreats, workshops and conferences, which expanded my horizon and supported my ability to focus on my projects. It was great to be part of your group and to do thrilling science. I hope that the project will further develop and be of use for more discoveries. Thank you very much for everything, Nils!

I am very grateful to Prof. Elena Rugarli to co-examine my thesis and Prof. Jan Riemer from the University of Cologne to preside the thesis committee.

I want to thank Prof. Aleksandra Filipovska and Prof. Oliver Rackham from the Harry Perkins Institute in Australia to give me opportunities to participate in interesting and productive projects.

I would like to express my sincere gratitude to Dr. Dusanka Milenkovic, Dr. Ana Bratic and Dr. Arnaud Mourier for being remarkably encouraging friends and scientists. Your guidance and critical sincerity helped me a lot to grow as a scientist. I am very grateful for your support, our discussions and the pleasant and productive atmosphere. Thanks a lot!

I highly appreciate everybody in the Larsson department for the friendly atmosphere. I want to thank Petra Kirschner, Dr. Min Jiang, Dr. Cristina Remes, Dr. Johanna Kauppila, Dr. Nina Bonekamp, Dr. Maria Miranda , Lysann Schmitz, Nadine Hochhard, Dr. Benedetta Ruzzenente, Dr. Marie Lagouge, Corry Schwierzy-Krämer, Dr. Miriam Krähling, Dr. Elisa Motori, and Dr. Henrik Spåhr for their help when needed and the fantastic years with science, X-mas market fun, cakes and cookies to fuel our brains.

I want to thank Dr. Xinping Li and Dr. Ilian Atanassov for the professional collaboration, advice on mass spectrometry, and for running an excellent proteomics core facility at the MPI for Biology of Ageing.

Moreover, I want to thank my friends Dr. Eduardo Silva Ramos for being an expert scientist reminding me to focus on what is important to finish, and MSc. Thomas Schöndorf, the strongest student in the universe, for his dedication and project support. Thanks a lot for many relaxing night outs with delicious food and entertaining movies. I wish you both all the best for your future and I hope that we meet again as scientists!

I would like to acknowledge the comparative biology department in particular Tamara Reiher, Tanja Schneider, Maria Hahn, Sarah Kranz, Iweta Gniadek, Katrin Behncke, Vera Musik and Frederick Boeddekker for animal caretaking contributing substantially to this project. I very much appreciate the generous financial support of the Max-Planck-Society.

Moreover, I very much appreciate the great teaching by my previous advisors from the institutes of Biochemistry and Genetics at the University of Cologne for training me to think critically about experiments and science.

Lastly yet importantly, I would like to thank my family, especially, Melanie, Ruth and Ute, for their encouragement and infinite support in the last years. Particularly, I want to acknowledge Melanie for her comprehension of my dedication to science. I am looking forward to the next 15 years!

7. Erklärung

"Ich versichere, dass ich die von mir vorgelegte Dissertation selbständig angefertigt, die benutzten Quellen und Hilfsmittel vollständig angegeben und die Stellen der Arbeit − einschließlich Tabellen, Karten und Abbildungen −, die anderen Werken im Wortlaut oder dem Sinn nach entnommen sind, in jedem Einzelfall als Entlehnung kenntlich gemacht habe; dass diese Dissertation noch keiner anderen Fakultät oder Universität zur Prüfung vorgelegen hat; dass sie − abgesehen von unten angegebenen Teilpublikationen − noch nicht veröffentlicht worden ist sowie, dass ich eine solche Veröffentlichung vor Abschluss des Promotionsverfahrens nicht vornehmen werde. Die Bestimmungen der Promotionsordnung sind mir bekannt. Die von mir vorgelegte Dissertation ist von Herrn Prof. Dr. Nils-Göran Larsson (am Max-Planck-Institut für Biologie des Alterns, Köln) betreut worden."

Köln, 30. November 2019

_____

(Jakob D. Busch)

8. Publications / Teilpublikationen

- **Busch, J.D.**, et al. (2019) MitoRibo-Tag Mice Provide a Tool for *In Vivo* Studies of Mitoribosome Composition. **Cell Reports**, Volume 29, ISSUE 6, P1728-1738.e9, November 05, 2019. https://doi.org/10.1016/j.celrep.2019.09.080

- Perks, K., […], **Busch J. D.**, et al. (2018) PTCD1 is required for 16S rRNA maturation complex stability and mitochondrial ribosome assembly. **Cell Reports** 23, 127–142. https://doi.org/10.1016/j.celrep.2018.03.033

- Rackham, O., **Busch, J. D.**, et al. (2016). Hierarchical RNA Processing Is Required for Mitochondrial Ribosome Assembly. **Cell Reports** 16, 1874-1890. https://doi.org/10.1016/j.celrep.2016.07.031

- Lagouge, M., […], **Busch, J. D**., et al. (2015). SLIRP Regulates the Rate of Mitochondrial Protein Synthesis and Protects LRPPRC from Degradation. **PLOS Genetics** 11, e1005423. https://doi.org/10.1371/journal.pgen.1005423